$5

November/December 2013

www.arrl.org

QEX

A Forum for Communications Experimenters

Issue No. 281

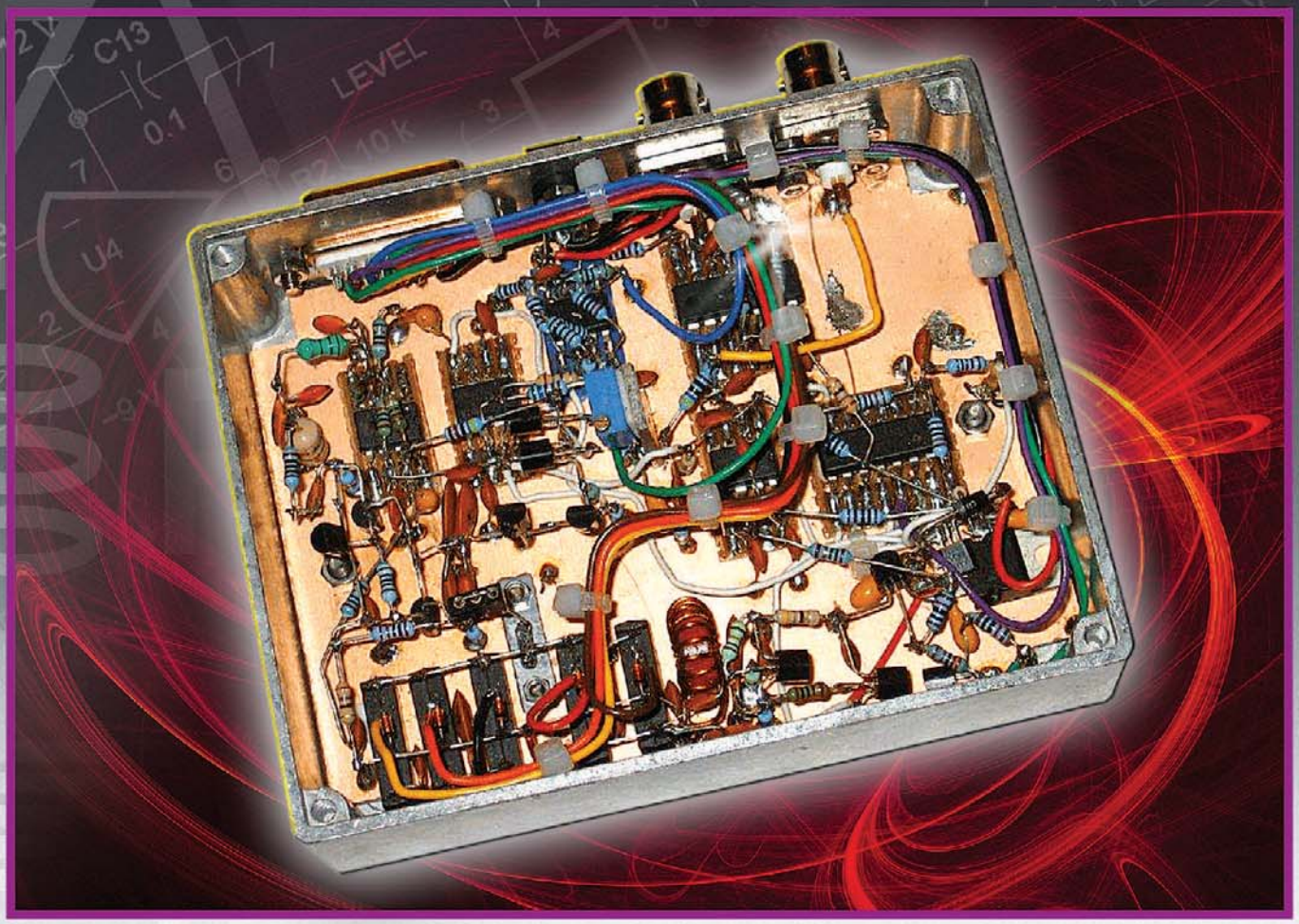

G3OTK describes an automated system for measuring the equivalent circuit components, or motional parameters of quartz crystals for the design of crystal ladder filters. With his microprocessor controlled test set he can measure up to 150 crystals in an hour.

ARRL *The national association for* *AMATEUR RADIO*™
225 Main Street
Newington, CT USA 06111-1494

EVENT HORIZON OF DX

TS-990S

Dual TFT Display & Dual Receiver HF/50 MHz Transceiver

The main receiver has an IP3 in the +40 dB class, and the sub receiver is the already famous TS-590S receiver. Capable of receiving two signals at once, on different bands. 7-inch and 3.5-inch color TFT displays allow displaying of independent contents. Simplification of complex operations at a glance. Make no mistake, this is not a toy. Finally a serious tool is available for getting the very most from your hobby, of course it's a Kenwood.

- Covers the HF and 50 MHz bands.
- High-speed automatic antenna tuner.
- USB, Serial and LAN ports.
- Various PC applications (free software): ARCP-990 enabling PC control, ARHP-990 enabling remote control, and ARUA-10 USB audio driver.
- Clean 5 to 200 W transmit power through the 50 V FET final unit.
- Built-in RTTY and PSK.
- Three Analog Devices 32-bit floating-point arithmetic DSPs.
- DVI output for display by an external monitor (main screen display only).

KENWOOD

Customer Support: (310) 639-4200
Fax: (310) 537-8235

Scan with your phone to download TS-990S brochure.

www.kenwoodusa.com

ISO9001 Registered
Professional Systems Business Group
JVCKENWOOD Corporation

ADS#11113

QEX (ISSN: 0886-8093) is published bimonthly in January, March, May, July, September, and November by the American Radio Relay League, 225 Main Street, Newington, CT 06111-1494. Periodicals postage paid at Hartford, CT and at additional mailing offices.

POSTMASTER: Send address changes to: QEX, 225 Main St, Newington, CT 06111-1494 Issue No 281

Offices

225 Main St, Newington, CT 06111-1494 USA
Telephone: 860-594-0200
Fax: 860-594-0259 (24 hour direct line)
e-mail: **qex@arrl.org**

Subscription rate for 6 issues:

In the US: ARRL Member $24, nonmember $36;

US by First Class Mail:
ARRL member $37, nonmember $49;

International and Canada by Airmail: ARRL member $31, nonmember $43;

Members are asked to include their membership control number or a label from their QST when applying.

In order to ensure prompt delivery, we ask that you periodically check the address information on your mailing label. If you find any inaccuracies, please contact the Circulation Department immediately. Thank you for your assistance.

About the Cover

Richard Harris, G3OTK, describes a method for measuring the equivalent circuit components, or motional parameters of quartz crystals for the design of crystal ladder filters. With his microprocessor controlled test set to measure motional inductance, capacitance and resistance, and then perform the calculations and display the data or output it to a computer and spreadsheet program, he can measure up to 150 crystals in an hour.

In This Issue

Features

Index of Advertisers

The American Radio Relay League

The American Radio Relay League, Inc, is a noncommercial association of radio amateurs, organized for the promotion of interest in Amateur Radio communication and experimentation, for the establishment of networks to provide communications in the event of disasters or other emergencies, for the advancement of the radio art and of the public welfare, for the representation of the radio amateur in legislative matters, and for the maintenance of fraternalism and a high standard of conduct.

ARRL is an incorporated association without capital stock chartered under the laws of the state of Connecticut, and is an exempt organization under Section 501(c)(3) of the Internal Revenue Code of 1986. Its affairs are governed by a Board of Directors, whose voting members are elected every three years by the general membership. The officers are elected or appointed by the Directors. The League is noncommercial, and no one who could gain financially from the shaping of its affairs is eligible for membership on its Board.

"Of, by, and for the radio amateur," ARRL numbers within its ranks the vast majority of active amateurs in the nation and has a proud history of achievement as the standard-bearer in amateur affairs.

A *bona fide* interest in Amateur Radio is the only essential qualification of membership; an Amateur Radio license is not a prerequisite, although full voting membership is granted only to licensed amateurs in the US.

Membership inquiries and general correspondence should be addressed to the administrative headquarters:

ARRL
225 Main Street
Newington, CT 06111 USA
Telephone: 860-594-0200
FAX: 860-594-0259 (24-hour direct line)

Officers

President: KAY C. CRAIGIE, N3KN
570 Brush Mountain Rd, Blacksburg, VA 24060

Chief Executive Officer: DAVID SUMNER, K1ZZ

The purpose of *QEX* is to:

1) provide a medium for the exchange of ideas and information among Amateur Radio experimenters,

2) document advanced technical work in the Amateur Radio field, and

3) support efforts to advance the state of the Amateur Radio art.

All correspondence concerning *QEX* should be addressed to the American Radio Relay League, 225 Main Street, Newington, CT 06111 USA. Envelopes containing manuscripts and letters for publication in *QEX* should be marked Editor, *QEX*.

Both theoretical and practical technical articles are welcomed. Manuscripts should be submitted in word-processor format, if possible. We can redraw any figures as long as their content is clear. Photos should be glossy, color or black-and-white prints of at least the size they are to appear in *QEX* or high-resolution digital images (300 dots per inch or higher at the printed size). Further information for authors can be found on the Web at **www.arrl.org/qex/** or by e-mail to **qex@arrl.org**.

Any opinions expressed in *QEX* are those of the authors, not necessarily those of the Editor or the League. While we strive to ensure all material is technically correct, authors are expected to defend their own assertions. Products mentioned are included for your information only; no endorsement is implied. Readers are cautioned to verify the availability of products before sending money to vendors.

Larry Wolfgang, WR1B

Empirical Outlook

This issue closes out another year. It seems like such a short time ago that we were working on the Jan/Feb issue of *QEX*! The end of one year and the beginning of the next always seems to draw reflections on where we have been as well as where we may be headed in the future.

From a personal perspective, 2013 started off with some medical challenges after knee replacement surgery. I'm happy to say that I've recovered from that trauma, and am now able to do some things that hadn't been possible for over 30 years. Gone is that nagging knee pain, and I am able to bend the new knee to be able to ride a bicycle. That may not seem like much, but for me it is huge!

Looking over the year's *QEX* articles, I am pleased with the range and the depth of coverage of some fascinating topics. We've had articles from (A)rduinos to (Z) Impedance Measurements and Matching – from Clark Sell's "Use Arduino Technology to Create a Clock/10 Minute Timer" to Ray Mack's "Using Time Domain Reflectometry for Transmission Line Impedance Measurement." There have been antennas – from "Multi-Element End Fire Arrays of K9AY Loops" by Richard Jaeger, "A 21 MHz Four Square Beam Antenna" by Garth Swanson, and Wayne Oppenlander's "Two Turn Magnetic-Loop Antenna for 30 Through 10 Meters" to "Some Ideas for Short 160 Meter Vertical Antennas" by Rudy Severns.

We have introduced what I believe to be new – at least to Amateur Radio – technology with "Motion Based Electrical Power Control" by James Lee and possibly extended our knowledge with articles such as "Fun With Voltage to Frequency Converters" by Sam Green and "Squeeze Every Last Drop Out of the AD8307 Log Amp" by Loftur Jónasson.

There have also been articles by well-known RF design engineers that have provided explanations and insight into various aspects of radio design, possibly even offering enhancements that could be used by equipment manufacturers. Cornell Drentea shared "Frequency Synthesis and Impacts on Receiver Performance – Reciprocal Mixing and Blocking Dynamic Range." Colin Horrabin also described the "HF7070 HF/LF Communications Receiver Prototype," a very high performance receiver that uses H mode mixers and a double-tank oscillator. While hams have been using H mode mixers for many years, they have not generally be incorporated into commercial designs.

Of course there were construction projects and other articles that I hope were of interest to many readers. In this issue you will find more articles of great interest. An antenna study by Al Christman, a quartz crystal article by Richard Harris, as well as a couple of articles involving circuit and systems simulations. Enjoy!

So what is ahead for 2014? That depends largely on you, our readers. What interests you? What are you working on that you can share with readers? Do you have the next technological breakthrough on your workbench? Are you playing with some of the newest ICs and other electronics circuitry? We can only print the articles that you write, so sit down at your computer and begin typing!

We do have a number of articles in the works that you are sure to enjoy in the coming issues. We have more projects, more theoretical articles and of course, more antenna articles. There is plenty to look forward to!

As most of you know by now, ARRL is celebrating our Centennial Anniversary during 2014. There are many special events planned, and I hope you will be able to participate in many of them. I know that *QEX* readers are interested in the technical aspects of our hobby. I hope many of you will take much pleasure in attending the ARRL National Convention in Hartford, CT next July 17-19 as well as the many Section and regional conventions that are being planned. You will want to take part in some of the technical presentations at those conventions, and hopefully some of you will also be giving those presentations.

Amateur Radio is also about on the air operating, and there will be a variety of operating activities. One activity that I recently learned about is the ARRL Centennial QSO Party. This year-long operating adventure includes contacting ARRL Members and various Officers and Appointees. The idea is to accumulate points for contacts made. Full details will be in the January 2014 issue of *QST*. Contacts with your *QEX* Editor will be worth 30 points. So, I will have a personal challenge to spend a lot more time on the air, looking to contact as many readers and other stations on as many different bands, using as many different modes as I can manage. It looks like 2014 could be a banner year for Amateur Radio activity at WR1B. How about your station?

Richard J. Harris, G3OTK

10 South Street, South Petherton, Somerset TA13 5AD, United Kingdom; **r.j.harris.g3otk@gmail.com**

An Automated Method for Measuring Quartz Crystals

G3OTK proposes a method for automatically measuring all of the components of the equivalent circuit of quartz crystals using a Colpitts oscillator.

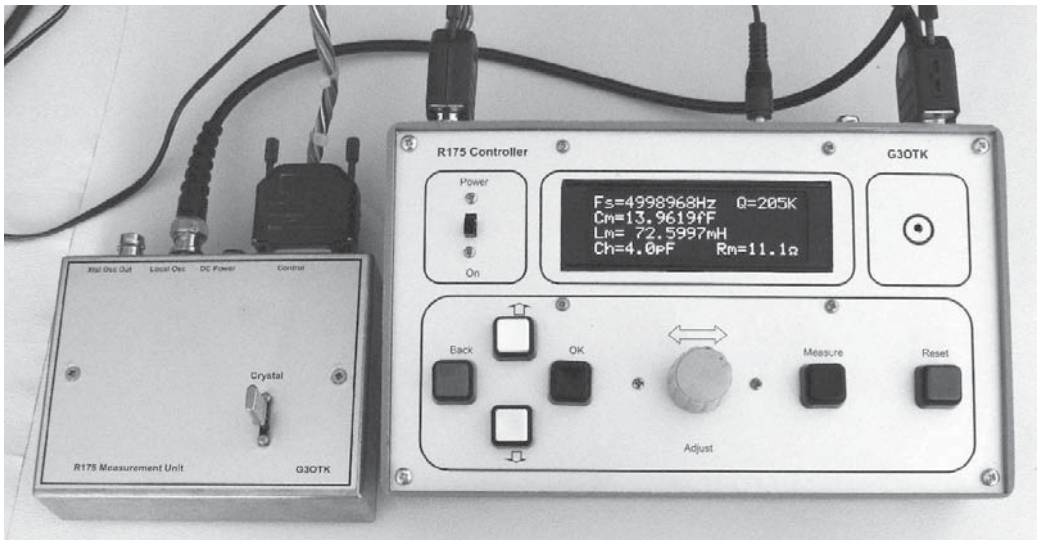

Ladder crystal filters have become popular in home-brew transceivers and QRP kits because of the availability of very low cost crystals. It seems to me that many projects use filters that have not been designed, but have been constructed on the "if it sounds right then it is right" principle. Although software for the design of ladder filters is available, a filter cannot be designed if the crystals have not been characterized and the equivalent circuit components, or motional parameters, determined with some accuracy.

Many methods for measuring the equivalent circuit of quartz crystals have been proposed over the years. These can be divided into two classes: those requiring a stable signal generator as an excitation source and those where the crystal is used in an oscillator. This latter class has the advantage that the principle item of test equipment is a frequency counter, which few serious experimenters will be without. Many years ago G3UUR proposed a simple method using a Colpitts oscillator, and many references can be found to it on the Internet.[1] As originally proposed, this method only gives a ball-park figure for the motional capacitance because it does not take into account the two capacitors of the Colpitts oscillator, nor the holder capacitance of the crystal. Also, it does not give any information about the motional resistance of the crystal or its series resonant frequency.

All of the methods for evaluating the motional parameters of quartz crystals that I have read about in Amateur Radio magazines require the measurements to be entered into formulae by hand to give the final parameter values. Making the measurements and undertaking the subsequent calculations for, say, 100 crystals is time consuming.

This article describes a further development of the oscillator technique that not only gives an accurate figure for the motional capacitance, motional inductance, holder capacitance and series resonant frequency but also gives a good estimate for the motional resistance. A microprocessor controls the measurements, makes the calculations, shows the results on an organic light emitting diode (OLED) display and also sends them to a computer running a spreadsheet program. Each crystal can be characterized in a few seconds and the results sorted into groups those with similar properties. The tabulated data will also give an insight into the spread of the motional parameters associated with inexpensive crystals. These are intended to be used in oscillators, and the information required for filter design is not part of the specification.

[1]Notes appear on page 8.

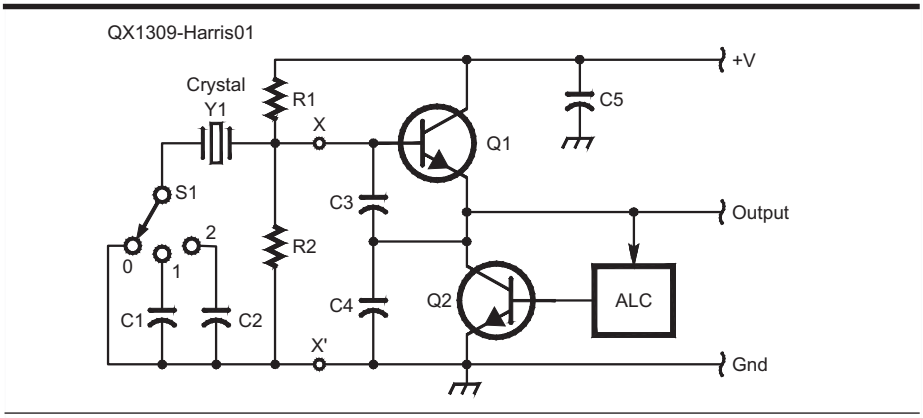

Figure 1 — This schematic is a basic crystal test circuit.

Outline of the Measurement Method

The outline is shown in Figure 1. The crystal under test, X1, is connected in series with a switch, SW1, which selects 0 V, C1 or C2. Q1, C3 and C4 form a Colpitts oscillator with the amplitude maintained at 1 mV by an Automatic Level Control (ALC) loop. At this low level, Q1 operates in a linear and predictable manner. For the amplitude to be constant, the motional resistance of the crystal must be balanced precisely by the negative resistance generated by the Colpitts Oscillator. This is proportional to the emitter current and gives a means of determining the motional resistance.

The loading effect of the bias resistors R1 and R2 is very small and can be ignored. At a frequency, f , the input impedance of the Colpitts oscillator at points X-X', as seen by the crystal, are given by Equation 1.

$$Z_{in} = B\left(\frac{-q\ I_e}{(2\pi f)^2\ C3\ C4\ K\ T}\right) - \frac{j}{2\pi f}\left(\frac{1}{C3}+\frac{1}{C4}\right) \qquad \text{[Eq 1]}$$

where:

K is Boltzmann's constant (1.3807 $\times 10^{-23}$ m^2 kg s^{-2} K^{-1})

T is the temperature in kelvins

q is the charge on an electron (1.6022 $\times 10^{-19}$ C)

I_e is the emitter current.

I have added the constant B to make a first order correction for the effects of the reduced current gain of Q1 at frequencies typical of the crystals used in CW and SSB filters. I will describe a method for determining it later. The 1 or 2 Ω emitter bulk resistance of the 2N3904 oscillator transistor can be ignored if C3 and C4 are chosen so that the emitter current is less than 0.5 mA. If the oscillator resistance, R_{osc}, is the real part of Z_{in}, then at a temperature of 21°C (70°F), it is given by Equation 2.

$$R_{osc} = -\left(\frac{B\ I_e}{f^2\ C3\ C4}\right) \qquad \text{[Eq 2]}$$

We will ignore the effect of the holder capacitance C_h because it is much smaller than the series combination of C3 and C4, and will be taken into account when the constant B is determined. The motional resistance, R_m, is equal to the magnitude of the oscillator resistance, R_{osc}, and so is proportional to the emitter current.

The imaginary part of Z_{in} is the series combination of C3 and C4. We will call this combination C_{osc}, which is given by Equation 3.

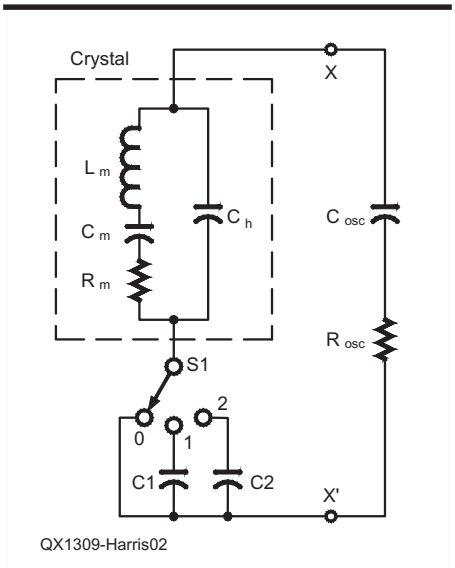

Figure.2 — Here is a diagram of an oscillator small signal equivalent circuit.

$$C_{osc} = \frac{C3\ C4}{C3+C4} \qquad \text{[Eq 3]}$$

The small signal equivalent circuit is shown in Figure 2. C_m, L_m and R_m are the motional parameters of the crystal. With the switch SW1 at position 0, the frequency of oscillation f_0 is given by Equation 4.

$$f_0 = \frac{1}{2\pi\sqrt{\frac{L_m\ C_m\left(C_h+C_{osc}\right)}{C_m+C_h+C_{osc}}}} \qquad \text{[Eq 4]}$$

With the switch in position n, where n is 1 or 2, the frequency f_n is given by Equation 5.

$$f_n = \frac{1}{2\pi\sqrt{\frac{L_m\ C_m\left(C_h+\frac{C_n\ C_{osc}}{\left(C_n+C_{osc}\right)}\right)}{C_m+C_h+\frac{C_n\ C_{osc}}{\left(C_n+C_{osc}\right)}}}} \qquad \text{[Eq 5]}$$

We can derive two equations for C_m by combining the equations for switch positions 1 and 0 (C_{m10}) and switch positions 2 and 0 (C_{m20}), eliminating L_m in the process.

$$C_{m10} = \frac{\left(\left(\frac{f_1}{f_0}\right)^2-1\right)}{\left(\frac{1}{\left(C_h+\frac{C1\ C_{osc}}{C1+C_{osc}}\right)}-\left(\frac{f_1}{f_0}\right)^2\frac{1}{C_h+C_{osc}}\right)} \qquad \text{[Eq 6]}$$

$$C_{m20} = \frac{\left(\left(\frac{f_2}{f_0}\right)^2-1\right)}{\left(\frac{1}{\left(C_h+\frac{C2\ C_{osc}}{C2+C_{osc}}\right)}-\left(\frac{f_2}{f_0}\right)^2\frac{1}{C_h+C_{osc}}\right)} \qquad \text{[Eq 7]}$$

The holder capacitance of the crystal will be the value of C_h that makes C_{m10} equal to C_{m20}, which will then be the motional capacitance C_m. I don't have an analytical solution for determining C_h, so I solve it numerically. For AT-cut crystals in standard or low profile HC49 packages, C_h will be within the range 1.5 to 6 pF. The microprocessor controller measures the three frequencies and then steps

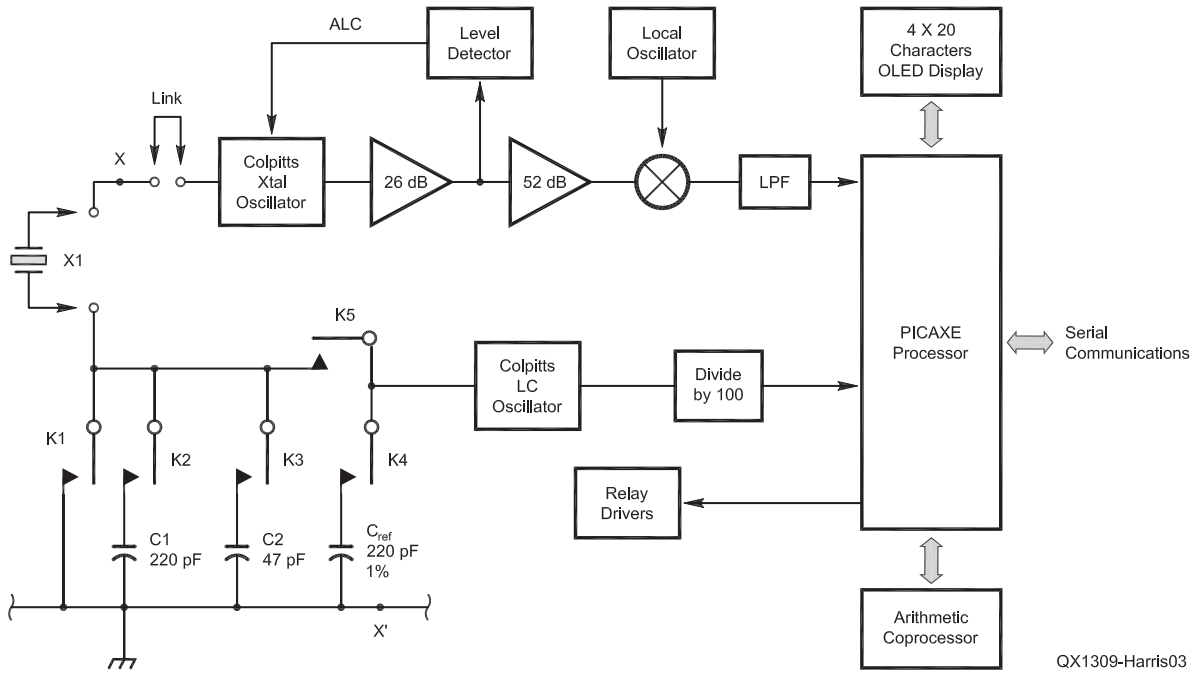

Figure 3 — The schematic/block diagram hybrid of the author's crystal measurement unit.

through the range of possible values for C_h in increments of 0.1 pF, calculating C_{m10} and C_{m20} at each step, until equality is found.

Once C_m and C_h have been determined, the series resonant frequency, f_s, of the crystal can be calculated from any of the three measurements of frequency. The simplest formula is when SW1 is in position 0.

$$f_s = f_0\left(1-\frac{C_m}{2\left(C_h+C_{osc}\right)}\right) \qquad \text{[Eq 8]}$$

The motional inductance L_m and Q can now be calculated by Equations 0 and 10.

$$L_m = \frac{1}{\left(2\pi f_s\right)^2 C_m} \qquad \text{[Eq 9]}$$

$$Q = \frac{2\pi f_s L_m}{R_m} \qquad \text{[Eq 10]}$$

We have now found all four of the component values and the Q of the equivalent circuit for the fundamental mode of operation.

A Practical Measuring Instrument

The block diagram of the measuring equipment is shown in Figure 3. Reed relays are used to switch capacitors in series with the crystal being measured. C1 (220 pF) and C2 (47 pF), both NP0 ceramic capacitors, could be measured before being fitted into the circuit, but relays K1, K2 and K3 add additional stray capacitance and the calculated motional and holder capacitances will be in error. My solution is to measure the capacitance in situ and this is the purpose of the Colpitts LC oscillator. Capacitance is measured relative to the reference capacitor C_{ref}. With the crystal oscillator turned off, and with K2 or K3 selected, three frequency measurements are made.

With relays K4 and K5 open, let the frequency be f_0. With K5 open and K4 closed let the frequency be f_{ref}. With K5 closed and K4 open let the frequency be f_x. K2 and K3 are open or closed as appropriate to the capacitor being measured. The unknown capacitance C_x can be calculated in terms of the ratio of the frequencies and the reference capacitor, C_{ref}.

$$C_x = C_{ref}\left(\frac{\left(\frac{f_0}{f_x}\right)^2-1}{\left(\frac{f_0}{f_{ref}}\right)^2-1}\right) \qquad \text{[Eq 11]}$$

This method is similar to that described by Carver.[2] I selected an NP0 ceramic capacitor for C_{ref}, which I measured to be 220.0 pF using an Almost All Digital Electronics (AADE) LC meter. The inductor and the Colpitts capacitors are chosen so that f_0 is about 7 MHz, midway between the frequencies of the crystals to be measured. The microprocessor that I use cannot measure frequencies above a couple of hundred kilohertz, and so the frequency is divided by 100 before being counted. I found that the stray capacitance associated with the relays was about 7 pF, a significant addition to C1 and C2.

When crystals are being assessed, the LC Colpitts oscillator is turned off and K5 opened. To bring the frequency within the counting range of the processor, the amplified output of the crystal oscillator is mixed with an external oscillator and converted down to an intermediate frequency of 1 to 3 kHz. A CMOS exclusive-OR gate is used as a digital mixer and an RC low pass filter cleans up the output for counting. The crystal oscillator frequency is calculated from that of the external oscillator and the intermediate frequency.

The processor is a PICAXE 40X2, a 40 pin PIC with an integral "PICAXE basic" interpreter, and which is very easy to program. It controls the measurement sequence and also communicates by means of I²C with a µM-FPU coprocessor that uses 32 bit float-

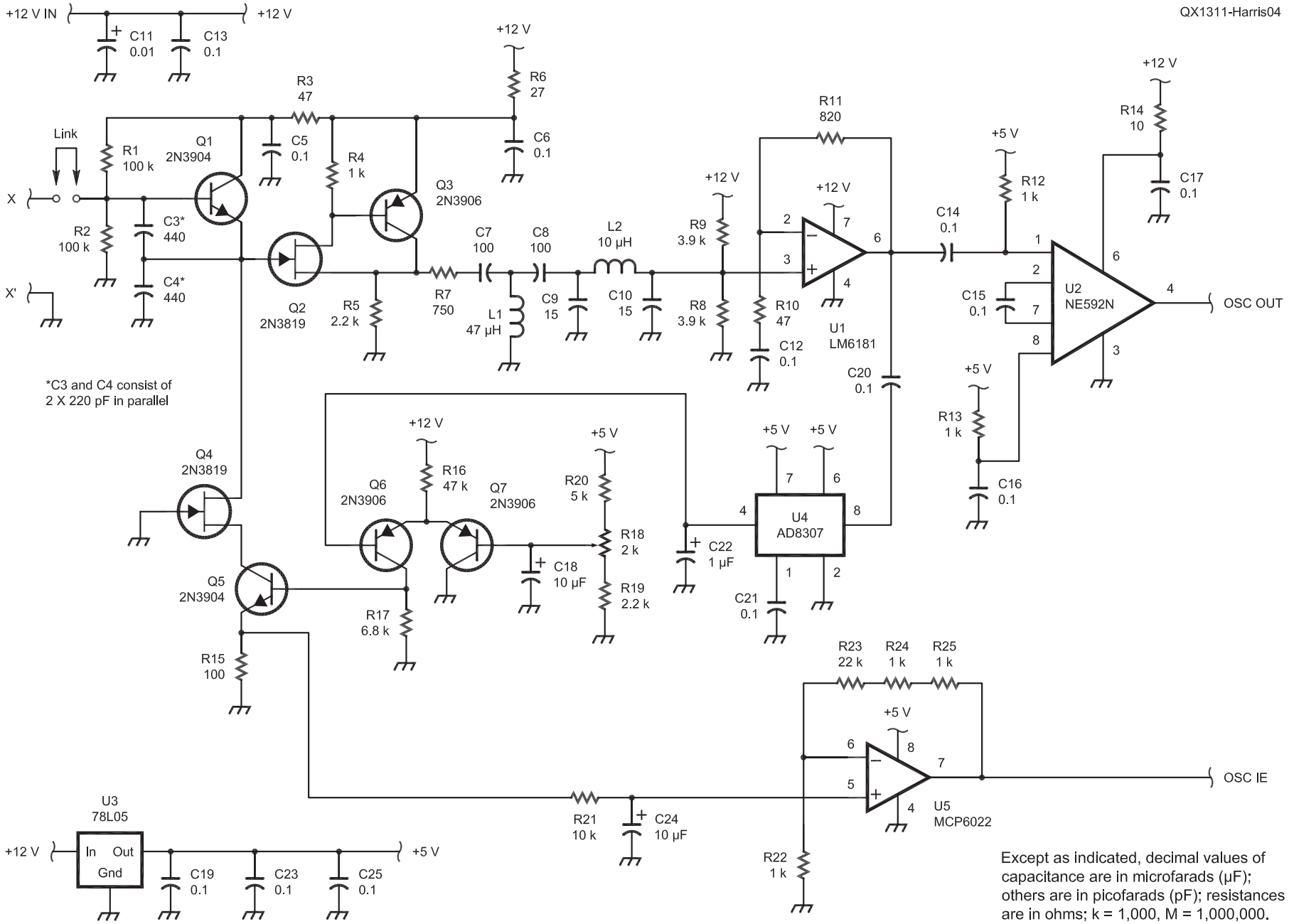

Figure 4 — This schematic shows the amplitude controlled Colpitts oscillator circuit used in the author's test system.

ing-point arithmetic. All of the calculations are made within the unit and the results are displayed on a 4 line by 20 character OLED display and are also sent to a computer running Microsoft *Excel*. Crystals can be measured at a rate of two or three a minute and the tabulated results sorted to group those with the similar values, such as motional inductance, series resonant frequency and motional resistance.

The level controlled crystal oscillator is at the heart of this unit and the schematic diagram is shown in Figure 4. The crystal and capacitor switching relays are connected to X-X'. Q1 with C3 and C4 form the Colpitts oscillator with the emitter current controlled by Q5. A unity gain buffer consisting of Q2 and Q3 drives a high pass filter, C7, L1 and C8, cascaded with a low pass filter,C9, L2 and C10, giving a pass band between 1 MHz and 20 MHz. U1 is a wideband current mode amplifier with a gain of approximately 20, which drives the ALC detector U4, an AD8307 logarithmic amplifier.

The long tailed pair Q6 and Q7compares the detected signal with a reference voltage set by R18 and the ALC loop is completed by means of Q5. A small voltage is developed across R15, amplified by U5, and then digitized and scaled by the processor to give the oscillator emitter current. Finally, U2 provides further amplification to drive the digital mixer.

The formula for the negative resistance of the oscillator has a constant, *B,* to correct for the deviation from the theoretical value of unity because the reduced current gain of Q1 at high frequencies lowers the input resistance of the transistor. We can make a reasonable estimate of *B* by first using the equipment to measure the motional resistance of a number of crystals and choosing the one with the lowest value. The link in series with the crystal is removed and several fixed resistors, for example 10, 15, 22 Ω, fitted in turn and measurements made again. The motional resistance now includes a known fixed resistor. The constant, *B,* is the best fit value that makes the increase in the measured resistances to be the same as the resistors used. For the 2N3904, I found that *B* was 1.20 for 5 MHz crystals and 1.35 for 10 MHz crystals.

The oscillator unit uses "Manhattan" style construction and is shown in Photo A. The crystal oscillator, capacitor switching relays and ALC circuit are on the left hand side. The lead photo on page 3 shows the assembled measurement unit and controller. The external oscillator, a homemade DDS signal generator, is not shown in the photograph. The calculated values of the motional capacitance and inductance are displayed to six significant digits, despite being only accurate

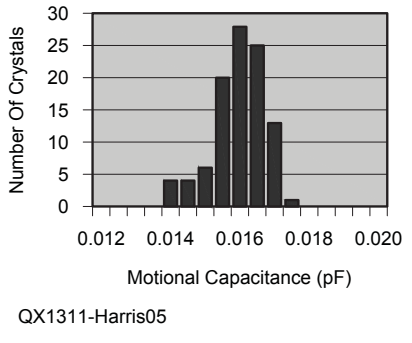

Figure 5 — This graph shows the spread of motional capacitance, C_m, for a batch of 100 crystals.

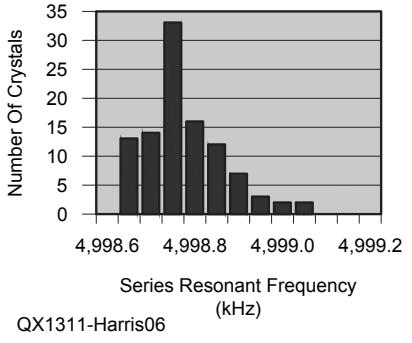

Figure. 6 — This graph shows the spread of series resonant frequencies, f_s, for the same 100 crystals.

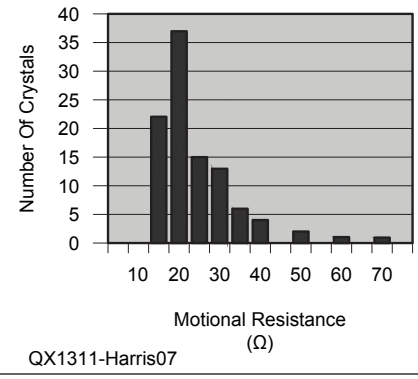

Figure. 7 — This graph shows the spread of motional resistance, R_m, for the batch of 100 crystals.

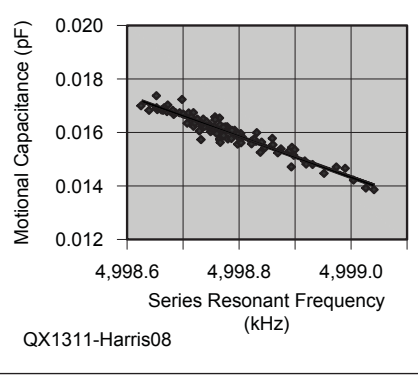

Figure. 8 — Here is a plot of the motional capacitance, C_m, versus series resonant frequency, f_s, for the batch of crystals.

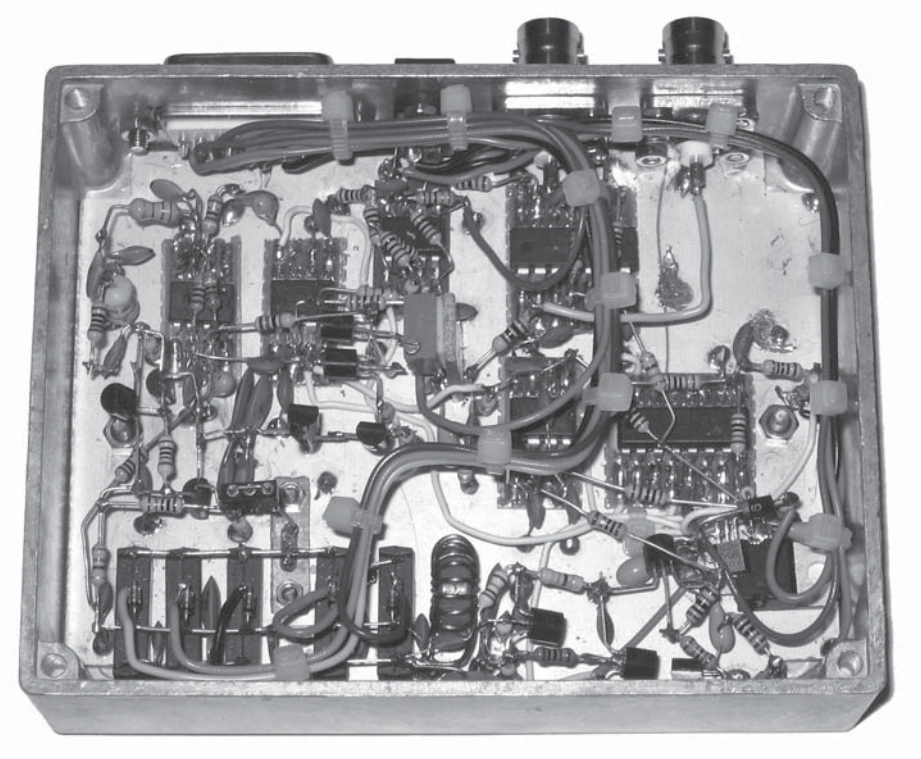

Photo A

to about 1%, because otherwise the center frequency of a filter design using values to, say, 3 significant figures could be in error by tens of kilohertz.

Some Results

I have measured several hundreds of crystals. I will describe the results of one batch consisting of 100 crystals purchased from a major UK component distributor. The nominal frequency was 5 MHz, with a load capacitance of 30 pF and a tolerance of 30 ppm. These were housed in HC49/U packages and cost less than 30 cents each.

Before we look at the spread of these motional parameters, it is worth considering what the selection priorities should be for crystals that are to be used in a filter. My personal view has been that the motional inductance is the first consideration, and the crystals should be selected to have as small a spread as possible. From this sub-set those with similar series resonant frequencies can be selected. Most crystals in a filter will be in series with capacitors to give the correct mesh frequencies and if necessary these capacitors can be adjusted to take into account small differences in the series resonant frequencies of the crystals. Finally, from this much smaller sub-set, those with similar, and small, motional resistances can be selected.

I numbered the crystals individually and measured the motional parameters of each one. The time taken to measure 100 crystals was about 40 minutes. The results were displayed in tabular form in an *Excel* spread sheet. The important motional parameters were sorted into various "bins," 0.5 *f* F wide for the motional capacitance, 50 Hz wide for the series resonant frequency and 5 Ω wide for the motional resistance. The distributions of these motional parameters are shown in Figures 5, 6 and 7. More than 25% of the crystals fell within one "bin" on each of the graphs but, unfortunately, there is no guarantee that the same crystals were in each of these bins.

Inexpensive crystals are manufactured for use in oscillators. Provided that the frequency with the specified parallel load capacitance is within the stated tolerance, then the motional capacitance and inductance can in principle take any value. The series resonant frequency is given by Equation 12.

$$f_s = f_p\left(1-\frac{C_m}{2\left(C_h+C_p\right)}\right) \qquad \text{[Eq 12]}$$

where f_p is the specified resonant frequency with the specified parallel load capacitance, C_p. So if C_m can take a range of values, then so can f_s. If motional capacitances are plotted against series resonant frequencies, however, then the result is a straight line with a slope given by Equation 13.

$$\frac{d\,f_s}{d\,C_m}=\frac{-f_p}{2\left(C_h+C_p\right)} \qquad \text{[Eq 13]}$$

where f_p is the nominal frequency with the load capacitance C_p. The slope is –73.5 Hz / *f* F for 5 MHz crystals with a specified load capacitance of 30 pF and holder capacitance of 4.0 pF. The motional capacitances and the series resonant frequencies of the crystals are shown in Figure 8, along with the least squares trend line, which has a slope of –76.1 Hz / *f* F, close to the calculated figure. The motional inductance has a similar relationship, although with a positive slope.

There is a fortunate consequence of this relationship. Crystals selected for a small spread of series resonance will also exhibit a small spread of both motional inductance and capacitance. Selecting crystals based solely on similar series resonant frequencies is a viable method. Furthermore, crystals from different manufacturers with the same nominal frequency, load and holder capacitances can be mixed and selected on this basis.

I constructed a 5 MHz pre-distorted linear phase filter designed from the tables of *k* and *q* values in Zverev using the average motional parameters of six crystals selected from this batch.[3] I added L-match circuits to the input and output of the filter to match to the 50 Ω terminations of the signal generator and detector. The plotted amplitude and phase responses overlaid those predicted by *SPICE* over a 60 dB amplitude range (the limit of the test equipment) and a phase range of 900°.

Accuracy

I have found that the measured motional capacitance and inductance of other crystals agreed with another method that I have described to within better than 1%.[4] Ultimately, all measurements are related to the accuracy of my LC meter, which is specified to be 1%.

As a check, I measured the series resonant frequencies of a sample of 30 crystals by connecting the output of a DDS signal generator to each crystal in turn through a series resistor and adjusting the frequency for minimum voltage across the crystal. I then re-measured the same crystals using the Colpitts oscillator method so that I could make a comparison at the same room temperature. The series resonant frequency using the direct measurement was on average 13 Hz higher than that found using the oscillator method. This discrepancy is probably due to the additional inductance of the wiring through the relays, which I estimate to be 60 nH.

I also calculated the motional resistances of the sample from the source voltage, the voltage across the crystals and series resistor value. The motional resistances agreed quite well with the oscillator method, being on average 6% higher. I have found that the motional resistance of some crystals, however, is not constant and varies with crystal current so that such comparisons are not entirely reliable.[5]

The holder capacitance was within 0.1 to 0.4 pF of that measured using an LC meter for 5 and 10 MHz crystals in both standard and low profile packages.

Conclusion

A Colpitts oscillator has been described that can be used as the basis of an instrument for measuring all of the motional parameters of quartz crystals. When controlled by a microprocessor, the results can be sent to a spreadsheet and displayed in tabular form to enable crystals with similar properties to be selected. With the present equipment, up to 150 crystals an hour can be measured.

Richard Harris was licensed as G3OTK in 1961. He received Bachelor and Master Degrees in Electrical Engineering from the University of Bath in the UK. He is a Member of the Institution of Engineering and Technology and a Chartered Engineer. Although he has spent much of his professional life undertaking electronic design, for the last ten years he has been responsible for Quality Assurance, Health and Safety and Environmental Management. He is a member of the Itchen Valley Amateur Radio Club.

Notes

[1]Wes Hayward, W7ZOI, Rick Campbell, KK7B and Bob Larkin, W7PUA, Experimental Methods in RF Design, published by the ARRL, 2009, ISBN: 978-087259-923-9; ARRL Publication Order No. 9239, $49.95. ARRL publications are available from your local ARRL dealer or from the ARRL Bookstore. Telephone toll free in the US: 888-277-5289, or call 860-594-0355, fax 860-594-0303; www.arrl.org/shop; pubsales@arrl.org.

[2]B. Carver, "The LC Tester," *Communications Quarterly,* Winter 1993, pp 19 – 27.

[3]A. I. Zverev, *Handbook of Filter Synthesis*, Wiley-Interscience.

[4]Richard J. Harris, G3OTK, "Crystal Bridge — A Balanced Bridge for Measuring Quartz Crystal Parameters", *Rad Com*, September 2011, pp 50 – 52.

[5]Richard J. Harris, G3OTK, "The Drive Level Sensitivity of Quartz Crystals," *QEX* Jan/Feb 2013 pp 14 – 21.

Al Christman, K3LC

Grove City College, 100 Campus Drive, Grove City, PA 16127-2104

Half Wavelength versus Quarter Wavelength Vertical Antennas

Is it worth the effort to build a ½ λ vertical antenna rather than a ¼ λ one? The author gives us some insight.

Vertical-monopole antennas are often used for working DX on the HF bands. They are relatively simple to construct, and their radiation pattern concentrates maximum signal strength at a low elevation angle. If the electrical height of the element is ¼ λ, then the resulting input impedance often provides a good match to 50 Ω coaxial cable. When the height of the radiator is increased to ½ λ, the peak gain will occur at an even lower take-off angle, but the feed point resistance tends to become very high.

This article was written to compare the performance of ¼ λ and ½ λ vertical antennas on several bands throughout the HF range. Three different ground systems were examined:

1) A single ground rod;
2) Sixty buried ¼ λ radials;
3) Sixty buried ½ λ radials.

Two detailed design examples are included in this article. I used a ½ λ tower vertical for 80 meters, and a ½ λ aluminum-tubing element for the 20 meter band.

Computer Simulations

In the first group of software models, lossless #12 AWG wire is used for the vertical monopole and the ground rod (if present), but the buried radials (where applicable) are lossless #18 AWG conductors. The element height was set to be either a physical ¼ λ or ½ λ, and no attempt was made to "tune" the system to resonance. The length of the buried radials (if used) was determined in a similar fashion. These radials were buried to a depth of 3 inches in "average" soil having a conductivity of 0.005 siemens per meter (S/m) and a dielectric constant of 13. All of the designs reviewed in this article were simulated with the *EZNEC* software package, which is available from Roy Lewallen, W7EL. [1]

Results on 80 Meters

Table 1 lists some of the key performance parameters for a ½ λ vertical, when the three ground systems described previously are employed. Compared to what can be obtained by simply feeding the monopole against an 8 foot ground rod driven into the soil at the base of the element, a conventional ground screen (consisting of sixty buried ¼ λ radials) improves the peak gain by only 0.39 dB. Doubling the length of these sixty radials from ¼ λ to ½ λ provides a further 0.27 dB of peak gain. In all cases, maximum gain occurs within a very narrow range of elevation angles between 17.1° and 17.7°.

EZNEC includes a convenient "average gain" feature, which can be used in several ways. The program calculates the power that is present in the far field of the antenna,

[1]Notes appear on page 15.

Table 1

Performance of a ½ λ vertical antenna system designed for operation on the 80 meter band at a frequency of 3650 kHz. The ground-based monopole has a height of 134.736 feet. Three different ground configurations are used. The first is simply an 8 foot ground rod, the second consists of sixty ¼ λ radials, and the last is made from sixty ½ λ radials, each with a burial depth of 3 inches. All conductors are lossless wires, either #12 or #18 AWG, and the soil is "average," with a conductivity of 0.005 siemens per meter (S/m) and a dielectric constant of 13.

	Ground Configuration		
Performance Parameter	*8 foot Ground Rod*	*Sixty ¼ λ Radials*	*Sixty ½ λ Radials*
Input Impedance (Ω)	2335 – *j* 1653	2247 – *j* 1729	2187 – *j* 1622
Peak Gain and Take-Off Angle (dBi and °)	+ 0.37@17.1°	+ 0.76@17.2°	+ 1.03@17.7°
Gain at 5° Take-Off Angle (dBi)	– 3.90	– 3.52	– 3.34
Gain at 10° Take-Off Angle (dBi)	– 0.65	– 0.27	– 0.07
Gain at 15°Take-Off Angle (dBi)	+ 0.29	+ 0.68	+ 0.92
Gain at 20°Take-Off Angle (dBi)	+ 0.25	+ 0.66	+ 0.96
Gain at 25°Take-Off Angle (dBi)	– 0.39	+ 0.03	+ 0.42
Gain at 30°Take-Off Angle (dBi)	– 1.50	– 1.04	– 0.55
Sky Wave Efficiency (%)	24. 8	27.5	30.1
Sky Wave Average Gain (dB)	– 6.05	– 5.61	– 5.22

and then divides this value by the input power delivered to the feed point. In an ideal scenario, when both the antenna and its surrounding environment have zero loss, the average gain will be exactly equal to 1, or 0 dB. Any losses in either the metallic structure of the antenna itself, or in the nearby soil, will reduce the average gain to a value that is less than unity (a negative number when expressed in dB). This information is presented in the Tables two different ways: first as "Sky Wave Efficiency" [%] and then as "Sky Wave Average Gain" [dB]. Since the "average gain" calculation is performed at a great distance from the source, it does not account for the ground-wave signal, or for that portion of the RF energy that was emitted by the antenna but absorbed by lossy earth. As a result, the Table values reported for these two parameters are quite low, although they can still be used for relative comparisons.

Table 2 shows what happens when the height of the monopole is reduced from ½ λ to ¼ λ. By comparing the peak gain values for the three different ground systems, it is easy to see that a good radial ground screen is critically important when using a ground-mounted ¼ λ vertical antenna. From the Table, we notice that the peak gain jumps by more than 5.3 dB (and the sky wave efficiency triples) when the 8 foot ground rod is replaced by a ground screen composed of sixty buried ¼ λ radials. A further 0.51 dB of peak gain can be obtained by doubling the length of these buried radials to ½ λ. In all three cases where a monopole height of ¼ λ is used, the take-off angle where peak gain occurs stays at either 24.7° or 25.8°.

If we compare these two tables with one another, we can see that, for *any* of the three different ground configurations, the taller radiator always generates more peak gain than does the shorter one. The ½ λ element, with only a ground rod at its base, produces almost as much peak gain as does the ¼ λ monopole with a ground screen comprised of sixty ¼ λ radials. Because of its greater height, the ½ λ antenna generates its maximum gain at an elevation angle that is nearly 8° lower than the corresponding ¼ λ version (17.3° versus 25.1° on average). Figure 1 is a plot of the elevation-plane radiation patterns for a ½ λ monopole driven against an 8 foot ground rod, versus a ¼ λ element with sixty ¼ λ radials in its ground screen.

Through an analysis of statistical information provided by Dean Straw, N6BV, in *The ARRL Antenna Book*, in Chapter 4 and on the included CD, I was able to calculate a weighted-average take-off/arrival angle for HF radio signals traveling between the Cleveland area and six different DX locations scattered across the globe. [2] (I chose Cleveland because it is the city included within the data-set that is closest to my QTH in western Pennsylvania.) A weighted-average "most-likely elevation angle" for every location and band was derived by multiplying each angle by the percentage of the time that specific angle was used, and then dividing the sum of these products by 100%. A review of the results, which are displayed in Table 3, indicates that a ½ λ vertical monopole, with its lower main lobe of radiation, would be superior for DX work on the 80 meter band, where the typical take-off/arrival angle is only 8°.

Table 2

Performance of a ¼ λ vertical antenna system designed for operation on the 80 meter band at a frequency of 3650 kHz. The ground–based monopole has a height of 67.368 feet. Three different ground configurations are used. The first is simply an 8 foot ground rod, the second consists of sixty ¼ λ radials, and the last is made from sixty ½ λ radials, each with a burial depth of 3 inches. All conductors are lossless wires, either #12 or #18 AWG, and the soil is "average," with a conductivity of 0.005 S/m and a dielectric constant of 13.

	Ground Configuration		
Performance Parameter	*8 foot Ground Rod*	*Sixty ¼ λ Radials*	*Sixty ½ λ Radials*
Input Impedance (Ω)	133.9 + *j* 11.83	40.36 + *j* 23.84	43.68 + *j* 25.92
Peak Gain and Take-Off Angle (dBi and °)	– 4.81@24.7°	+ 0.51@24. 7°	+ 1.02@25.8°
Gain at 5° Take-Off Angle (dBi)	– 10.41	– 5.10	– 4.72
Gain at 10° Take-Off Angle (dBi)	– 6.90	– 1.59	– 1.20
Gain at 15° Take-Off Angle (dBi)	– 5.53	– 0.21	+ 0.21
Gain at 20° Take-Off Angle (dBi)	– 4.95	+ 0.36	+ 0.82
Gain at 25° Take-Off Angle (dBi)	– 4.81	+ 0.51	+ 1.01
Gain at 30° Take-Off Angle (dBi)	– 4.96	+ 0.37	+ 0.93
Sky Wave Efficiency (%)	10.2	34.7	40.0
Sky Wave Average Gain (dB)	– 9.92	– 4.59	– 3.98

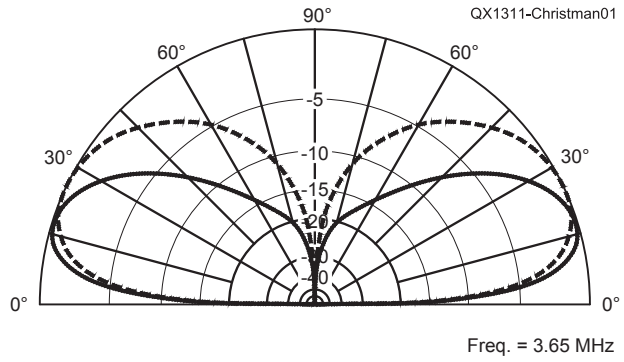

Figure 1 — Performance comparison on 80 meters between a ½ λ antenna element with an 8 foot ground rod (solid trace: peak gain = + 0.37 dBi at a 17.1° take-off angle) and a ¼ λ antenna element with sixty ¼ λ radials (dashed trace: peak gain = + 0.51 dBi at a 24.7° take-off angle).

Results on 40 Meters

The outcomes for a ½ λ vertical antenna when operating on the 40 meter band are given in Table 4. This time, adding a conventional ground screen (sixty ¼ λ buried radials) in lieu of a 6 foot ground rod increases the maximum gain by 0.46 dB, while an additional 0.32 dB can be picked up by extending the length of the radials from ¼ λ to ½ λ. For all three configurations, peak gain takes place at an elevation angle between roughly 18° and 19°.

The results for a ¼ λ antenna system appear in Table 5. On this band, installing a ground-screen of sixty buried ¼ λ radials yields an extra 5.11 dB of gain, as compared to what can be achieved with just a 6 foot ground rod. Doubling the length of the radials boosts the gain by another 0.73 dB. The take-off angle always stays within the range from about 26° to 28°.

Examining Tables 4 and 5 together, we can see that the ½ λ element easily provides more peak gain than the ¼ λ version, *except* when an extended ground screen (with ½ λ radials) is used. For that particular configuration,

the shorter antenna edges out the longer one by a scant 0.03 dB. Of course, the taller radiator always produces a main lobe that peaks at an elevation angle that is lower, with the difference amounting to slightly more than 8° (18.6° versus 26.8° on average). A quick glance at Table 3 reveals that the best take-off/arrival angle for 40 meter DX work is 6.2°, so the ½ λ antenna is (once again) preferred for this application. Figure 2 is a plot of the elevation-plane radiation patterns for a ½ λ monopole driven against a 6 foot ground rod, versus a ¼ λ element with 60 ¼ λ radials in its ground screen.

Results on 20 Meters

Table 6 lists the important performance parameters for a ½ λ 20 meter band radiator, if driven against the three ground systems described earlier. When compared to what can be obtained by just feeding the vertical against a 4 foot ground rod driven into the soil at the base of the monopole, the inclusion of a conventional ground screen (consisting of sixty buried ¼ λ radials) improves the peak gain by 0.46 dB. Doubling the length of these sixty radials from ¼ λ to ½ λ provides an extra 0.26 dB of peak gain. For all three configurations, the elevation angle for maximum gain occurs within a limited range between about 19° and 20°.

Next, Table 7 indicates what happens when the height of the monopole is cut in half, from ½ λto ¼ λ. Just as we found on 80 and 40 meters, it is vital to employ a good system of radials when using a ground-mounted vertical whose height is ¼ λ. On this band, we can see that the peak gain jumps by almost 4.5 dB when the 4 foot ground rod is replaced by a ground screen composed of sixty buried ¼ λ radials. A further 0.8 dB of peak gain can be obtained by doubling the length of these buried radials. The take-off angle where peak gain occurs varies somewhat, but hovers in the vicinity of roughly 27° to 29°.

Comparing Tables 6 and 7 with one another, we can see that, for *any* of the various ground configurations, the taller radiator generates more peak gain than does the shorter one. With only a ground rod at its base, the ½ λ element generates more peak gain than the ¼ λ monopole with a ground screen comprised of sixty ¼ λ radials. Due to its greater height, the ½ λ antenna generates its maximum gain at an elevation angle that is more than 8° lower than the corresponding ¼ λ version (19.4° versus 27.7° on average). Figure 3 is a plot of the elevation-plane radiation patterns for a ½ λ monopole driven against a 4 foot ground rod, versus a ¼ λ element with sixty ¼ λ radials in its ground screen. From a review of Table 3, we find that the most-likely take-off/arrival angle for DX signals on the 20 meter band is only 5.8°, so

Table 3

The most likely elevation angles for HF signals traveling between Cleveland and six different DX locations around the world, on four amateur bands from 80 through 10 meters. For each band and QTH, a weighted average is calculated by multiplying every angle by the percentage of the time that particular angle is used, and then dividing the sum of these products by 100%.

DX location	*80 meters*	*40 meters*	*20 meters*	*10 meters*
Southern Africa	5.9°	5.4°	5.5°	4.2°
South America	9.6°	9.0°	8.4°	7.3°
South Asia	—	2.7°	4.3°	3.8°
Europe	11.5°	9.5°	7.6°	7.0°
Japan	8.5°	5.9°	4.7°	4.1°
Oceania	4.4°	4.9°	4.5°	2.9°
Band Average	8.0°	6.2°	5.8°	4.9°

Table 4

Performance of a ½ λ vertical antenna system designed for operation on the 40 meter band at a frequency of 7150 kHz. The ground-based monopole has a height of 68.781 feet. Three different ground configurations are used. The first is simply a 6 foot ground rod, the second consists of sixty ¼ λ radials, and the last is made from sixty ½ λ radials, each with a burial depth of 3 inches. All conductors are lossless wires, either #12 or #18 AWG, and the soil is "average," with a conductivity of 0.005 S/m and a dielectric constant of 13.

	Ground Configuration		
Performance Parameter	*6 foot Ground Rod*	*Sixty ¼ λ Radials*	*Sixty ½ λ Radials*
Input Impedance (Ω)	2085 – j 1450	1988 – j 1535	1929 – j 1376
Peak Gain and Take-Off Angle (dBi and °)	+ 0.14@18.3°	+ 0.60@18.5°	+ 0.92@19.1°
Gain at 5° Take-Off Angle (dBi)	– 4.72	– 4.29	– 4.09
Gain at 10° Take-Off Angle (dBi)	– 1.19	– 0.75	– 0.53
Gain at 15° Take-Off Angle (dBi)	– 0.04	+ 0.42	+ 0.68
Gain at 20° Take-Off Angle (dBi)	+ 0.10	+ 0.58	+ 0.91
Gain at 25° Take-Off Angle (dBi)	– 0.39	+ 0.12	+ 0.54
Gain at 30° Take-Off Angle (dBi)	– 1.34	– 0.78	– 0.25
Sky Wave Efficiency (%)	24.4	27.6	30.5
Sky Wave Average Gain (dB)	– 6.13	– 5.59	– 5.16

Table 5

Performance of a ¼ λ vertical antenna system designed for operation on the 40 meter band at a frequency of 7150 kHz. The ground based monopole has a height of 34.3905 feet. Three different ground configurations are used. The first is simply a 6 foot ground rod, the second consists of sixty ¼ λ radials, and the last is made from sixty ½ λ radials, each with a burial depth of 3 inches. All conductors are lossless wires, either #12 or #18 AWG, and the soil is "average," with a conductivity of 0.005 S/m and a dielectric constant of 13.

	Ground Configuration		
Performance Parameter	*6 foot Ground Rod*	*Sixty ¼ λ Radials*	*Sixty ½ λ Radials*
Input Impedance (Ω)	119.7 + *j* 1.59	39.26 + *j* 25.01	45.0 + *j* 27.08
Peak Gain and Take-Off Angle (dBi and °)	– 4.89@26.1°	+ 0.22@26.3°	+ 0.95@27.9°
Gain at 5° Take-Off Angle (dBi)	– 11.17	– 6.08	– 5.58
Gain at 10° Take-Off Angle (dBi)	– 7.40	– 2.31	– 1.78
Gain at 15° Take-Off Angle (dBi)	– 5.84	– 0.74	– 0.18
Gain at 20° Take-Off Angle (dBi)	– 5.14	– 0.03	+ 0.59
Gain at 25° Take-Off Angle (dBi)	– 4.90	+ 0.21	+ 0.90
Gain at 30° Take-Off Angle (dBi)	– 4.97	+ 0.15	+ 0.93
Sky Wave Efficiency (%)	10.0	32.4	39.5
Sky Wave Average Gain (dB)	– 10.01	– 4.89	– 4.04

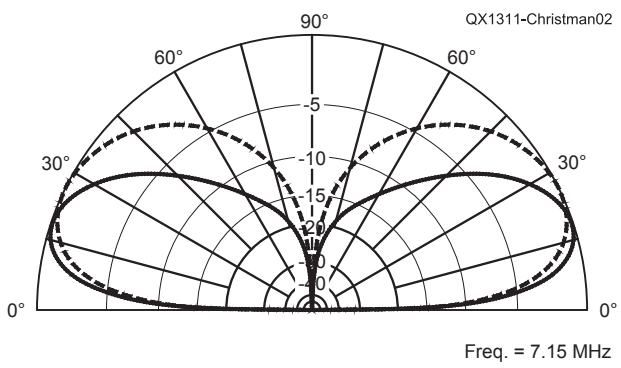

Figure 2 — Performance comparison on 40 meters between a ½ λ antenna element with a 6 foot ground rod (solid trace: peak gain = + 0.14 dBi at an 18.3° take-off angle) and a ¼ λ antenna element with sixty ¼ λ radials (dashed trace: peak gain = + 0.22 dBi at a 26.3° take-off angle).

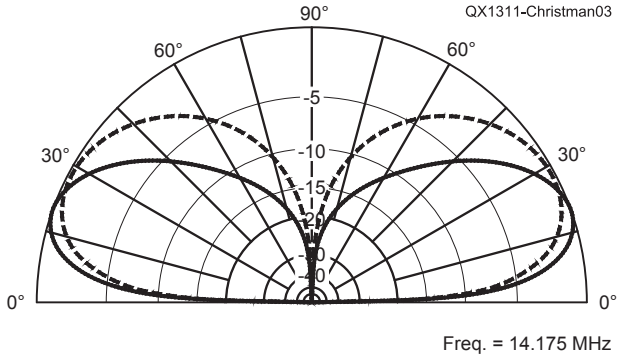

Figure 3 — Performance comparison on 20 meters between a ½ λ antenna element with a 4 foot ground rod (solid trace: peak gain = + 0.45 dBi at a 19.0° take-off angle) and a ¼ λ antenna element with sixty ¼ λ radials (dashed trace: peak gain = + 0.33 dBi at a 27.1° take-off angle).

(as usual) a vertical antenna with a height of ½ λ would be advantageous for working DX on this band.

Results on 10 Meters

The findings for a ½ λ vertical antenna when operating on the 10 meter band are supplied in Table 8. Now, installing a conventional ground screen (sixty ¼ λ buried radials) in place of the 4 foot ground rod raises the maximum gain by 0.61 dB, while another 0.18 dB of gain can be gleaned by extending the length of the radials from ¼ λ to ½ λ. In all three scenarios, peak gain takes place at an elevation angle between roughly 19° and 20° above the horizon.

The outcomes for a ¼ λ monopole appear in Table 9. Surprisingly, adding a ground screen of sixty buried ¼ λ radials generates nearly 8 dB of extra gain, as compared to what can be achieved when using only a 4 foot ground rod. Doubling the length of the radials increases the gain by a further 0.79 dB. The take-off angle where peak gain occurs lies within the range between 27° and 30°.

Examining Tables 8 and 9 together, we can see that the ½ λ element *always* outperforms the ¼ λ version, in terms of the maximum gain it provides. This extra gain is produced at a lower elevation angle, with the difference amounting to nearly 8.5° (19.7° versus 28.1° on average). A review of Table 3 indicates that the most likely take-off/arrival angle for working DX on this band is just 4.9°, so the ½ λ antenna is (yet again) the better performer. Figure 4 is a plot of the elevation-plane radiation patterns for a ½ λ monopole driven against a 4 foot ground rod, versus a ¼ λ element with sixty ¼ λ radials in its ground screen.

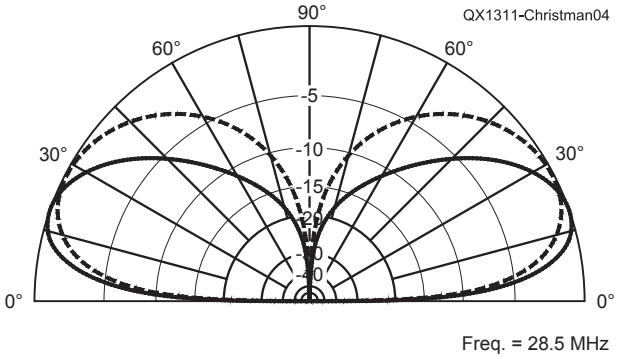

Figure 4 — Performance Comparison on 10 meters between a ½ λ antenna element with a 4 foot ground rod (solid trace: peak gain = + 0.60 dBi at a 19.4° take-off angle) and a ¼ λ antenna element with sixty ¼ λ radials (dashed trace: peak gain = + 0.50 dBi at a 27.4° take-off angle).

Table 6

Performance of a ½ λ vertical antenna system designed for operation on the 20 meter band at a frequency of 14.175 MHz. The ground based monopole has a height of 34.694 feet. Three different ground configurations are used. The first is simply a 4 foot ground rod, the second consists of sixty ¼ λ radials, and the last is made from sixty ½ λ radials, each with a burial depth of 3 inches. All conductors are lossless wires, either #12 or #18 AWG, and the soil is "average," with a conductivity of 0.005 S/m and a dielectric constant of 13.

	Ground Configuration		
Performance Parameter	*4 foot Ground Rod*	*Sixty ¼ λ Radials*	*Sixty ½ λ Radials*
Input Impedance (Ω)	1886 – *j* 1221	1795 – *j* 1309	1747 – *j* 1113
Peak Gain and Take-Off Angle (dBi and °)	+ 0.45@19.0°	+ 0.91@19.3°	+ 1.17@19.9°
Gain at 5° Take-Off Angle (dBi)	– 4.71	– 4.30	– 4.16
Gain at 10° Take-Off Angle (dBi)	– 1.05	– 0.64	– 0.47
Gain at 15° Take-Off Angle (dBi)	+ 0.21	+ 0.64	+ 0.85
Gain at 20° Take-Off Angle (dBi)	+ 0.44	+ 0.90	+ 1.17
Gain at 25° Take-Off Angle (dBi)	+ 0.05	+ 0.55	+ 0.90
Gain at 30° Take-Off Angle (dBi)	– 0.80	–0.25	+ 0.20
Sky Wave Efficiency (%)	26.8	30.3	32.8
Sky Wave Average Gain (dB)	– 5.71	– 5.18	– 4.84

Detailed Examples

The first sample design is a ½ λ antenna system for operation on the 80 meter band, with the center frequency at 3650 kHz, where ½ λ = 134.736 feet (for simplicity, this value was rounded to 135 feet). In the computer model, the vertical element is constructed from triangular tower sections with a face width of 12 inches, and there is an 8 foot ground rod at the base. I assumed that the entire system is made from zinc, and the soil is "average" (conductivity = 0.005 S/m, dielectric constant = 13). The *EZNEC* model also incorporates a capacitance of 15 pF to simulate the effects of the base insulator. Table 10 includes the performance parameters for this antenna (note that the input impedance shown here takes the capacitance of the base insulator into account). An impedance matching network was included, consisting of a series inductance of 17.647 µH to cancel the antenna's capacitive input reactance at 3650 kHz, along with an "un-un" transformer to reduce the input resistance of 290 Ω down to 50 Ω. When these two components are added to the computer model, a frequency sweep yields the SWR plot given in Figure 5. From 3500 to 3800 kHz, the worst-case SWR is just 1.51:1, so the network provides a good impedance match across both the DX phone and DX CW sub-bands.

The second sample is a ½ λ antenna designed to operate on the 20 meter band, with a center frequency of 14.175 MHz, where ½ λ = 34.694 feet (this value was rounded to 35 feet). In the computer model, the vertical element is assembled from tapered sections of metal tubing, with diameters ranging from 2 inches at the bottom to 0.5 inches at the upper tip of the monopole. The length of the ground rod is 4 feet, and the complete antenna is constructed from aluminum. As above, the soil is assumed to be "average," with a conductivity of 0.005 S/m and a dielectric constant of 13. This

Table 7

Performance of a ¼ λ vertical antenna system designed for operation on the 20 meter band at a frequency of 14.175 MHz. The ground based monopole has a height of 17.347 feet. Three different ground configurations are used. The first is simply a 4 foot ground rod, the second consists of sixty ¼ λ radials, and the last is made from sixty ½ λ radials, each with a burial depth of 3 inches. All conductors are lossless wires, either #12 or #18 AWG, and the soil is "average," with a conductivity of 0.005 S/m and a dielectric constant of 13.

	Ground Configuration		
Performance Parameter	*4 foot Ground Rod*	*Sixty ¼ λ Radials*	*Sixty ½ λ Radials*
Input Impedance (Ω)	95.04 + *j* 8.74	38.56 + *j* 27.72	46.59 + *j* 28.59
Peak Gain and Take-Off Angle (dBi and °)	– 4.04@26. 8°	+ 0.33@27. 1°	+ 1. 13@29. 3°
Gain at 5° Take-Off Angle (dBi)	– 10.65	– 6.31	– 5.81
Gain at 10° Take-Off Angle (dBi)	– 6.76	– 2.42	– 1.88
Gain at 15° Take-Off Angle (dBi)	– 5.12	– 0.77	– 0.19
Gain at 20° Take-Off Angle (dBi)	– 4.35	+ 0.01	+ 0.66
Gain at 25° Take-Off Angle (dBi)	– 4.06	+ 0.31	+ 1.04
Gain at 30° Take-Off Angle (dBi)	– 4.10	+ 0.29	+ 1.13
Sky Wave Efficiency (%)	12.1	33.3	41.4
Sky Wave Average Gain (dB)	– 9.17	– 4.78	– 3.83

Table 8

Performance of a ½ λ vertical antenna system designed for operation on the 10 meter band at a frequency of 28.5 MHz. The ground based monopole has a height of 17.256 feet. Three different ground configurations are used. The first is simply a 4 foot ground rod, the second consists of sixty ¼ λ radials, and the last is made from sixty ½ λ radials, each with a burial depth of 3 inches. All conductors are lossless wires, either #12 or #18 AWG, and the soil is "average," with a conductivity of 0.005 S/m and a dielectric constant of 13.

	Ground Configuration		
Performance Parameter	*4 foot Ground Rod*	*Sixty ¼ λ Radials*	*Sixty ½ λ Radials*
Input Impedance (Ω)	1828 – j 913.5	1668 – j 1049	1621 – j 832.5
Peak Gain and Take-Off Angle (dBi and °)	+ 0.60@19.4°	+ 1.21@19. 6°	+ 1.39@20.1°
Gain at 5° Take-Off Angle (dBi)	– 4.68	– 4.12	– 4.04
Gain at 10° Take-Off Angle (dBi)	– 0.98	– 0.41	– 0.31
Gain at 15° Take-Off Angle (dBi)	+ 0.32	+ 0.91	+ 1.04
Gain at 20° Take-Off Angle (dBi)	+ 0.60	+ 1.21	+ 1.39
Gain at 25° Take-Off Angle (dBi)	+ 0.24	+ 0.89	+ 1.14
Gain at 30° Take-Off Angle (dBi)	– 0.56	+ 0.14	+ 0.46
Sky Wave Efficiency (%)	28.0	32.8	34.5
Sky Wave Average Gain (dB)	– 5.52	– 4.84	– 4.62

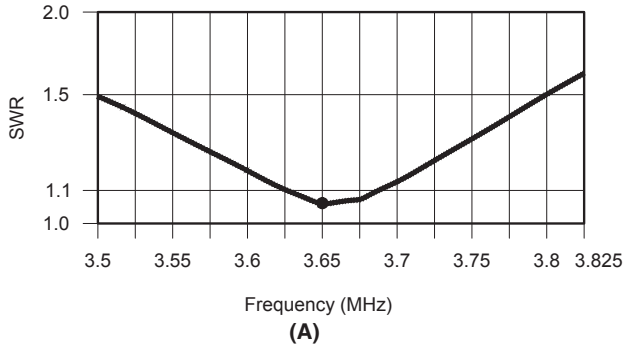

(A)

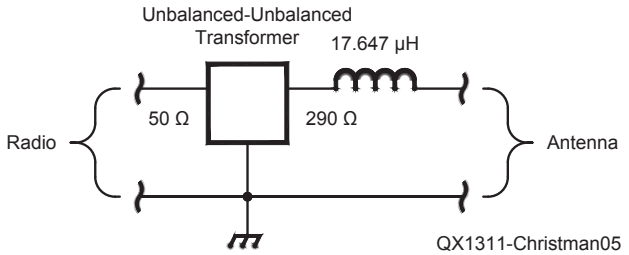

(B)

Figure 5 — Part A is the SWR Plot for the ½ λ 80 meter antenna made from zinc tower sections, when the matching network shown in Part B is used ($Z_{Reference}$ = 50 Ω).

Table 9

Performance of a ¼ λ vertical antenna system designed for operation on the 10 meter band at a frequency of 28.5 MHz. The ground based monopole has a height of 8.628 feet. Three different ground configurations are used. The first is simply a 4 foot ground rod, the second consists of sixty ¼ λ radials, and the last is made from sixty ½ λ radials, each with a burial depth of 3 inches. All conductors are lossless wires, either #12 or #18 AWG, and the soil is "average," with a conductivity of 0.005 S/m and a dielectric constant of 13.

	Ground Configuration		
Performance Parameter	*4 foot Ground Rod*	*Sixty ¼ λ Radials*	*Sixty ½ λ Radials*
Input Impedance (Ω)	204.5 + *j* 129.9	39.38 + *j* 33.31	49.06 + *j* 32.25
Peak Gain and Take-Off Angle (dBi and °)	– 7.43@27.0°	+ 0.50@27.4°	+ 1.29@29.9°
Gain at 5° Take-Off Angle (dBi)	– 14.13	– 6.27	– 5.80
Gain at 10° Take-Off Angle (dBi)	– 10.21	– 2.34	– 1.84
Gain at 15° Take-Off Angle (dBi)	– 8.54	– 0.66	– 0.11
Gain at 20° Take-Off Angle (dBi)	– 7.76	+ 0.14	+ 0.77
Gain at 25° Take-Off Angle (dBi)	– 7.46	+ 0.46	+ 1.18
Gain at 30° Take-Off Angle (dBi)	– 7.48	+ 0.46	+ 1.29
Sky Wave Efficiency (%)	5.5	34.6	43.0
Sky Wave Average Gain (dB)	– 12.57	– 4.60	– 3.66

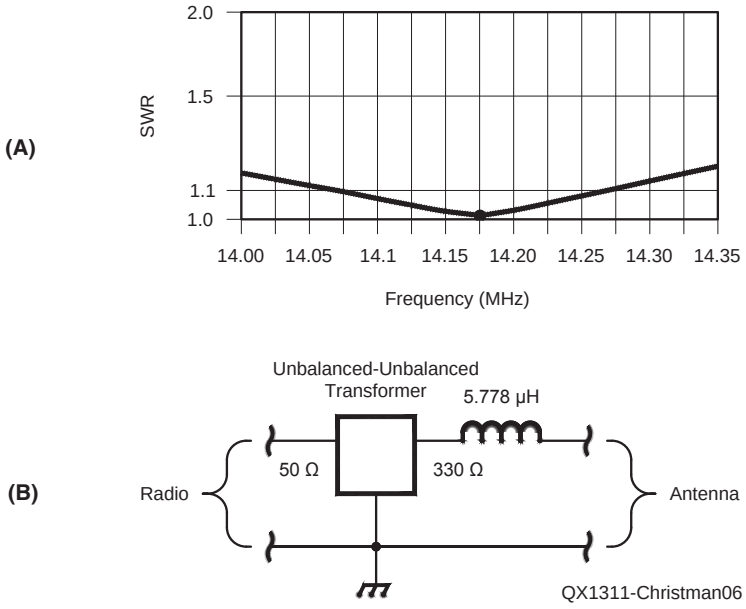

Figure 6 — Part A is the SWR Plot for the ½ λ 20 meter antenna made from aluminum tubing, when the matching network shown in Part B is used ($Z_{Reference}$ = 50 Ω).

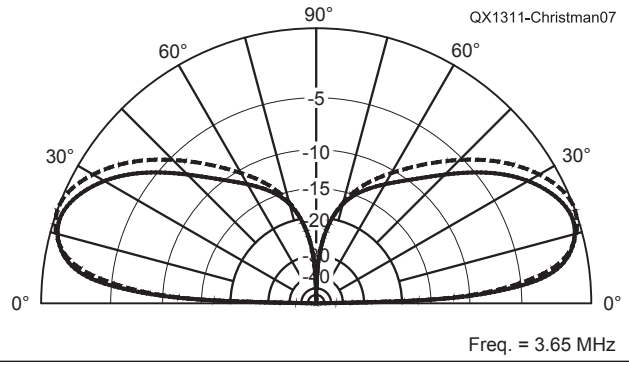

Figure 7 — Elevation–plane radiation patterns for the two detailed examples described in the text. The solid trace is the 135 foot element made of zinc tower sections, with an 8 ft ground rod. The operating frequency is 3650 kHz, and the peak gain is 0.34 dBi at a 17° take-off angle. The dashed trace is the 35 foot element made of aluminum tubing, with a 4 foot ground rod. The operating frequency is 14.175 MHz and the peak gain is 0.62 dBi at a 19.1° take-off angle.

EZNEC model also includes a base-insulator capacitance of 5 pF. Performance data for the antenna is listed in Table 10, alongside the information for the 80 meter example. In this case, impedance matching is accomplished with a network that includes an inductance of 5.778 µH in series with the feed point, plus an "un-un" transformer with a 330 Ω to 50 Ω ratio. Figure 6 displays a plot of the SWR, which remains below 1.2:1 across the entire band.

Figure 7 is a plot of the elevation-plane radiation patterns for these two ½ λ antennas. With the addition of suitable ground-screens, the 80 meter element could easily function as a ¼ λ antenna on 160 meters, while the 20 meter monopole would also serve well as a low-angle radiator on both 40 and 30 meters.

Effects of Ground-Rod Length

The various ½ λ vertical elements described in this article rely solely upon a ground rod to provide their connection to earth, and one might expect that the length of this rod would have a definite impact upon the performance of the overall system. Table 11 lists the peak gain for the pair of sample antennas described above, as the length of the accompanying ground rod is varied in two-foot increments. Interestingly, we can see that the gain of the 80 meter antenna reaches a maximum when its ground rod length is roughly 14 feet, and the improvement over what was obtained with a 2 foot rod is considerable (more than a full decibel). The performance of the 20 meter system is optimized when the ground rod is about 4 feet long.

To investigate further, I decided to calculate the wavelength of the RF signal as it travels through the soil beneath the two antennas. This parameter is dependent upon the frequency of operation, along with the conductivity and dielectric constant of the soil. The corresponding wavelengths are found to be 59.64 feet at 3650 kHz, and 18.73 feet at 14.175 MHz. (Notice that the wavelengths in the ground are much shorter than the values in free space.) Comparing these results with the data shown in Table 11, we can see that for maximum gain, the length of the ground rod should be slightly less than ¼ of the wavelength of the RF signal as it travels through the soil.

I decided to explore this idea in more detail, so I ran the *EZNEC* models for the 80 meter and 20 meter antennas several more times. Here, I reduced the incremental change in the length of the ground rods to see if I could get more accurate results. Best performance for the 80 meter system occurred when the ground rod length was centered around a value of 14.22 feet while

the gain for the 20 meter antenna peaked when the length of the ground rod was in the vicinity of 4.15 feet. Of course, the overall gain of either system can be increased still further by installing a conventional radial ground screen beneath the vertical monopole.

Losses

The feed point impedance for all of the versions of the ¼ λ antenna that employ radials has a real part that lies between roughly 38 and 49 Ω, along with an inductive-reactance component. As a result, the inclusion of a series capacitor at the feed point can provide a good impedance match to 50 Ω coaxial cable for any of these installations. In contrast, each of the ½ λ systems has an input impedance that is quite high, and a matching network (such as those described previously) will definitely be needed to bring the input SWR down to a reasonable value. These networks will dissipate a certain amount of transmitter power, but this factor has been ignored in the analysis. When this power loss is properly taken into account, the effective gain of the various ½ λ antennas will be somewhat lower than the values given in the various tables.

Conclusions

This article has compared the performance of a variety of ground-mounted ½ λ and ¼ λ vertical antennas on several of the HF bands between 80 and 10 meters. Computer analysis reveals that, in most cases, a ½ λ radiator that is driven against a single ground rod will generate as much peak gain as a ¼ λ monopole with sixty ¼ λ radials. The optimum length for this ground rod appears to be slightly less than ¼ of the wavelength of the radio signal in the soil. Further, the "nose" of the main lobe of radiation from the taller antenna will be at an elevation angle that is about 8° lower than that of the shorter element, which is advantageous for working DX.

Table 10

Performance of two different ½ λ vertical antenna systems. The first is made from zinc tower sections and is designed for operation on the 80 meter band at a frequency of 3650 kHz. The second is constructed of aluminum tubing and designed for operation on the 20 meter band at 14.175 MHz.

Performance Parameter	*80 Meter Band Antenna*	*20 Meter Band Antenna*
Input Impedance (Ω)	287 – *j* 420	328 – *j* 516
Peak Gain and Take-Off Angle (dBi and °)	+ 0.34@17.0°	+ 0.62@19.1°
Gain at 5° Take-Off Angle (dBi)	– 3.89	– 4.54
Gain at 10° Take-Off Angle (dBi)	– 0.65	– 0.88
Gain at 15° Take-Off Angle (dBi)	+ 0.28	+ 0.38
Gain at 20° Take-Off Angle (dBi)	+ 0.22	+ 0.61
Gain at 25° Take-Off Angle (dBi)	– 0.44	+ 0.23
Gain at 30° Take-Off Angle (dBi)	– 1.55	– 0.59
Sky Wave Efficiency (%)	25.1	28.3
Sky Wave Average Gain (dB)	– 6.01	– 5.49

Table 11

Performance of a ½ λ vertical antenna system as a function of ground rod length. The 80 m antenna is composed of zinc tower sections and has a height of 135 feet, while the 20 m antenna is composed of tapered aluminum tubing, with an overall height of 35 feet. The soil is "average," with a conductivity of 0.005 S/m and a dielectric constant of 13. These are the two antennas described in detail in the text, and also in Table 10.

	Peak Gain and Take-Off Angle	
Ground Rod Length	*80 meters (f = 3.65 MHz)*	*20 meters (f = 14.175 MHz)*
2 feet	Gm = – 0.63 dBi at 17.0°	Gm = 0.56 dBi at 19.1°
4 feet	Gm = – 0.03 dBi at 17.0°	Gm = 0.62 dBi at 19.1°
6 feet	Gm = + 0.22 dBi at 17.0°	Gm = 0.57 dBi at 19.1°
8 feet	Gm = + 0.34 dBi at 17.0°	Gm = 0.36 dBi at 19.1°
10 feet	Gm = + 0.42 dBi at 17.0°	
12 feet	Gm = + 0.45 dBi at 17.0°	
14 feet	Gm = + 0.47 dBi at 17.0°	
16 feet	Gm = + 0.46 dBi at 17.0°	
18 feet	Gm = + 0.44 dBi at 17.0°	

Al Christman, K3LC, is a Professor of Electrical Engineering at Grove City College in western Pennsylvania. He obtained his PhD from Ohio University in 1990. Al has been licensed since 1974, and former calls include WA3WZD, WD8CBJ, and KB8I. He is an ARRL Life Member who enjoys DXing on 20 meter phone, where he still needs two countries to reach the top of the Honor Roll. When the weather is nice, Al may be found riding the back roads on his motorcycle.

Notes

[1] *EZNEC* antenna-simulation software is available from Roy Lewallen, W7EL, PO Box 6658, Beaverton, OR 97007.

[2] H. Ward Silver, NØAX, Ed., *The ARRL Antenna Book*, 22nd edition, 2011, ARRL, Newington, CT 06111. ISBN: 978-0-87259-694-8; ARRL Publication Order No. 6948, $49.95. ARRL publications are available from your local ARRL dealer or from the ARRL Bookstore. Telephone toll free in the US: 888-277-5289, or call 860-594-0355, fax 860-594-0303; **www. arrl. org/shop**; **pubsales@arrl. org**.

Ulrich L. Rohde, N1UL

990 Cape Marco Dr, PH2, Marco Island, FL 34145;
ulr@synergymwave.com, Synergy Microwave Corporation

Rucha Lakhe

201 McLean Blvd, Patterson, NJ 07410
rula_tronix@yahoo.com

Mathematical Stability Problems in Modern Nonlinear Simulation Programs

The authors provide some insight into the inner workings and background calculations for circuit simulation programs.

The use of nonlinear components such as bipolar transistors, GaAs FETs, and microwave diodes makes it necessary to predict large signal-handling performance. The traditional tools to do this were the *SPICE* approach and Volterra series expansion. The *SPICE* program is a program operating solely in the time domain. *SPICE* is an outstanding workhorse for dc analysis as a function of bias and temperature and transient analysis. Some drawbacks of *SPICE* are:

- The lack of an optimizer;
- The lack of distributed elements such as tee junctions, crosses, and others;
- The slow execution speed related to the time-domain approach.[1, 2, 3] The purpose of this paper is to show the limitations of past nonlinear *SPICE* programs and to show a solution which is mathematically sound.[4]

Another approach that has been tried is Volterra series expansion. This approach is a simulation where the actual computation time is somewhat independent of the values of the components used in a circuit. Once the number of harmonics goes up, however, Volterra series expansion also becomes very time consuming. The Volterra series can be regarded as a nonlinear generalization of the familiar convolution integral.

The Volterra series also has the limitation that the degree of nonlinearity must be mild, as the representation otherwise requires an intractably large number of details for adequate modeling. The recently developed harmonic balance method avoids many of the time consuming mathematical approaches mentioned previously. This method is a hybrid time- and frequency-domain approach, which allows all the advantages of a time-domain device model, combined with the strength of the steady-state frequency-domain technique, to be presented in the lumped and distributed circuit elements in which the device is embedded. The time-domain model can be completely general, thus bypassing complicated determination of coefficients by curve fitting over different bias levels.

How does the Modern Nonlinear Program Work?

For a fixed circuit topology (analysis case), the frequency domain is passed through only once; the admittance matrix of the linear subnetwork is computed and stored for subsequent use. In the time-domain path, the state-variable harmonics are first used to compute the corresponding time-domain waveforms. As mentioned earlier, these are fed to nonlinear device equipment to produce the time-domain device port voltages and currents. Voltage and current harmonics are then described by one- or two-dimensional fast Fourier transforms (FFTs) for the cases of single-tone and two-tone excitation, respectively. The voltage harmonics are used to generate "linear" current harmonics via the linear subnetwork admittance matrix. The two sets of current harmonics are finally compared to produce individual harmonic balance errors and a combined (global) harmonic balance error to be used in a convergence test.

In well-conditioned cases (such as FET circuits), a standard Newton-Raphson iteration may be used successfully as an update mechanism even though no starting-point information is available (for example, if zero initial values are assumed for all harmonics). In such cases the harmonic balance errors are used via a simple perturbation mechanism to generate a Jacobian matrix. The latter is then inverted and applied to the error vector to generate the updated harmonic vectors. The algorithm is fast and accurate.

For circuits containing strongly nonlinear devices, such as microwave diodes, a simple Newton iteration may sometimes fail to converge. The best stable *SPICE* type program is SpectreRF by Cadence Design Systems. Another *SPICE* type program that also overcomes this difficulty is Ansys *Designer 8* or higher, which incorporates a second iteration scheme based on a variable metric algorithm (quasi-Newton iteration), which is slower although considerably more robust than the regular Newton method. In reality the designer program is a harmonic balance based *SPICE* program. There is a free Student Edition of Designer 8 available for download from the Ansys website, for those who qualify. Go to **https//support.ansys.com/portal/site/AnsysCustomerPortal/student/template.REGISTER**. This includes the software user manual. In addition, you can purchase the user manual at **www.ansys.com/Support/Documentation**.

In ill-conditioned cases, the quasi-Newton iteration may be used to approach the required solution. After this has been done to a satisfactory extent, automatic switchover to Newton iteration takes place, so that the approach solution can quickly be refined

[1]Notes appear on page 26.

to any desired accuracy.

When circuit optimization is requested, the algorithm flowchart is modified. Harmonic balance errors are computed in the same way, but now the variable circuit parameters are also updated and the linear subnetwork admittance is computed at each iteration. An objective function is defined as a combination of harmonic balance error and a contribution arising from the electrical specifications. Such an objective is then minimized by the variable metric algorithm until a minimum close enough to zero is reached. Circuit parameters and state-variable harmonics are updated simultaneously, thus avoiding the nesting of nonlinear analysis and circuit optimization loops. Ansys *Designer 8* is a general tool using the harmonic balance method for microwave. The harmonic balance method is a generic mathematical approach and is used for the first time in commercial CAD software. Today the program of interest is Ansys *Designer 8*. These modern programs are written mathematically so well that stability problems in oscillators do not occur in amplifiers.

Harmonic Balance Analysis (HBA)

Harmonic balance analysis is performed using a spectrum of harmonically related frequencies, similar to what you would see by measuring signals on a spectrum analyzer. The fundamental frequencies are the frequencies whose integral combinations form the spectrum of harmonic frequency components used in the analysis. On a spectrum analyzer you may see a large number of signals, even if the input to your circuit is only one or two tones. The harmonic balance analysis must truncate the number of harmonically related signals so it can be analyzed on a computer.

Analysis parameters such as No. of Harmonics specify the truncation and the set of fundamental frequencies used in the analysis. The fundamental frequencies are typically not the lowest frequencies (except in the single-tone case) nor must they be the frequencies of the excitation sources. They simply define the base frequencies upon which the complete analysis spectrum is built.

A project for harmonic balance analysis must contain at least the following: A top-level circuit, at least one nonlinear active device, and a frequency specification (including the number of harmonics of interest). The five categories of harmonic balance analysis are:

- Single-tone analysis (single RF signal)
- Two-tone intermodulation analysis (two RF signals)
- Two-tone mixer analysis (one RF signal and one LO signal)
- Three-tone intermodulation analysis (three RF signals)
- Three-tone mixer analysis (two RF signals and one LO signal).

Formation of the Harmonic Balance Equations

Harmonic balance analysis involves the periodic steady-state response of a fixed circuit given a pre-determined set of fundamental tones.[5, 6] The analysis is limited to periodic responses because the basis set chosen to represent the physical signals in the circuit are sinusoids, which are periodic. The Fourier series is used to represent these signals. In the single-tone case, a signal is given by Equation 1.

$$x(t) = \sum_{k=-NH}^{NH} \left(X_k e^{jk\omega_0 t} \right) \qquad \text{[Eq 1]}$$

where:

$X_k = X_{-k}^*$

ω_0 is the fundamental frequency

NH is the number of harmonics chosen to represent the signal.

In harmonic balance, the circuit is usually divided into two subcircuits connected by wires forming multiports. One subcircuit contains the linear components of the circuit and the other contains the nonlinear device models, as shown in Figure 1. The linear subcircuit response is calculated in the frequency domain at each harmonic component ($k \times \omega 0$) and is represented by a multiport Y matrix. This is the function performed by linear analysis.

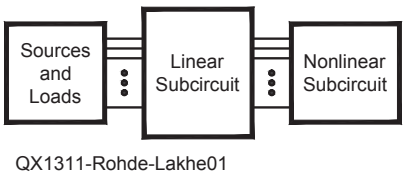

Figure 1 — General block diagram showing the two subcircuits in the harmonic balance program.

Separation of the Linear and Nonlinear Subcircuits

The nonlinear subcircuit contains the active devices whose models compute the voltages and currents at the intrinsic ports of the device (parasitic elements are linear and absorbed by the linear subnetwork). The port voltages (v) and currents (i) are analytic or numeric functions of the device state variables (x). Often the state variables represent physical voltages such as diode junction voltage or FET gate voltage, but are not restricted to physical quantities. The port voltages and currents are often functions of the time derivatives of the state variables (when a nonlinear capacitor is involved) and of time-delayed state variables (such as a time-delayed current source). Generally, the nonlinear device equations are of the form:

$$v(t) = \Phi\left[x(t), \frac{dx}{dt}, K, \frac{d^n x}{dt^n}, x(t-\iota) \right] \qquad \text{[Eq 2]}$$

$$i(t) = \Phi\left[x(t), \frac{dx}{dt}, K, \frac{d^n x}{dt^n}, x(t-\iota) \right] \qquad \text{[Eq 3]}$$

The device state variables, port voltages, and currents are transformed to the frequency domain using the discrete Fourier transforms as $\boldsymbol{X}$, $\boldsymbol{V_k(X)}$ and $\boldsymbol{I_k(X)}$, respectively. Kirchhoff's current law is applied to the interface between the subcircuits at each harmonic frequency:

$$Y_k V_k(X) + I_k(X) + J_k = 0 \qquad \text{[Eq 4]}$$

where $\boldsymbol{J_k}$ are the Norton equivalents of the applied generators. This constitutes the harmonic balance equations at each harmonic frequency. The object of the analysis is to find the set of state variables, $\boldsymbol{X}$, to satisfy Equation 4.

When the analysis begins, the state variables are typically set to zero and the left side of Equation 4 is non-zero. We can write an error vector:

$$E_k(X) = Y_k V_k(X) + I_k(X) + J_k \qquad \text{[Eq 5]}$$

whose Euclidean norm $\boldsymbol{E}^t \boldsymbol{E} = \|\boldsymbol{E}\|$ is called the Harmonic Balance Error (HBE). If the HBE is reduced below a tolerance, we say that Equation 4 is satisfied and a solution has been obtained.

Solving Methods

The process of solving the harmonic balance equations is an iterative one. An estimate of $\boldsymbol{X}$ is inserted into Equation 5, $\boldsymbol{E}$ is calculated and if it is not below the tolerance then a new value of $\boldsymbol{X}$ must be determined and tried. Each such loop is termed an iteration. There have been several methods used in the past to determine new

values of $\boldsymbol{X}$ and two that have proven to be the most general and efficient are discussed here.

The state variables, $\boldsymbol{X}$, and harmonic balance residuals, $\boldsymbol{E}$ are complex values. In practice these are decomposed into their real and imaginary parts so that the number of real unknowns in $\boldsymbol{X}$ is $\boldsymbol{ND} \times (2 \times \boldsymbol{Nt} + 1)$ where $\boldsymbol{ND}$ is the total number of nonlinear device ports and $\boldsymbol{Nt}$ is the number of frequency components (= $\boldsymbol{NH}$ for single tone analysis). Now we can write $\boldsymbol{E}(\boldsymbol{X}) = 0$ as a Taylor series expansion truncated after the first derivative term.

$$E\left(X\right) = 0 \approx E\left(X^{(n)}\right) + J\left(X^{(n)}\right)\left(X - X^{(n)}\right) \qquad \text{[Eq 6]}$$

where $\boldsymbol{J}$, the Jacobian matrix, is the first derivative matrix of $\boldsymbol{E}$ with respect to $\boldsymbol{X}$ and superscript n indicates the current iteration. Solving for $\boldsymbol{X}$ and using this for the next trial, we get Equation 7.

$$X^{(n+1)} = X^{(n)} - J^{-1}\left(X^{(n)}\right)E\left(X^{(n)}\right) \qquad \text{[Eq 7]}$$

This is the Newton-Raphson update method where the last right-hand term is the update. This method works in one iteration if the set of equations is linear, but will take an unknown number of iterations if nonlinear. Often the update is reduced by a factor called the Newton damping factor so the method takes smaller steps with each iteration. Convergence to a solution is not guaranteed and the iterations may diverge if not controlled. Some *SPICE* programs used enhanced versions of the Newton-Raphson method to improve convergence and speed.

The *SPICE* program can use an algorithm that dynamically changes the Newton damping factor during solving, based on the rate of convergence. If the solver has trouble converging, the factor will be made smaller to improve convergence. If it has been reduced by more than a predetermined factor, the solver will stop and an error will be reported.

An important aspect to note is the size of the Jacobian. If $\boldsymbol{X}$ contains $\boldsymbol{ND} \times (2 \times \boldsymbol{Nt} + 1)$ elements, then $\boldsymbol{J}$ contains this number squared. As a practical example, if $\boldsymbol{ND} = 10$ (5 FETs) and $\boldsymbol{Nt} = 4$, then there are 8100 entries in $\boldsymbol{J}$, which takes 63 kBytes. This is relatively small, but $\boldsymbol{Nt}$ becomes much larger when multi-tone excitation is considered.

Some of the controlling functions are made accessible through the CTRL block in the project (see the Control Blocks chapter of the User's Guide). The HBE tolerance can be changed from its default by: HBTOL *x* where *x* is the tolerance per device port per frequency component.

The absolute harmonic balance error allowed is scaled by the number of device ports and number of frequency components so that large circuits with many frequency components meet HBE criteria similar to those of small circuits. The default for HBTOL is 1.0×10^{-6}. For the case of two-tone intermodulation analysis and three-tone analysis, the allowed harmonic balance is also scaled by the relative currents of the circuit. This reduces the allowed error (effectively reducing HBTOL) to provide better accuracy of the intermodulation products.

The number of allowed iterations before the program stops can be changed from its default value of 400 by: **MAXITER** *n*, where *n* is an integer.

Multi-Tone Analysis

The discussion above was based on single-tone analysis for conceptual simplicity. Multi-tone analysis is simply an extension of single-tone analysis.[7, 8, 9] In the single-tone case, a circuit is excited with an RF source and harmonics of that source are produced by the nonlinearities of the circuit. The set of harmonics, the frequency of excitation and DC are called the *spectrum* of the analysis. The single-tone spectrum is defined as: $S_1 = k \times f_0$ where $k = 0, 1, \ldots \boldsymbol{NH}$, and f_0 is the fundamental frequency. In multi-tone analysis the spectrum is modified to include the harmonic products of each fundamental tone. The harmonic products are just integer functions of the fundamental frequencies and indicate the allowed "bins" for power conversion within a circuit. The rest of the harmonic balance analysis is exactly the same.

The conversion between time-domain waveforms and Fourier coefficients is accomplished by the discrete Fourier transform in single-tone analysis. For each additional fundamental tone, a dimension is added in the transform. This allows efficient computation between domains, but becomes CPU-intensive when more than three-dimensions are encountered.

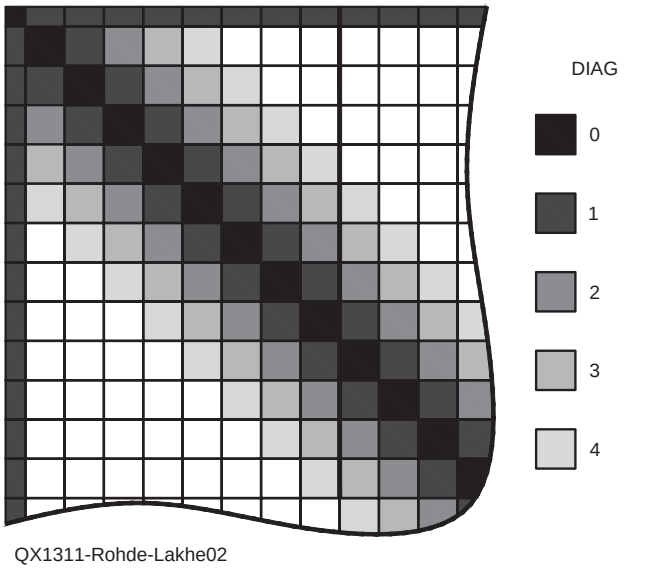

Figure 2 — Sparse Jacobian block structure.

Local Oscillator Spectrum Initialization of Mixer Circuits

For mixer analysis cases where the primary interest is the conversion gain and the RF signal powers are small compared to the LO, the circuit can be analyzed using the LO signal only and the conversion gain is determined using small-signal (linear) frequency-conversion methods. This is performed using the Small-Signal Mixer Analysis option.

For cases where the RF signal power is not insignificant compared to the LO, a full mixer spectrum must be used. Compression of the conversion gain due to high RF power can then be analyzed. Here, the mixer problem can be divided into two parts to help speed the analysis. First, the LO signal is analyzed using single-tone analysis; the RF signal is turned off. Single-tone analysis is usually very fast compared with a full two-tone analysis. Once the LO signal spectrum is found, the results are used to initialize the full mixer spectrum and the RF signal is turned back on. The full spectrum is then analyzed.

This method is most useful for three-tone mixer problems, due to the large number of spectral components used in the analysis. The primary use of the three-tone mixer analysis is to determine the intermodulation products of the IF products. This precludes the use of small-signal mixer analysis (since the intermodulation products cannot be determined using linear frequency conversion methods), but the RF signals are generally small compared to the LO. By solving the

LO problem first, which is the primary nonlinear problem, and then introducing the RF signals, the analysis time can be reduced by a factor of about three. The actual time reduction depends on the circuit, the RF power levels, and the conversion gain.

Using the LO harmonic spectrum to initialize the full mixer spectrum is the default for three-tone analysis. The option is not the default for two-tone analysis, because significant time improvements have not been observed.

Number of Spectral Components and Reduced Spectrum Option

The number of spectral components considered in each type of analysis is related to the number of fundamental tones and the nonlinearity specified. Tables 1, 2, and 3 list the number of spectral components for several nonlinearities considered in two-tone and three-tone analyses. The reduced spectrum option removes selected spectral components where significant harmonic power is not expected. The results of the analysis will not degrade at low power levels, but may yield different results for high power levels, depending on the circuit. Usually, the difference in results is negligible for practical cases.

The reduced spectrum option is especially useful for three-tone mixer analysis where the primary objective is to obtain the intermodulation intercept point with the IF. Low RF signal power levels are used and the analysis results are unaffected by the reduced

Table 1
Number of Spectral Components (excluding DC) for Two-Tone and Three-Tone Intermodulation Analysis

Nonlinearity INTM m	*Two-Tone Full (Default)*	*Two-Tone Reduced*	*Three-Tone Full (Default)*	*Three-Tone Reduced*
3	12	8	31	21
4	20	12	64	31
5	30	22	115	79
6	42	30	188	115
7	56	44		209
8	72	56		
9	90	74		
10	110	90		

Table 2
Number of Spectral Components (excluding DC) for Two-Tone Mixer Analysis

	#SB (M2) = 1		*#SB (M2) = 2*		*#SB (M2) = 3*	
#LO (M1)	*Full (Default)*	*Reduced*	*Full (Default)*	*Reduced*	*Full (Default)*	*Reduced*
2	7	7	12	12	17	17
4	13	13	22	18	31	23
6	19	19	32	24	45	29
10	31	31	52	36	73	41
15	46	46	77	51	108	56
20	61	61	102	66	143	71
25	76	76	127	81	178	86
30	91	91	152	96	213	101

Note: #LO is the number of local oscillator harmonics; #SB is the number of RF sidebands

Table 3
Number of Spectral Components (excluding DC) for Three-Tone Mixer Analysis

	INTM (M2) = 3		*INTM (M2) = 5*	
# LO (M1)	*Full*	*Reduced (Default)*	*Full*	*Reduced (Default)*
2	62	42	152	112
4	112	52	274	122
6	162	62		132
10	262	82		152
15		107		177
20		132		202
25		157		227
30		182		252

Notes: Entries that have been filled-in can be simulated
#LO is the number of local oscillator harmonics; INTM is the intermodulation order

spectrum option (the number of LO harmonics is not affected).

The total number of spectral components grows very quickly with the level of nonlinearity and number and fundamental tones.

• Two-tone or three-tone intermodulation spectrum: The highest order group of spectral components, except those in the fundamental group (the intermodulation products), are ignored. In this case, the *n* in REDUCED*n* is ignored.

• Two-tone mixer analysis: All sidebands except the first sideband above the n^{th} local oscillator harmonic will be ignored.

• Three-tone mixer analysis: All sideband groups at or below the n^{th} local oscillator harmonic will be the same as the reduced two-tone intermodulation spectrum; all the sidebands above the n^{th} local oscillator harmonic will contain the two fundamental frequencies only.

Understanding the reduced spectrum is a little complicated. If the analysis is run with several reduced spectrum values and the spectrums are compared, then a better understanding of the spectral selections will be attained. Many studies were conducted and showed that the (default) reduced spectrum option for three-tone mixer intermodulation analysis affected analysis accuracy only slightly.

Sparse Jacobian Techniques

The Jacobian matrix, when properly arranged, can be treated as a sparse matrix by pre-setting some entries to zero. (See Note 7.) The physical reason for doing this is that most of the power transfer takes place between the harmonic frequencies of the fundamentals and much less takes place between the other frequencies in the spectrum. We can therefore set these derivatives to zero within the Jacobian. When this criterion is not met, the band of non-zero entries is widened to include cross-harmonic terms.

Because the Jacobian structure is properly arranged, sparse matrix techniques are efficiently employed. General purpose sparse matrix solvers that analyze the sparsity structure are avoided and specialized solvers can be used that are much more efficient. The *SPICE* programs should (as for example in *Designer 8*) automatically set the bandwidth of the sparse tridiagonal matrix and dynamically alter it if the nonlinearity of the circuit is too great for the sparse assumptions. In this way the simulator achieves convergence using the minimal amount of computation time and memory that is possible for a given problem. For circuits with many devices under multi-tone operation, the CPU time may be decreased by a factor of 40.

A control parameter is made available to override the initial default sparsity parameter that controls the Jacobian bandwidth. The initial setting is 0 and can be changed by DIAG ***n*** where ***n*** will be the initial sparsity parameter. Typical values range between 0 and 6. The sparsity parameter will still be dynamically altered during execution if needed. If ***n*** is greater than ***Nt*** / 3 (***Nt*** is the number of frequencies), then the program will use the full Jacobian. If only the full Jacobian is desired, then set ***n*** to a large number.

Using a sparse Jacobian does not affect the final values or accuracy of the results. It will only affect the convergence properties of the particular problem.

Iterative Newton Method

One of the shortcomings of harmonic-balance methods is the large memory requirements when a circuit has many nonlinear devices and/or multi-tone analysis is needed. Modern versions of the *SPICE* program can handle more than 1 million transistors without a significant loss of accuracy. The Jacobian system matrix grows large and must be stored and factored. Sparse methods may not be enough to keep the problem within the memory bounds and acceptable computational resources of desktop computers. The *SPICE* program uses a technique that efficiently solves large systems of equations without direct factorization of the system matrix. In this way, there is no simplification or approximation made to the problem and the full accuracy of the conventional harmonic-balance method is completely maintained. The convergence and power-handling capabilities of conventional harmonic-balance analysis are also fully maintained. The method is completely automatic and does not require any user intervention. An internal software switch detects when the new method should be used and automatically invokes it.

A brief summary of the method and its advantages is given: Conventional harmonic-balance computes and stores the Jacobian matrix. The iterative solution of the harmonic-balance equations requires factorization of the Jacobian to obtain updates of the circuit voltages. As the number of nonlinear devices in the circuit increases and the number of spectral components used to analyze the circuit increases, the Jacobian matrix can become very large, requiring tens or hundreds of megabytes of storage and several minutes of CPU time to factor it. The calculation and factorization of the Jacobian typically occurs several times during a single harmonic-balance solution. The new method, based on an iterative approach known as *Krylov Subspace Methods*, avoids direct storage and factorization of the Jacobian. Rather, a series of matrix-vector operations replaces the full storage and factorization steps while retaining full numerical accuracy.

Observed speed-up factors depend on the number of nonlinear devices in the circuit and the number of spectral components used in the analysis as well as the convergence properties of the harmonic-balance algorithm. Speed improvements over conventional harmonic balance analysis from 2× to 10× for circuits consisting of a few transistors under two and three-tone excitation have routinely been observed. A circuit containing 20 FETs under three-tone analysis exhibited a speed improvement factor of 30×. Memory requirements have also been tremendously reduced. The 20 FET circuit originally required >200 Mbytes and now will analyze with 64 Mbytes. As the circuit becomes more "complex" the new methods provide better speed and memory improvements.

The *SPICE* program Outputs

During analysis, *SPICE* programs like *Designer 8*, generate a number of output files that are used to store textual, graphical and initialization information. The files generated are:

myfile.aud

The audit file contains textual information about the analysis. In its basic form it contains the final results of the network functions. Additional information can be requested by setting the verbosity flag in the control block as:

VERBOSE *n*

where 0 ***n*** $\leq$ 4. The higher the verbosity number is, the more output that is generated about the final and initial points at each sweep step.

Sweeping Frequency, Power and Voltage Sources

Each source in the design can be swept in amplitude. Also, the tones defined for the analysis can be swept. When more than one source or frequencies are swept, an ambiguity arises as to the order of precedence. The following rules apply in the cases of multiple sweeps:

1) When more than one source is swept and no frequencies are swept, then the sources sweep in unison. That is, each source is stepped at the same time. This is a one-dimensional sweep.

2) When more than one frequency is swept and no sources are swept, then the frequencies sweep in unison. This is also a one-dimensional sweep.

3) When frequencies and sources are both swept, the program

performs a two-dimensional sweep where the sources are swept in the innermost loop. A matrix results where the source sweep is the most rapidly changing index. An exception to this case is during noise analysis, where the swept frequency deviation will be the innermost loop.

Generating Large-Signal S-Parameters

Since large-signal S-parameters are poorly defined, but widely used, we will show two methods of generating them. If your definition of large-signal S-parameters is different, you can redefine the example to suit your own needs. Here lies the ambiguity as to what one means by large-signal S-parameters. It will depend on the specific application and must be tailored in each case. Figure 3 presents one interpretation.

The calculation of *S*-parameters in the large-signal regime is not as straightforward as it is in the linear, small-signal regime. The large-signal *S*-parameters are dependent on the power of the excitation sources at each external circuit port as well as the circuit bias and terminations. Guidelines will be given here on using *Designer 8* to generate large-signal *S*-parameters, but the proper use of these S-parameters in circuit design is up to you.

Consider a two-port circuit whose large-signal *S*-parameters are desired. If we apply a source at port 1 with port 2 terminated, we could measure the reflected and transmitted waves, and conversely for a source applied to port 2.[10, 11, 12] This assumes that when the device under test is actually used, however, it will be terminated in the same impedance as it was tested. This is rarely the case. Typically the device is embedded in some matching network that presents a complex impedance to the device. Therefore, the operating regime of the device will change and its large-signal *S*-parameters will be altered.

We could then hypothesize that a source can be placed at each port and the traveling waves could be measured at each port. The problem here is that it is not possible to distinguish between the reflected wave at a port and the transmitted wave due to the source at the other port because the sources are the same frequency. If we perturb the frequency of one of the sources, then the reflected and transmitted waves due to each source can be resolved. This, however, requires a two-tone analysis. The situation is illustrated in Figure 3A, for a two-port device under test.

The difference in frequency between the two sources can be made small, on the order of 0.001%. This is recommended for circuits of large *Q*. Typically the difference used is about 0.1% because the S-parameters of the device under test do not change rapidly with frequency.

This example shows some of the inconsistencies associated with large-signal *S*-parameters. For example, what happens to the power that is converted to other harmonic products? These will depend on the bias point, harmonic terminations, and so on. In practice, the powers measured include all harmonic powers incident on the detector, whereas in the calculations we can pick out the precise fundamental powers. Also, we chose incident power levels as 10 dBm and 8 dBm, but how do we know if these are correct until *after* the design is done? There are several approximations like these that are assumed to be small when using large-signal *S*-parameters in active circuit design. Nonetheless, these parameters persist in design and can be computed using *Designer 8*.

In some cases where it can be approximated that one or more ports will be conjugately matched so a source doesn't need to be present there, higher port parameters can also be computed using repetitive analyses.

Other so-called conversion parameters can be computed. For example, if a mixer conversion matrix is desired between the RF and IF frequencies, the corresponding transmission parameters can be computed using TG between the proper harmonic numbers. The reflection coefficients can be found by using RL at the source ports and source harmonics.

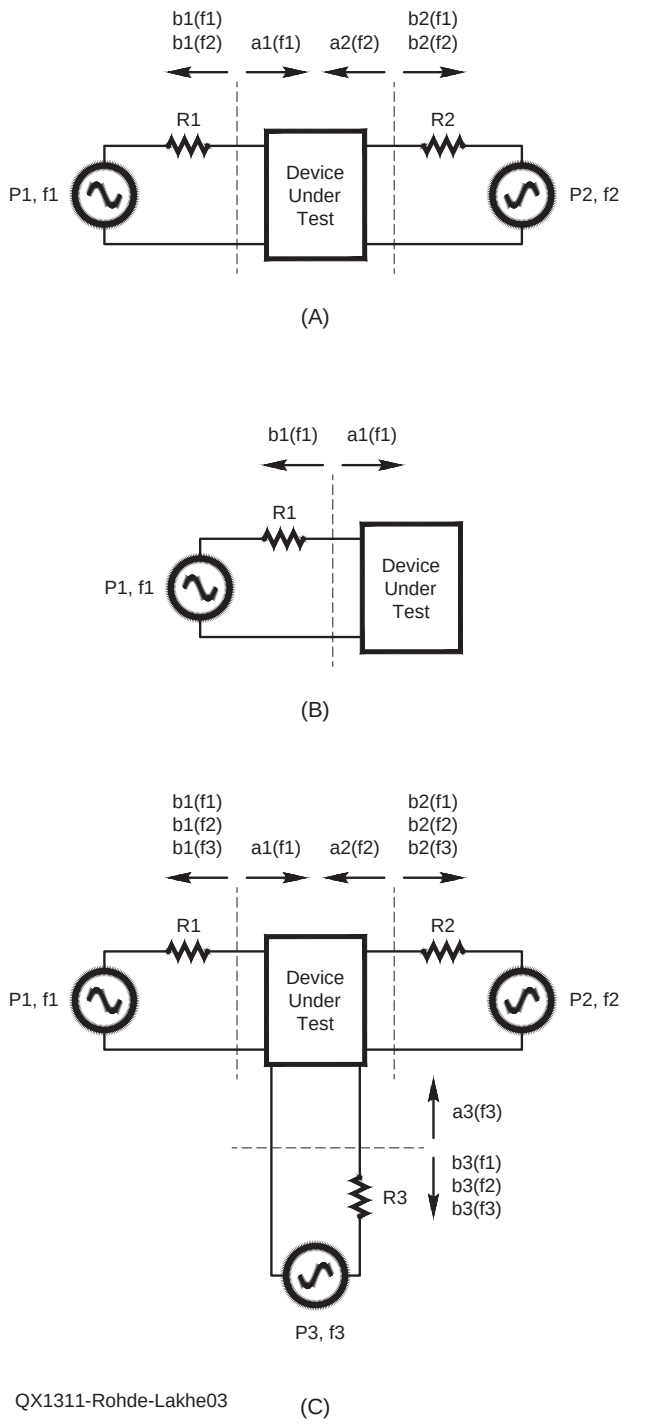

Figure 3 — Schematic diagram: Generating large-signal S-parameters.

Algorithm for Single-Tone Y-Parameters: Evaluation of Nonlinear Systems

For single-tone band-pass analysis, it is assumed that a nonlinear element's measurements are obtained when both the source and load have a 50 Ω termination and the input is a band-pass single-tone signal. The measurements obtained are directly related to the large signal S-parameters of the two-port nonlinear element and the power

available at the input and output ports.[13]

For a given single-tone input, we can refer to large signal S-parameters as the operating point of the nonlinear two-port element when operating independently and terminated in 50 Ω. One would certainly expect this operating point to change when this nonlinear element is embedded in a nonlinear topology system (as in Figure 4) composed of linear and nonlinear components.

The new operating point (for large-signal S-parameters) is determined for each nonlinear element using an iterative algorithm where the levels of the incident powers at both ports are interpolated iteratively until the algorithm converges to the actual operating point. This nonlinear frequency domain iterative algorithm accounts for all nonlinearities and inter-stage mismatches in the system.

For the multi-channel nonlinear topology in Figure 4, it is always assumed that parallel nonlinear channels connected to the same linear electrical subsystem are not coupled (in other words, non-interacting). This, in simple terms, implies that signals traveling in one nonlinear path do not spill over into the other nonlinear path (by virtue of the S-parameters describing the linear electrical subsystem).

This effectively implies that the signals in nonlinear channels are not coupled, and as a result, the impedances Zs_n, Zin_n, $Zout_n$, and Zl_n for the n^{th} nonlinear element ($1 \leq n \leq N$) in Figure 4 are well defined. With that important assumption, the iterative algorithm used for evaluating the operating point for each nonlinear element proceeds as follows (refer to Figure 4):

1) Assume an initial guess of $P1_n(0) = P2_n(0) = 0$ for the first iteration ($k = 0$) for the n^{th} nonlinear element ($1 \leq n \leq N$).

2) Calculate the power-dependent S-parameters for the n^{th} nonlinear element ($1 \leq n \leq N$) at the k^{th} iteration ($k \leq 0$). For the first iteration ($k = 0$), this would basically yield the n^{th} nonlinear element small signal S-parameters since the initial estimate for the incident powers is zero.

3) Calculate the entire system ***Y*** matrix, the impedances shown in Figure 4— $Zs_n(k)$, $Zin_n(k)$, $Zout_n(k)$, and $Zl_n(k)$, and the nodal voltages at the input and output ports of the n^{th} nonlinear element at the k^{th} iteration.

4) Recalculate the incident powers at each port with ($1 \leq n \leq N$) and ($k \leq 0$) according to Equation 8

$$P1_n(k+1) = \frac{\left| \frac{v1_n(k)\left[zin_n(k) + zs_n(k) \right]}{zin_n(k)} \right|^2}{4\,\mathrm{Re}\left\{ zs_n(k) \right\}}$$

[Eq 8]

$P1_n(k + 1)$ = the power available at the input port of the n^{th} nonlinear element at the k^{th} iteration when the output port is terminated in $Zl_n(k)$.

and

$$P2_n(k+1) = \frac{\left| \frac{v2_n(k)\left[zout_n(k) + zl_n(k) \right]}{zout_n(k)} \right|^2}{4\,\mathrm{Re}\left\{ zl_n(k) \right\}}$$

[Eq 9]

$P2_n(k + 1)$ = the power available at the output port of the n^{th} nonlinear element at the k^{th} iteration when the input port is terminated in $Zs_n(k)$.

5) Form the error function, Equation 10.

$$Error(k) = \frac{\sum_{n=1}^{N} \sqrt{\left[P1_n(k+1) - P1_n(k+1) \right]^2 + \left[P2_n(k+1) - P2_n(k+1) \right]^2}}{\sum_{n=1}^{N} \sqrt{\left[P1_n(k) \right]^2 + \sqrt{\left[P2_n(k) \right]^2}}}$$

[Eq 10]

The algorithm is assumed convergent if the condition $Error(k) \leq N \times 10^{-6}$ is met. If this convergence condition is not satisfied, steps 2 to 5 above are repeated until the algorithm converges. If the algorithm fails to converge after 30 iterations, an error in analysis message will be displayed.

Linear Electrical Discrete Time Simulation

During signal analysis, all electrical components and sub-designs are converted to time domain behavioral models (unidirectional models). This time domain model is extracted from the corresponding frequency response evaluated during the course of the simulation.

The extracted time domain behavioral models will typically contain the transient, steady state, and noise responses of the electrical sub-design (all in accordance with the frequency-domain signal and noise response of the electrical sub-design as well as impedance mismatches within the sub-design). Therefore, the processing of modulated signals through electrical components/sub-designs will include the transient, steady state, group delay, and noise effects.

There are two techniques available for discrete time simulation of linear electrical components and sub-designs: Convolution and Impulse Invariance.

Setting Discrete Time Simulation Control Parameters

For the discrete time simulation of a mixed-mode communications system, the user must carefully select the following control parameters:

1) $t_s = 1 / f_s$ = Simulation time step (which may assume different

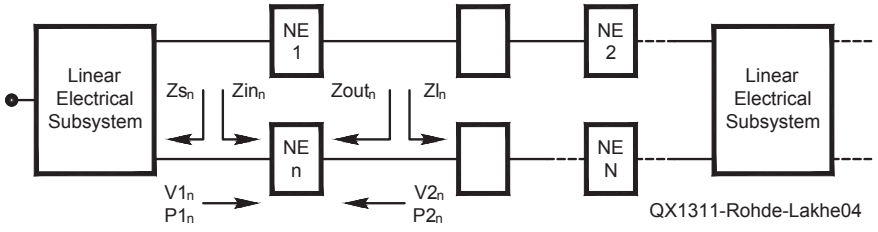

Figure 4 — General nonlinear electrical topology containing N nonlinear elements (NE = nonlinear elements).

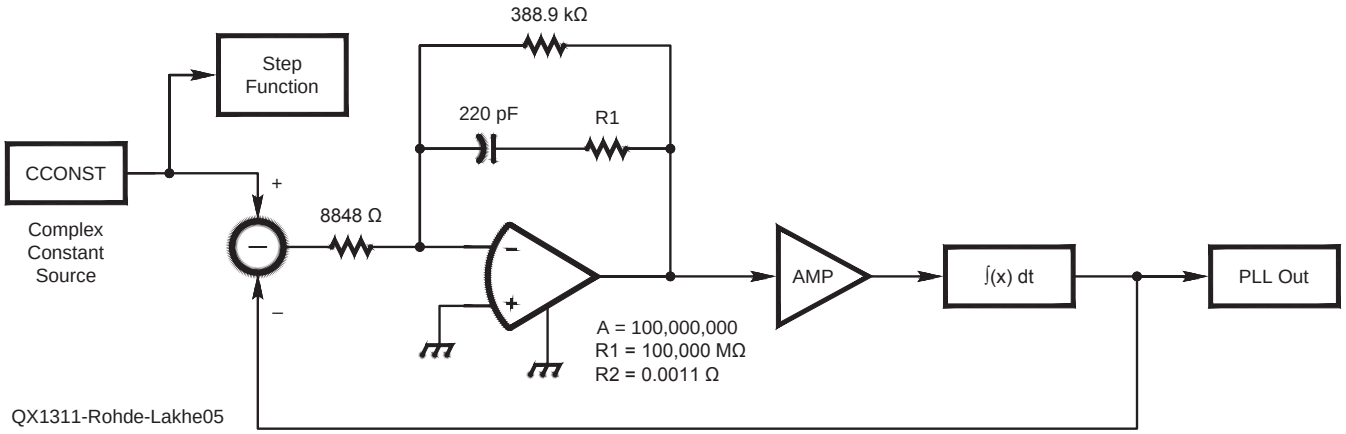

Figure 5 — Example of PLL project to show the time domain response.

values at different points in the system)

2) *MIN_BW* = Minimum bandwidth of an electrical component or sub-design in the complete mixed mode system.

3) *MAX_RATIO* = Ratio of a local maximum to the global maximum in the impulse response.

Step 1: Choosing the Simulation Time Step

Choosing the simulation time step, t_s, is not a direct process in discrete time signal analysis. For a typical wireless communications system, the user always begins by setting the bit rate for binary data sources (or sampling rate if a source happens to be a waveform source).

Binary source components (BSRC) have a parameter that determines their output bit rate. In a typical baseband modulation process, binary bits (at a user-defined bit rate) are mapped unto information symbols (to yield a given symbol rate). Each symbol is then represented by a user-selected number of samples (typically by up-sampling or repeating each symbol) to finally yield a desired sampling rate, f_s, and the corresponding simulation time step of $t_s = 1 / f_s$. These samples are then filtered to yield the discrete baseband modulation waveform $S(nt_s)$ described above.

When choosing the simulation time step caution should be exercised to preserve the Nyquist criterion for the signal $S(t)$. In other words, the user must ensure that the discrete signal $S(nt_s)$ (at any point in the system) has at least a Nyquist sampling rate or higher, where the Nyquist sampling rate is equal to twice the bandwidth of the continuous signal $S(t)$.

At the same time, the simulation time step must be chosen in accordance with the Nyquist criterion for system bandwidth. In other words, if the bandwidth of a filter or electrical sub-design is BW, then, $f_s \leq 2BW$. Good results may be obtained for values of $f_s \leq 5BW$.

In conclusion, the simulation time step, t_s, must be chosen in accordance with the expected (baseband or band-pass) signal, $S(t)$, and (baseband or band-pass) system bandwidths. For most practical applications, the signal and system bandwidths are of the same order, but in general, t_s at any point in the system must be chosen in accordance with the larger of the signal bandwidth and system bandwidth at that point.

In some applications, the user may be interested in generating direct waveforms without having to convert binary information to symbols and symbols to samples. There exists a good number of waveform sources that can generate a variety of periodic and transient waveforms. In addition, arbitrary waveforms may be imported for the discrete time system analysis from *MATLAB*, *WinIQSim* and other

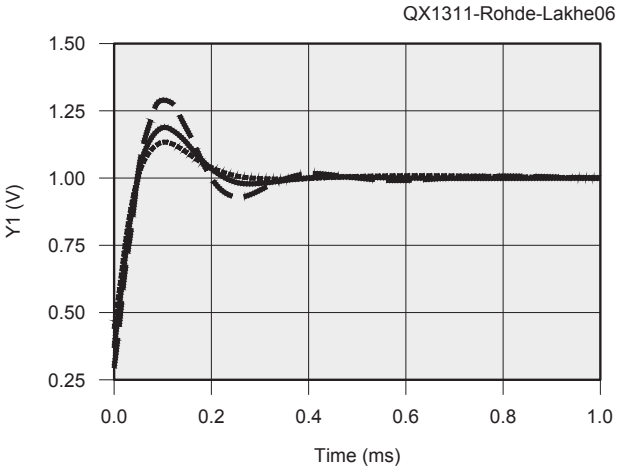

Figure 6 — PLL time domain response for 3 different R1 values in the loop filter. Simulation sampling rate, f_s = 50 kHz. (Values of R1 used are R1 = 74800 Ω, R1 = 174800 Ω, R1 = 274800 Ω.)

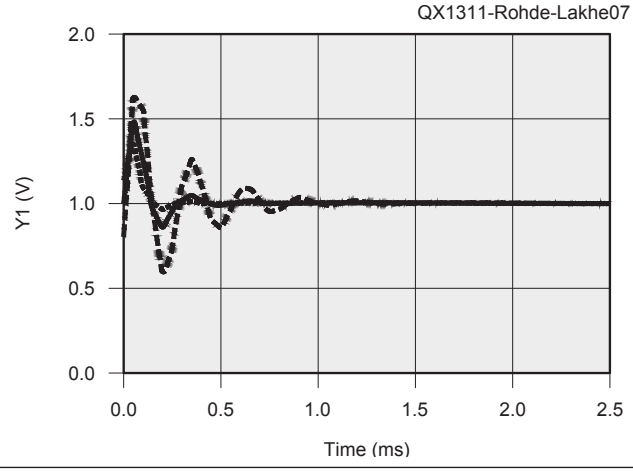

Figure 7 — PLL time domain response for 3 different R1 values in the loop filter. Simulation sampling rate, f_s = 20 kHz. (Values of R1 used are R1 = 74800 Ω, R1 = 174800 Ω, R1 = 274800 Ω.)

system simulators by means of an external waveform file.

All waveform source components in the *Designer 8* system have a parameter that determines the desired sampling rate, f_s, which in turn will set the desired simulation time step.

As an example, consider the second order (type 1) **PLL** project shown in Figure 5. Note that the sample rate parameter for the complex constant source (CCONST) is set to 50 kHz (well beyond the Nyquist rate of the electrical sub-design or loop filter of the Phase Locked Loop). This sampling rate implies a time step of 20 μs. After analyzing the project, the PLL time domain response shown in Figure 6 will be displayed.

If the sample rate of the CCONST source is readjusted to 20 kHz and the project is re-analyzed, the resulting change in time domain response for the PLL can be seen in Figure 7 in terms of the "smoothness" of the output curves. There is a warning message displayed for this step.

As we can see from Figure 6 and Figure 7, choosing a higher sampling rate results in more accurate simulation results. In Figure 6 and Figure 7 the x axis is time in milliseconds and the vertical axis is the impulse response of the PLL system.

Step 2: Choosing the Minimum Bandwidth Control Variable

Another important control parameter for analyzing mixed systems is *MIN_BW*, which is the minimum bandwidth of an electrical component or sub-design. It is up to the user to define this minimum bandwidth as the point where the frequency domain response is down by 3 dB, 10 dB or more. The simulation speed and accuracy of mixed mode systems largely depends on selecting this control parameter. The parameter *MIN_BW* may be specified through the Discrete Time Domain System solution setup. To specify a reasonable value for *MIN_BW*, it may be worthwhile to evaluate the frequency response ($S_{21}(f)$) of electrical sub-designs using the single tone frequency domain sweep analysis discussed in the Frequency Domain Analysis topic. This will help identify the *MIN_BW* in the system more appropriately.

The number of frequency points used to evaluate the frequency response of an electrical component/sub-design (during discrete time analysis) is given by the next power of 2 greater than or equal to *K*, where

$K = \{\text{Minimum power of } 2 \leq (10 f_s / MIN\_BW)\}$

and the frequency step is given by

$df = (f_s / K) \leq (MIN\_BW / 10) =$ Sweep resolution used for warning message in the discrete time domain analysis dialog, where f_s is the sampling rate of the input signal(s) to the electrical component/sub-design.

Step 3: Choosing the Maximum Ratio Control Variable

Once the frequency response of a linear electrical RF sub-design is obtained, the impulse response is extracted from the frequency response by means of the inverse FFT operation and the pre-defined variable *MAX_RATIO* ($0 < MAX\_RATIO \leq 1$).

MAX_RATIO is a critical parameter used to determine the actual length of the impulse response used for discrete time simulation. Since the inverse FFT of the frequency response yields an impulse response of length $K / 2$ samples, not all of these samples will be used in the actual discrete time domain simulation. Starting at the last impulse response sample at time $Kt_S / 2$ and moving towards $t = 0$ (see Figure 8), the pre-defined variable *MAX_RATIO* is used to truncate the impulse response at the point where the ratio of the impulse response local maximum to the global maximum is $\leq$ *MAX_RATIO*. Thus, specifying a smaller *MAX_RATIO* value will typically result in longer impulse responses (and longer simulation time) but more accuracy.

The default value for *MAX_RATIO* is $1e^{-10}$, which should produce the most accurate results. At the expense of accuracy, the user may specify larger values for *MAX_RATIO* if a shorter simulation time is desired.

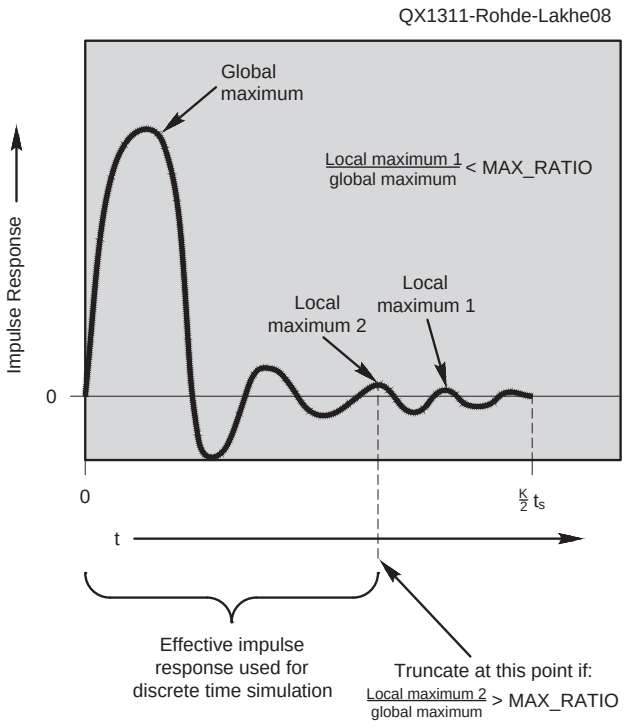

Figure 8 — Graphical illustration of the significance of the maximum ratio control parameter.

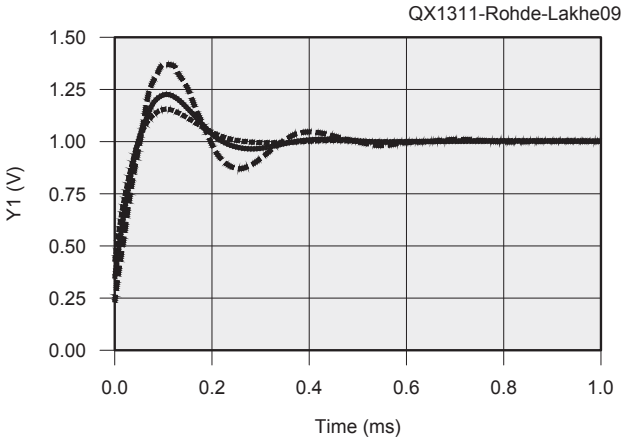

Figure 9 — PLL response from *MAX_RATIO* = 0.001.

A graphical illustration of the effects *MAX_RATIO* has on determining the length of the impulse response is shown in Figure 8.

Consider the PLL example discussed above. The responses shown in Figures 9 and 10 reflect two different values for the *MAX_RATIO* control parameter, namely 0.001 in Figure 9 and 0.1 in Figure 10, with a fixed sampling rate of 50 kHz. Clearly, the impact of choosing a larger *MAX_RATIO* (Figure 10) can be seen. This is due to the fact that a larger *MAX_RATIO* resulted in a premature truncation of the impulse response of the PLL electrical loop filter, and consequently,

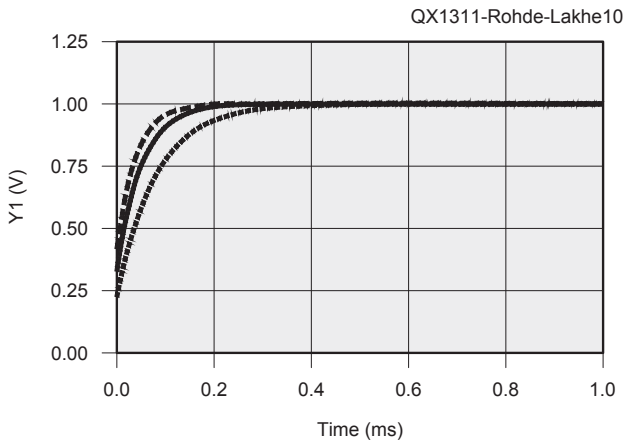

Figure 10 — PLL response from *MAX_RATIO* = 0.1.

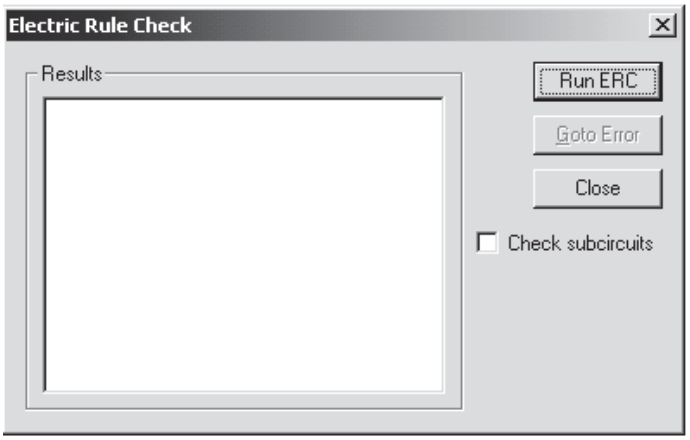

Figure 11 — The Electric Rule Check screen opens this dialog screen, with space for results and error messages when you run the ERC.

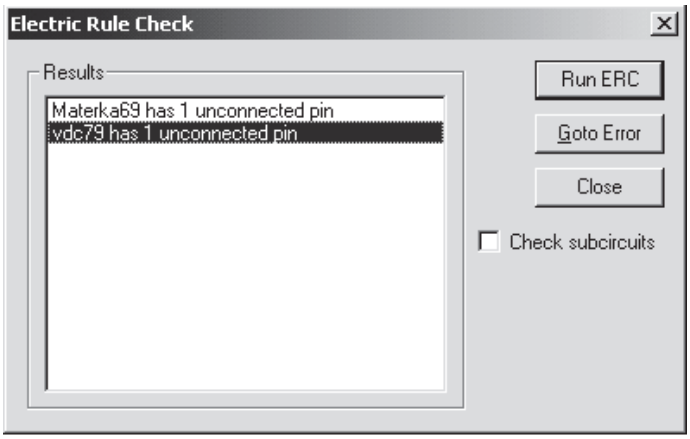

Figure 12 — Here is an example of an Electric Rule Check dialog screen showing two error messages. Note that the Goto Error button will take you to the object in the Schematic Editor that caused the error.

the simulation results are inaccurate. In general, a longer discrete time impulse response (smaller *MAX_RATIO*) requires a longer simulation time, but will tend to yield more accurate results. In Figure 9 and Figure 10 the x axis is time in milliseconds and the vertical axis is the impulse response of the PLL system.

If starting at Kt_s / 2 and moving towards $t = 0$, the search process fails to detect a local maximum/global maximum ratio that is less than *MAX_RATIO*, a warning message will be displayed at the end of the simulation.

Checking Connectivity

The Electric Rule Check (ERC) feature checks the circuit for valid connectivity. ERC automatically conducts rule checking for ports, connections, and components of the active schematic.

To test for connectivity, select Schematic > Electric Rule Check, which opens the ERC dialog shown in Figure 9.

Select Check Subcircuits to run the electric rule check on subcircuits of the active schematic display.

Click Run ERC to begin the error check.

If an error is displayed in the Results window double-click the error message or select the message and click Goto Error to go directly to the object in the Schematic Editor that caused the error. Figure 10 shows an example.

Possible Causes of Electric Rule Check Error Messages

• Unconnected Pins — A component, or port, with a pin that is not connected to anything else.

• Overlapping Components — A component that completely overlaps another, such that the two components appear as one component. (Often caused by accidentally clicking twice when placing a component.)

• Nets with Multiple Output Pins — A net that has more than one output pin connected to it. (This is rare since most component pins are labeled as input and output.)

If You Encounter Convergence Difficulties

The nonlinear solvers have been greatly improved, but you may still have convergence problems with some circuits, particularly highly nonlinear circuits with bipolar transistors, or circuits with high drive levels may pose a problem. For such circuits, the following hints are suggested to enable finding a solution.

1) Check the circuit connections. Improper node connections and/or missing units on parameters are the most common causes for convergence problems and messages that indicate "Singular Jacobian." This commonly happens when the active devices are not biased properly or the signal path is not connected. Use the **Show Bias Point** option on the **Analysis** dialog to check for proper bias.

2) Check that the bias sources are properly connected. If constant current sources are used, make sure the current flows in the desired direction.

3) Add losses in the circuit. When initial designs are simulated it is common to use ideal elements that don't have losses (for example, transmission lines using characteristic impedance and electrical length only). This may pose problems in the analysis of the linear subcircuit at DC or when computing the Jacobian for nonlinear analysis.

4) Approach the solution point incrementally. By sweeping the source voltage or power toward the desired level, the circuit is driven gradually into the region where convergence is difficult to obtain. During a source sweep, the results of the previous step are used for the initial iterate of the subsequent step, the starting point is closer to the vicinity of the desired solution than a "cold" start from zero initial values. *Designer 8* also employs automatic step reduction on power sweeps, whereby the step size is halved if convergence was not obtained on the previous step.

5) A similar solution to the one in point 4 is to start the analysis from the previous solution. The *.VAR file should be backed up, the

solution options should start from a previous solution, and the DC initialization should be disabled. This method can also be useful when manually tuning the circuit to achieve a desired response (if it is a single-point analysis).

6) If insufficient sampling points are used to represent the time-domain waveforms, there will be significant aliasing errors in the FFT.

Notes

[1]G. Vendelin, A. Pavio, U.L. Rohde, N1UR, *Microwave Circuit Design Using the Linear and Nonlinear Techniques*, Wiley, New York, 2005.
[2]U.L. Rohde, N1UR, and D. Newkirk, W9VES, *RF/Microwave Circuit Design for Wireless Applications*, Wiley, New York, 2000.
[3]U.L. Rohde, N1UR, A.K. Poddar, and G. Boeck, *The Design of Modern Microwave Oscillators for Wireless Applications: Theory and Optimization*, Wiley, New York, 2005.
[4]Ulrich L. Rohde, N1UR, and Hans Hartnagel, www.mes.tu_darmstadt.de/media/mikroelektronische_systeme/pdf_3/eweme2010/proceedings/sessionvii/rohde_paper.pdf
[5]V. Rizzoli, A. Lipparini, and Ernesto Marazzi, "A General-Purpose Program for Nonlinear Microwave Circuit Design," *IEEE Transanctions on Microwave Theory and Techniques*, Vol. 31, No. 9, September 1983, pp 762-770.
[6]V. Rizzoli, A. Lipparini, A. Costanzo, F. Mastri, C. Cecchetti, A. Neri, and D. Masotti, "State-of-the-Art Harmonic-Balance Simulation of Forced Nonlinear Microwave Circuits by the Piecewise Technique," *IEEE Transactions on Microwave Theory and Techniques*, Vol. 40, No. 1, January 1992, pp 12-28.
[7]V. Rizzoli, C. Cecchetti, A. Lipparini, "A General-Purpose Program for the Analysis of Nonlinear Microwave Circuits Under Multitone Excitation by Multidimensional Fourier Transform," *17th European Microwave Conference*, September 1987, pp 635-640.
[8]V. Rizzoli and A. Neri, "State-of-the-Art and Present Trends in Nonlinear Microwave CAD Techniques," IEEE Transactions on Microwave Theory and Techniques, Vol. 36, No. 2, February 1988, pp. 343-365.
[9]V. Rizzoli, C. Cecchetti, A. Lipparini, and F. Mastri, "General-Purpose Harmonic-Balance Analysis of Nonlinear Microwave Circuits Under Multitone Excitation," *IEEE Transactions on Microwave Theory and Techniques*, Vol. 36, No. 12, December 1988, pp 1650-1660.
[10]V. Rizzoli, F. Mastri, F. Sgallari, V. Frontini, "The Exploitation of Sparse-Matrix Techniques in Conjunction with the Piecewise Harmonic-Balance Method for Nonlinear Microwave Circuit Analysis," *1990 MTT-S International Microwave Symposium Digest*, June 1990, pp 1295-1298.
[11]V. Rizzoli, A. Lipparini, and F. Mastri, "Computation of Large-Signal S-Parameters by Harmonic-Balance Techniques," *Electronics Letters*, Vol. 24, March 1988, pp 329-330.
[12]V. Rizzoli, F. Mastri, F. Sgallari, and G. Spaletta, "Harmonic-Balance Simulation of Strongly Nonlinear Very Large-Size Microwave Circuits by Inexact Newton Methods," *IEEE Microwave Theory and Techniques Society*, 1996, pp 1357-1360.
[13]Ansys *Designer 8* Manual.
[14]Andrei Vladimirescu, *The SPICE Book,* Wiley NY, 1994.

Ulrich L. Rohde, N1UL, studied electrical engineering and radio communications at the Universities of Munich and Darmstadt, Germany. He holds a PhD in electrical engineering (1978) and a ScD (Honorary, 1979) in radio communications, a Dr-Ing (2004), University of Berlin, Germany in oscillator circuits and several honorary doctorates. In 2011 he earned a Dr-Ing Habil. Degree from the University of Cottbus, Germany.

He is President of Communications Consulting Corporation; Chairman of Synergy Microwave Corporation, Paterson, New Jersey; and a partner of Rohde & Schwartz, Munich, Germany. Previously he was President of Compact Software, Inc, Paterson, New Jersey; and Business Area Director for Radio Systems of RCA, Government Systems Division, Camden, New Jersey. He is a Professor of RF Microwave Circuit Design at Cottbus and has held Visiting Professorships at several universities in the United States and Europe.

Dr Rohde holds 25 patents and has published more than 200 scientific papers and has written or contributed to many books.

Dr Rohde is an ARRL Life Member, and is a Fellow of the IEEE, with positions on many IEEE Committees and Societies. In addition to his US call sign, he has held German call signs (DJ2LR/DL1R) since 1956 as well as Swiss call sign HB9AWE.

Rucha Lakhe completed her Bachelor of Engineering degree from Mumbai University, India in 2001 and her MS degree from Syracuse University in 2006. She is currently enrolled as a Dr-Ing student at B. T. U., Cottbus, Germany.

She is currently working as a design engineer in the oscillator group for Synergy Microwave Corporation as part of the EE Team. Previously she has worked for MtronPti as an Advanced Design Engineer, designing microwave/RF filters and crystal oscillators. She has been working in the field of RF and microwave circuits since 2006.

Her research interests are RF and microwave communications systems and circuits, specifically transistor modeling using nonlinear parameters and RF-MEMs, microwave, millimeter wave oscillators and filters. She is an IEEE Member.

Bill Kaune, W7IEQ

160 Cedarview Dr, Port Townsend, WA 98368; **w7ieq@arrl.net**

Using GPS to Fine-Tune a Rubidium Frequency Standard

The author describes the control circuitry he developed to adjust the frequency of a Rb oscillator to lock the output signal to a GPS clock signal.

I have long been interested in instruments used to make measurements. Thus, when I saw an article in the Nov/Dec 2007 issue of *QEX* by John Raydo, KØIZ, entitled "A Low-Cost Atomic Frequency Standard," I immediately decided to build one. This device is based on a surplus LPRO-101 10 MHz rubidium oscillator module manufactured by a company named Datum. I purchased one on eBay for about $75 including shipping from Hong Kong. I purchased a 24 V, 3 A power supply from a surplus house (Marlin P. Jones, Inc.), and constructed a box out of aluminum sheet metal and a ¼ inch base plate that also served as a heat sink. I mounted these items in the box, rigged up a simple circuit that used the "lock" output from the LPRO-101 to turn on a front panel LED when the oscillator locked to the rubidium (Rb) vapor standard, and included a small cooling fan (RadioShack 273-240). I turned it on and it achieved lock after about three minutes.

I subsequently built a simple circuit that started with the 10 MHz output of the Rb frequency standard, and divided repeatedly by 2, 5, and multiples of 10. Using this circuit, I can generate Rb-stabilized frequencies from 10 MHz to 0.2 Hz in the above-mentioned steps. Over time, however, I became progressively more bothered by the fact that I had no way to independently determine the accuracy of the frequency standard, or even that it was working properly.

Then, one day I read that the global positioning satellites (GPS) use cesium clocks that are extremely accurate, and that you can purchase GPS receivers that generate time reference pulses essentially as accurate as the GPS clocks. I fired up my web browser, went to eBay, and started looking for GPS receivers. I soon found a receiver circuit board that was advertised as a Trimble Resolution-T Timing Receiver. I purchased it for $28 including shipping from Hong Kong. I also purchased a Trimble GPS antenna for $11, including shipping.

GPS Receiver

The next step was to figure out what I needed to do to get a functioning receiver at home. The first thing I discovered was that the receiver board was not actually the board that was advertised on eBay but was, instead, a Trimble GPS SMT integrated circuit installed on a "carrier" board. After reading the manual for this device, I decided it was probably superior to the Resolution-T receiver that I thought I had purchased, because of its higher-speed internal clock.

The Trimble receiver is designed to work with a computer via a "serial" interface between the two. USB ports have largely replaced the serial (COM) ports included in computers for so long. I thought it was about time for me to learn about USB ports so I purchased a book titled *USB Complete: The Developers Guide* by Jan Axelson. It did not take much reading to learn that USB ports are complicated, and I decided there had to be an easier way. I next purchased a book on serial interfaces entitled *Serial Port Complete: COM Ports, USB Virtual Ports, and Ports For Embedded Systems*, again by Jan Axelson. The key thing I learned from this book was that you could have a "USB virtual port." To do this, you buy a cable that has some embedded electronics that converts from USB at the computer end to serial at the other end and you load a software driver into the computer that has the effect of making the computer's USB port look like a serial port to any computer application software. I purchased one of these cables (Future Technologies Devices International Ltd part # TTL-232R-5V-AJ) from Digi-Key (part # 768-1068-ND) and downloaded the drivers from the FTDI website.

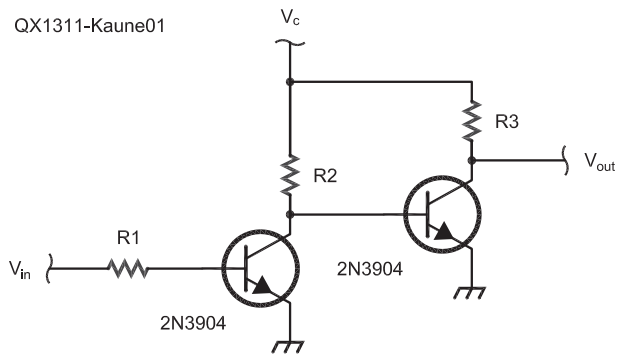

Figure 1 — This is a voltage level shifting circuit used in the GPS Interface. To shift from 3.3 V to 5 V, Vc = 5.0 V, V_{in} = 3.3 V, V_{out} = 5.0 V R1 = 100 kΩ and R3 = 220 Ω. To shift from 5 V to 3.3 V, Vc = 3.3 V, Vin = 5.0 V, Vout = 3.3 V, R1 = 150 kΩ, R2 = 7kΩ and R3 = 220 Ω.

The Trimble receiver operates with a 3.3 V power supply, whereas the low noise amplifier in the GPS antenna and the FTDI cable operate at 5.0 V. Consequently, you need two power supply voltages and two voltage level-shifting circuits, one to shift the 3.3 V serial output pulses from the GPS receiver to the 5.0 V required by the FTDI cable and the other to shift the 5.0 V serial pulses coming from the FTDI cable to 3.3 V. (I could have bought a 3.3 V cable from FTDI, but I had additional uses in mind that would require a 5 V cable.) The simple circuit I built to accomplish both of these level shifts is shown in Figure 1. The resistors R1, R2, and R3 have different values, listed in the caption, depending on the direction of voltage shift. The circuit in Figure 1 is not very fast (rise time about 0.300 µs), but it is simple and fast enough for this application. (The serial port runs at 9600 baud, which means a minimum pulse width of 104 µs.)

I bundled these two circuits, two voltage regulators and the GPS receiver board into a small metal box and named it my GPS Receiver and Interface. I downloaded from the Trimble website software named *Trimble GPS Studio*, Version 1.08.0. I connected everything together, applied power to the GPS interface, started the *GPS Studio* on my computer, and soon observed that the GPS unit seemed to be working fine. Wonders never cease!

The Trimble GPS receiver outputs a pulse every second that is synchronized nearly exactly with the GPS cesium clock. I say *nearly* exactly because in this receiver there is a little time jitter in the timing pulse, amounting to ±15.6 ns. This jitter is called "pps quantitization error" in the user manual for this device. It averages to 0 over time, and arises because the output clock pulse is synchronized with the receiver's own internal 64 MHz clock.

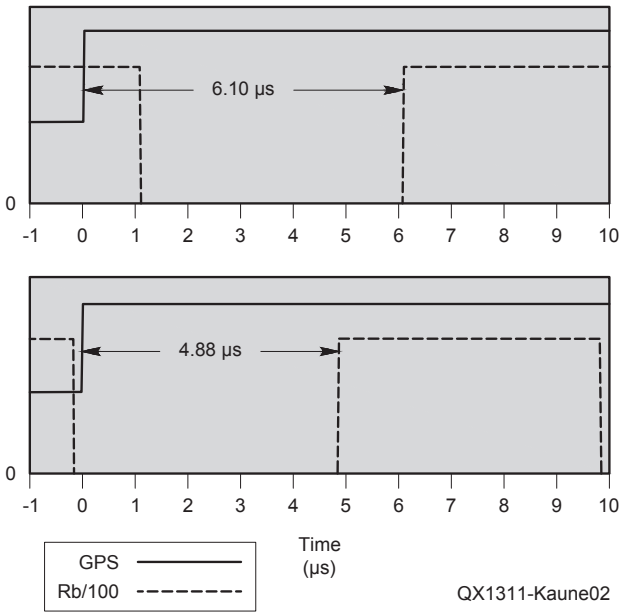

Figure 2 — Here is an oscilloscope plot showing movement in time of the Rubidium pulse relative to the GPS timing pulse during one hour.

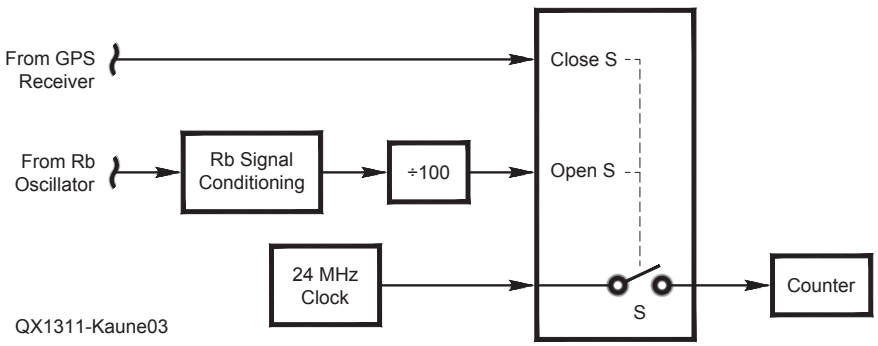

Figure 3 — This is the block diagram of the phase detector.

Measuring Frequency Error of the Rb Oscillator

I next connected the timing-pulse output of the GPS receiver to Channel 1 of my Rigol DS1052E digital oscilloscope, the output of my Rb oscillator, divided in frequency by 100, to Channel 2, and set the scope to trigger on Channel 1. The resulting display is shown in the top of Figure 2. The scope display was rewritten every second as a new GPS timing pulse arrived, but the display did not materially change. In other words, the GPS timing and frequency-divided Rb pulses were synchronized in time. This is what you would expect if the divided Rubidium frequency of 100 kHz were an exact integral multiple of the 1 Hz GPS frequency. If the Rb frequency were slightly in error — that is not exactly 10 MHz — however, one would expect that the Rb pulse shown in the oscilloscope trace would move horizontally relative to the GPS pulse over time. In fact, as I watched the traces, I observed that the Rb pulse did move slightly. The lower part of Figure 2 reproduces the oscilloscope trace one hour later than the top trace. The Rb pulse has moved to the left by an amount of 1.22 µs.

By noting the amount of movement of the Rb pulse relative to the GPS timing pulse, the error in the Rb frequency can be calculated. The change in phase, $\Delta\theta$, between the GPS and Rb pulse that occurs during an elapsed time *t* is given by Equation 1.

$$\Delta\theta = -2\pi\delta f_R' t, \qquad \text{[Eq 1]}$$

where $\Delta\theta$ is measured in radians (2π radians = 360° phase shift) and $\delta f_R'$ is the error in the Rb frequency divided by 100, that is, $\delta f_R' = \left(f_R - 10\text{ MHz}\right)/100 = \delta f_R / 100$. An alternative way to measure the change in phase would be to note the time between the occurrence of a GPS pulse and the first subsequent Rb pulse. In this method, a change of phase of one cycle (2π radians) would be a change in this time difference equal to the period of one cycle, that is, $1/f_R'$ = 10 µs, where f_R' = 100 kHz is the nominal frequency of the Rb oscillator divided by 100. Equation 2 compares these two ways of measuring phase.

$$\frac{\Delta T}{1/f_R'} = \frac{\Delta\theta}{2\pi} \qquad \text{[Eq 2]}$$

where ΔT is the change in time between the GPS and frequency-divided Rb pulse that accumulates during an elapsed time t. Combining Equations 1 and 2, solving for the error in the Rb oscillator frequency, and using the fact that $\delta f_R'/f_R' = \delta f_R/f_R$, we find Equation 3.

$$\delta f_R = -f_R \frac{\Delta T}{t} \qquad \text{[Eq 3]}$$

From Figure 2, $\Delta T = -1.22 \times 10^{-6}$ s. Also, t = 60 minutes = 3600 s and f_R = 10 MHz, so δf_R = 0.0034 Hz = 3.4 mHz. In this way, I was able to determine the accuracy of my Rb oscillator.

In order for this analysis to be valid, we need to know that the Rb oscillator frequency, divided by 100, is within ± 0.5 Hz of 100 kHz; for example, a frequency of 101 kHz would also have produced a stable display. This frequency range corresponds to a range of ± 50 Hz for the Rb oscillator. Fortunately, my HP5316 frequency counter indicated the frequency of the Rb oscillator was within 1 Hz of 10 MHz.

Using GPS to Fine-Tune the Frequency of the Rb Oscillator

The LPRO-101 Rb oscillator includes a screwdriver adjustment that can be used to shift its frequency slightly. Using this capability, the frequency of the Rb oscillator could be adjusted to minimize its error. This would be relatively simple to do and would probably be adequate for nearly all uses of the Rb frequency standard. I, however, decided to go further and develop a controller that would continually monitor

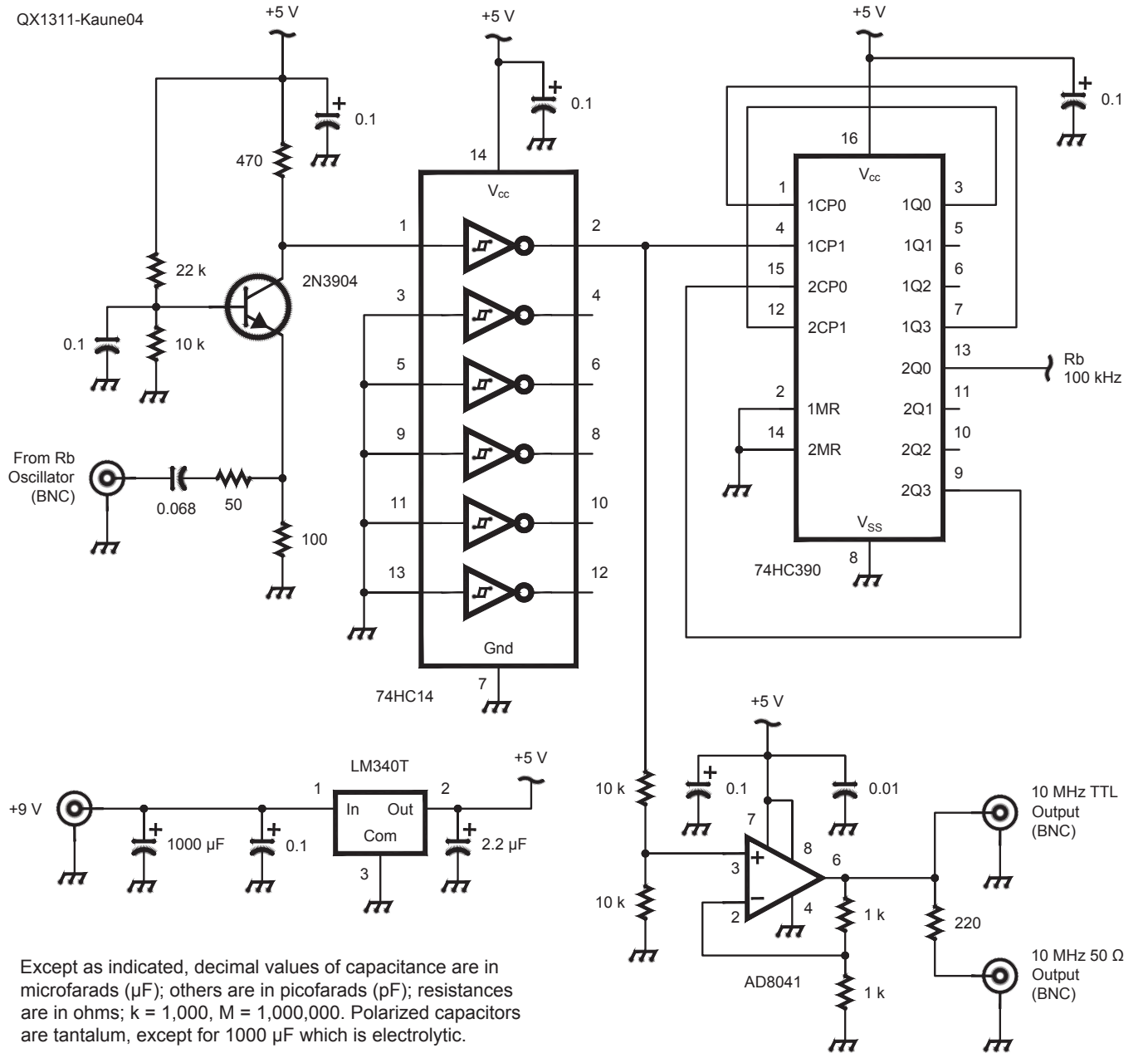

Except as indicated, decimal values of capacitance are in microfarads (µF); others are in picofarads (pF); resistances are in ohms; k = 1,000, M = 1,000,000. Polarized capacitors are tantalum, except for 1000 µF which is electrolytic.

Figure 4 — The schematic diagram of the Rubidium oscillator signal conditioning, frequency dividing, and power supply circuitry.

the time difference between the GPS pulses and the subsequent Rb pulses and adjust the frequency of the Rb source to hold this time difference as constant as possible. I decided to do this because it sounded interesting and I thought I would learn a lot.

I started looking around on the Internet and soon came across a July, 1998 *QST* article titled "A GPS-Based Frequency Standard" by Brooks Shera, W5OJM. This paper describes a system that uses GPS time information to control the frequency of an oscillator. I read through it and then started designing my system. The first challenge was to design a circuit that could measure the time difference between the occurrence of a GPS pulse and the first following Rb pulse. I followed closely Brooks' strategy. Figure 3 is a conceptual diagram showing the phase detector. The occurrence, once per second, of a pulse from the GPS receiver turns on switch S. Pulses from the 24 MHz clock start to be counted. Counting continues until the next Rb pulse, divided in frequency by 100, arrives, which opens switch S and terminates the count. Once the count is complete, it will be read by a microprocessor (not shown in Figure 3) and the counter reset to zero in preparation for the next GPS pulse.

Figures 4 and 5 show the schematic diagrams of the circuits that I developed for the GPS controller. The Rb signal conditioning and divide-by-100 electronics are shown in Figure 4. The signal from the Rb oscillator is a sine wave with a peak magnitude of about 0.8 V when terminated in 50 Ω. This signal is amplified by the 2N3904 stage in Figure 4 and is routed to a Schmitt trigger inverter (74HC14) that converts it into a 5 V peak square wave. This signal is sent to both a dual decade counter (74HC390) and an AD8041 amplifier. The counter is configured to divide by 100. The output of the amplifier provides both a square wave output with peak amplitude of 5.0 V, suitable to drive most types of logic circuitry, and a 0.9 V peak output suitable for 50 Ω loads; these outputs are available on the front panel of the controller.

Figure 4 also shows the voltage regulator that provides +5.0 V for all circuitry. I use a 9 V, 300 mA wall-wart to power the voltage regulator. Because most wall warts have poor filtering, I placed a 1,000 μF electrolytic capacitor across the input.

The switch S and associated open and close circuitry shown in Figure 3 were implemented with the dual J-K flip flop (74HC109) and two-input NOR gate (74HC02) shown in Figure 5. Both flip flops are initially off. The positive-logic output, 1Q (pin 6), from the first flip flop is applied to the reset input, 2R– (pin 15), of the second flip flop. Since the reset input is *negative* logic, the flip flop is held in reset and will not respond to any inputs on its clock (2CP, pin 12). The negative-logic output of flip flop 2 (2Q–, pin 9) is applied to the reset pin of flip flop 1 (1R–, pin 1). Since this level is high when flip flop 2 is cleared, flip flop 1 is armed and will respond to pulses arriving at its input.

The J-K inputs of both flip flops are connected so that the *rising edge* of any input causes the flip flop to set. Now suppose a GPS pulse arrives at the clock input (1CP, pin 4) to the first flip flop. This raises the output 1Q high, and removes the reset from flip flop 2. Flip flop 2 then responds to the next Rb pulse, divided in frequency by 100, that arrives at its clock input. When this pulse arrives, its negative-logic output, 1Q–, goes low, resetting flip flop 1, which then resets flip flop 2.

In this way, a strobe pulse, 1Q, is generated that is high during the time interval between the leading edge of a GPS pulse and the leading edge of the next Rb pulse. The inverse of this pulse, 1Q–, is applied to one input of a dual-input NOR gate. The output of this gate will be high only if both inputs are low. The 24 MHz clock (ECS Inc. ECS-2100A-240, Digi-Key part # X221-ND) is applied to the other input. Thus, during the strobe pulse, the output of the NOR is high whenever the clock pulse is low. The 74HC393 eight-bit binary counter counts the clock pulses that make it through the NOR gate. An eight-bit counter is sufficient because the longest time the NOR gate can be open is 10 μs, which gives a maximum count of 240.

The peak voltage of the timing pulse from the Trimble receiver is 3.3 V. I initially planned to use a circuit to shift this level up to 5 V, but I discovered that 3.3 V was sufficient to reliably trigger the J-K flip flop. Consequently, in Figure 5, the input timing pulse is sent directly to the J-K flip flop.

The strobe pulse for the J-K flip flop is also sent to the interrupt input (pin 21) of a PIC 16F876A microprocessor. Whenever the processor receives this pulse, it stops whatever it is doing, waits until the count is completed, reads the 8-bit value, and sets the counter back to 0. The processor uses this and previous counts to determine a correction to the Rb oscillator frequency and outputs this correction factor to a 12-bit digital-to-analog converter (DAC7611 in Figure 5). The resulting analog value, whose range is from 0 to 4.095 V, is amplified by the OPA342 stage to cover 0 to 5.0 V, the range needed for the Rb oscillator frequency control, and is sent to the Rb oscillator to fine tune its frequency. I selected the OPA342 operational amplifier because it was advertised as a "rail-to-rail" amplifier, which means it is capable of output voltages ranging all the way from its negative supply voltage (in our case 0 V) to its positive supply voltage (5 V).

Much of the frequency controller logic is implemented in the software for the PIC processor. Figure 6 is a block diagram of the overall process. (This diagram is, essentially, the diagram of a phase-locked-loop.) The phase detector, implemented in hardware (Figure 5), determines the phase count every second in response to an incoming GPS pulse. The PIC processor reads these values and averages 120 of them during a period of 2 minutes; the average value is denoted C in Figure 6. C is compared to a target value, C_t, and a digital "error" voltage, V_1, is generated according to Equation 4.

$$V_1 = G\left(C - C_t\right) + V_{off} \qquad \text{[Eq 4]}$$

where G is the "gain" of the phase detector and V_{off} is an offset voltage. The target count, C_t, is set equal to the current count at the time that a front panel switch, discussed later, is moved from the "Open Loop" to the "Close Loop" position. The offset voltage was initially set to 2.5 V and was later changed to 2.155 V. The output digital voltage, V_1, from the phase detector is passed through a low-pass single-pole digital filter in the processor software to filter out noise and to shape the response. The digital output is converted to an analog voltage in hardware (Figure 5) and sent to the Rb oscillator.

When I started this project, I knew little about digital filters. I got a book on the subject and quickly learned that designing digital filters can be a complicated business involving Laplace and z transforms. What I needed for this project, however, was a simple low-pass filter and while fiddling around with this, I found a simple design procedure. The input to this filter is a series of numbers, x_0, x_1, x_2, and so on. This series can be denoted x_i, $i = 0, 1, 2, \ldots$. The filter output will also be a series of numbers, y_i, $i = 0, 1, 2, \ldots$. I experimented with two different filter equations, given as Equation 5A and Equation 5B.

$$y_i = Ax_i + By_{i-1} \qquad \text{[Eq 5A]}$$
$$y_i = A\left(x_i + x_{i-1}\right) + By_{i-1} \qquad \text{[Eq 5B]}$$

where A and B are constants. Using digital filter terminology, the first filter will be called the "one-tap" filter because it uses only one value of x, and the second filter will be called the "two-tap" filter. The question I addressed was how to choose A and B for each filter to obtain a filter with the desired time constant (and bandwidth).

The classic analog single-pole low-pass filter is a series resistor-capacitor. The input voltage is applied across the two and the output is taken across the capacitor. If a

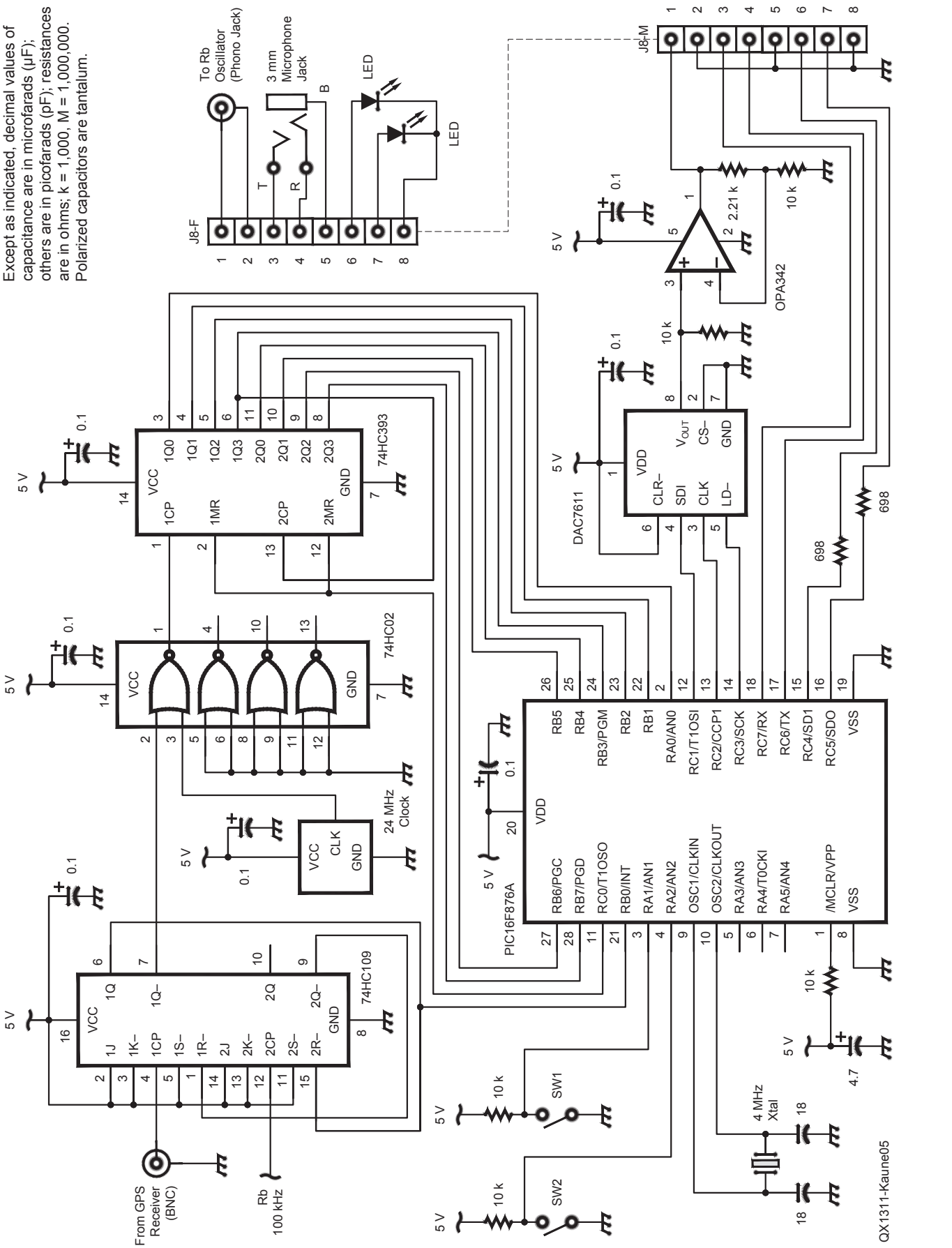

Figure 5 — Here is the frequency controller schematic diagram.

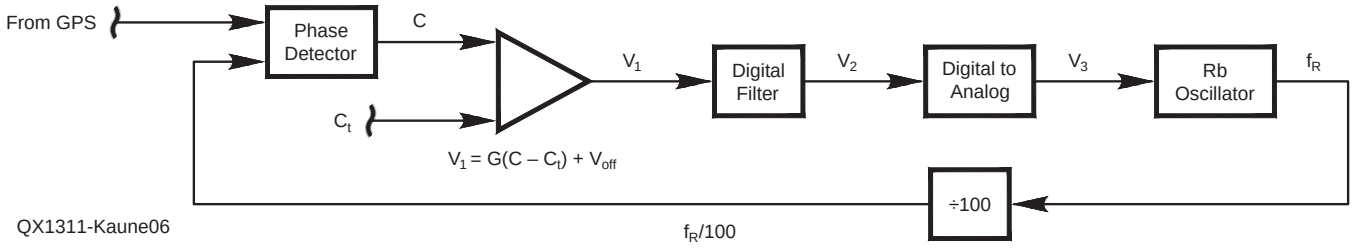

Figure 6 — This block diagram shows the frequency control logic.

steady dc voltage of 1 is applied, the output will equal the input. Our digital filter should act in the same way. Thus, if $y_{i-1} = 1$ and $x_i = 1$ for all i, then y_i must also equal 1. Placing these values in Equations 5A and 5B, we get Equations 6A for the one-tap filter and 6B for the two-tap filter.

$$1 = A + B \quad \text{[Eq 6A]}$$
$$1 = 2A + B \quad \text{[Eq 6B]}$$

Now suppose that a steady voltage of 1 is applied until time 0, at which point the voltage is instantly reduced to 0. In the case of the series resistor-capacitor filter, the voltage across the capacitor will decay exponentially with a time constant τ. That is expressed as Equation 7.

$$y = e^{-t/\tau} \quad \text{[Eq 7]}$$

where t is time > 0 and τ is the filter time constant.

For the digital filter, $x_i = 0$ for $i \leq 0$ and $y_0 = 1$. Using Equation 5A or 5B repeatedly:

$$y_1 = By_0 = B$$
$$y_2 = By_1 = B(B) = B^2$$
$$y_3 = By_2 = B(B^2) = B^3$$
$$\vdots \quad \vdots \quad \vdots$$

Therefore, we see that

$$y_N = B^N \quad \text{[Eq 8]}$$

where N is related to time. If the time interval between samples is T_S, then $N = t / T_S$. Thus, Equation 8 becomes Equation 9.

$$y = B^{t/T_S} \quad \text{[Eq 9]}$$

In order for the responses of the analog [Equation 7 and digital Equation 9] filters to be the same, we need the condition established by Equation 10.

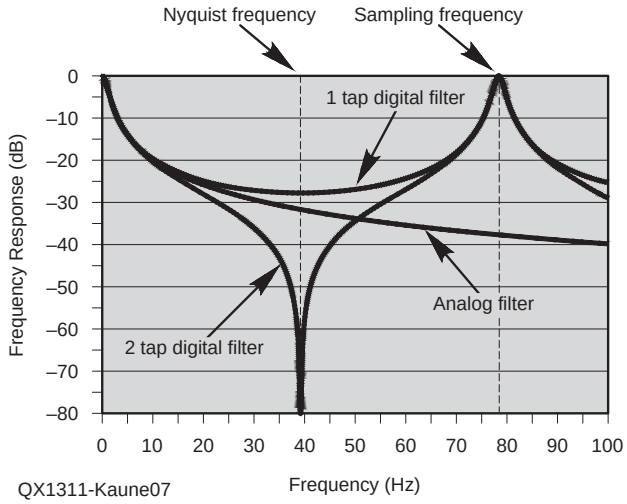

Figure 7 — This plot shows the frequency responses of the digital filters and equivalent analog filter.

$$B^{t/T_S} = e^{-t/\tau} \quad \text{[Eq 10]}$$

This equation may be solved for B and Equation 6 used to calculate the value for A.

$B = e^{-T_S/\tau}$ and $A = 1 - B$ for the one-tap filter [Eq 11A]

$B = e^{-T_S/\tau}$ and $A = (1 - B) / 2$ for the two-tap filter [Eq 11B]

In this way, we have related the parameters of the digital filter to those of its analog counterpart.

I next tested these two filters using computer-generated sine-wave inputs. Figure 7 shows the frequency responses of both digital filters and a corresponding analog filter for a time constant chosen to give a bandwidth of 1 Hz and a sampling frequency of 78.57 Hz. (The sampling frequency was chosen to yield the same product of the time constant and sampling frequency as the filter used in the final GPS frequency controller.) The frequency response of the analog filter decreases steadily with frequency. Both digital filters have essentially the same frequency response as their analog counterpart up to about 20 Hz. Above this frequency, the response of the one-tap filter starts to flatten out while the response of the two-tap filter steepens. At ½ of the sampling frequency, called the Nyquist frequency, the response of the one-tap filter is flat while the two-tap filter becomes almost zero. Things get more complicated as the input frequency, f, is increased above the Nyquist frequency. The temporal pattern of the samples of this input is exactly the same as the pattern obtained when sampling an input frequency of $2f_N - f$ (f_N = Nyquist frequency). Thus, the response of the filter is the same for input signals with frequencies of f and $2f_N - f$, with the result that the magnitude of the filtered signal rises, reaching 1 (0 dB) at twice the Nyquist frequency. Figure 7 shows that the response of the filter is symmetrical around the Nyquist frequency.

I was initially quite surprised to find that

the attenuation of the two-tap filter was so great near the Nyquist frequency until I realized that at the Nyquist frequency, $x_i + x_{i-1} = 0$ for all i. I selected the two-tap digital filter for use in the frequency controller software.

The output from the digital filter is converted to an analog voltage in hardware (Figure 5), amplified slightly, and used to fine-tune the Rb oscillator. I measured the oscillator frequency error for different control voltages using the method described earlier and summarized by Equation 3. Figure 8 shows the results. The measured points are shown as plus signs, and the straight line is the best linear fit to these data. This line is given by Equation 12.

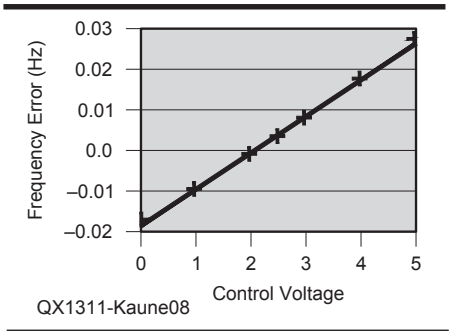

Figure 8 — This graph shows the Rubidium oscillator frequency error as a function of the control voltage. Measured data are shown as "+" signs. The straight line is a linear fit to the measured data.

Figure 9 — Here is a photograph showing the front panel of the Rubidium-GPS frequency controller.

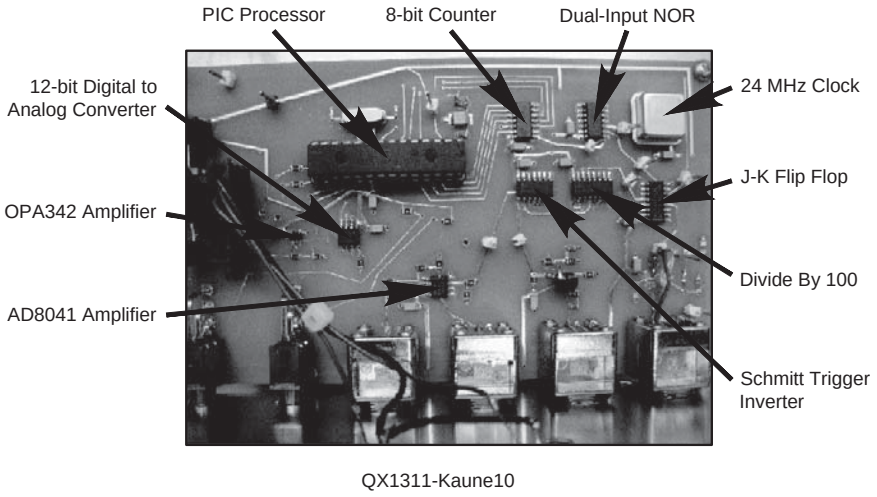

Figure 10 — This shot shows the frequency controller circuit board with the various components labeled.

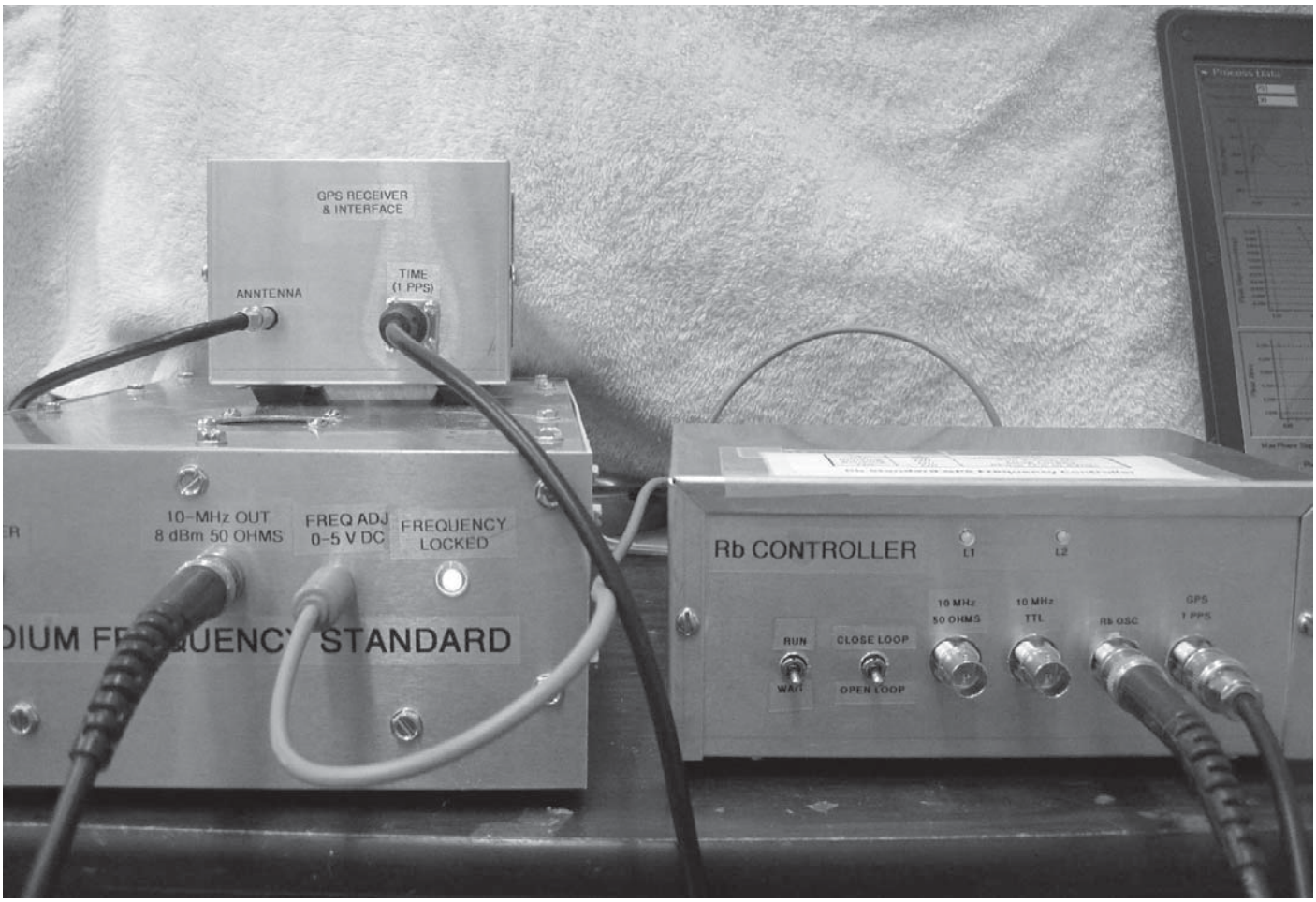

Figure 11 — Here is a view of the complete Rubidium oscillator frequency control system.

$$\delta f_R = -0.0188 + (0.0090)V \qquad \text{[Eq 12]}$$

where δf_R is the frequency error of the Rb oscillator in hertz, and V is the control voltage applied to the oscillator. (Actually, the data show a slight upwards curvature and a slightly better fit is provided by the quadratic form $\delta f_R = -0.0178 + 0.00775\ V + 0.00025\ V^2$.)

I wrote assembly-language software for the PIC processor to implement Figure 6 and to also continually send phase counts, averaged over the two minute measurement period discussed earlier, and control voltages to a computer, connected to the PIC via the same serial cable used earlier to connect the GPS Receiver-Interface to a computer. The data sent to the computer enabled me to monitor the GPS frequency controller operation. I spent considerable time developing this software and experimenting with different values for the phase detector gain, G, that appears in Equation 4, and the time constant, τ, of the digital filter. In selecting these values, I obtained guidance from phase-locked-loop theory. I also had to develop a method of determining when the Rb oscillator became "locked" to the GPS timing pulse.

My final selections for G were 0.06 before lock was achieved and 0.012 after. For the filter time constant, I selected 300 s before lock was achieved and 1500 s after. I found by having two selections for each of these parameters, I could substantially reduce the time to the achievement of lock. Once lock was achieved, the increase in τ and corresponding decrease in G provided increased immunity against noise.

I found that a suitable way to determine lock status was when the variation in the phase count became sufficiently small. My ultimate algorithm takes a consecutive sequence of 11 phase count measurements, covering a period of 22 minutes, and determines their standard deviation. Lock was achieved when this standard deviation became sufficiently small.

Figure 9 is a photograph of the front panel of the controller. The left-most switch can be used to place the controller in a WAIT mode, where it does nothing. In the RUN position, the controller starts to make phase measurements and send these data to a computer connected to it. The next switch determines whether the controller will ("Close Loop") or won't ("Open Loop") adjust the control voltage to achieve phase lock. The left-most two BNC connectors provide the 10 MHz 50 Ω and TTL outputs mentioned earlier. The right-most two BNC connectors are inputs for the Rb oscillator and GPS timing pulse, respectively. The two LEDs above the BNC connectors, marked L1 and L2, show the status of the controller. If both are off, the controller is in WAIT mode. If L1 is blinking once a second, the controller is in RUN mode. If, in addition, L2 is lit, the controller has locked the frequency of the Rb oscillator to the GPS timing pulses. Finally, if both lights are steadily on, the controller has found the phase count too close to its minimum value (0) or to its maximum value (240). In this case, the controller will adjust the control voltage to most rapidly move the phase count into an acceptable range.

Figure 10 is a photograph of the circuit board of the controller with most of the major components labeled. Most components were

surface mounted; the PIC processor was not since I needed to be able to remove it for programming. (If you look closely, you can see two places on the board where I made corrections.) The two switches and the four BNC connectors were mounted directly on the computer board. The control voltage output, the 9 V dc power input, and the serial input/output jack were mounted on the back cover of the enclosure. As you can see from Figure 10, I could have made the board considerably smaller and more compact, and thus saved on fabrication costs.

Figure 11 is a photograph of the entire system. The Rb oscillator is at the lower left in the picture. Sitting on top of it is the GPS Receiver and Interface unit. The frequency controller is at the lower right. You can just see the left-hand part of the computer screen being used to monitor the system.

Testing the Complete System

For testing I connected my notebook computer to the frequency controller through a serial interface as described earlier. I wrote

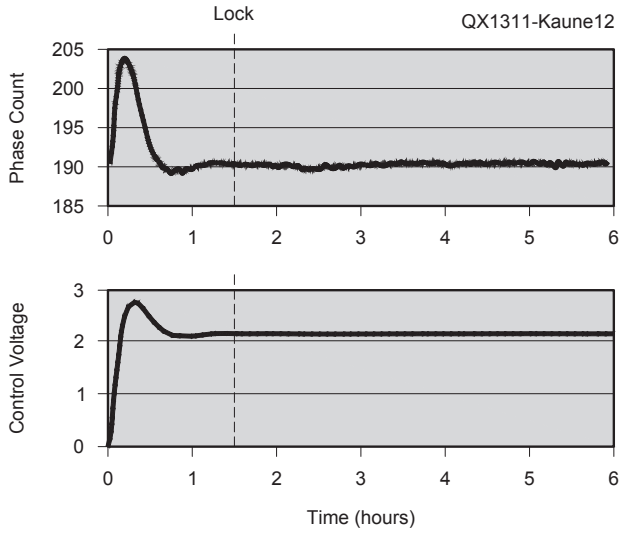

Figure 12 — Test run of the Rubidium-GPS frequency control system. The initial frequency error was –17 mHz.

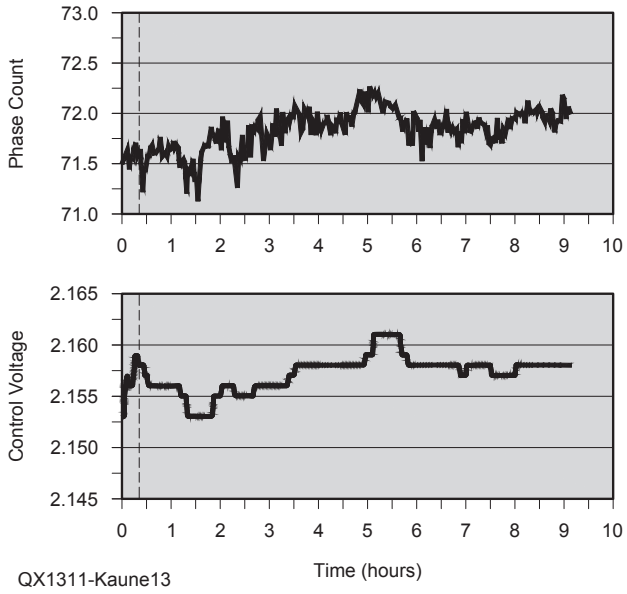

Figure 13 — Here is another test run of the Rubidium-GPS frequency control system. The initial frequency error was very small.

software for the computer using *Visual Basic* Version 6.0. This version of *Visual Basic* includes a serial port (COM) "control" that implements a software interface to the serial port. My application software receives phase count and control voltage data every 2 minutes and additional information regarding when the front-panel Open/Close Loop switch is placed in the Close Loop position and when lock is achieved. The software displays six graphs: Phase count versus time; control voltage versus time; rate of change of phase count versus time; rate of change of control voltage versus time; residual jitter in phase count versus time; and residual jitter in control voltage versus time. The software can also be used to save data for later off-line analysis.

I tested the system in various ways. Figure 12 shows the phase count and control voltage as functions of time during one test where I initially set the control voltage to 0 to induce an initial Rb oscillator frequency error of about –17 mHz. The figure shows an initial transient period, lasting a bit more than 1 hour, where the control voltage is adjusted upwards, initially overshooting its final value of about 2.15 V. The system determined that frequency lock was achieved at 1.45 hours. I could have reduced or eliminated the overshoot by adjusting the phase detector gain and/or the digital filter time constant, but doing so would not have materially decreased, and could have substantially increased, the time to final lock.

A series of tests showed that a control voltage near 2.15 V was consistently needed to bring the error in the frequency of the Rb oscillator to 0. Consequently, I altered the PIC program to always start with an initial control voltage of 2.153 V. Figure 13 shows the results of a test after this change was made. Note that frequency lock was achieved at 0.35 hours. This graph illustrates clearly the noise in the phase count signal. There are at least three sources of noise: the 1 pps quantitization error mentioned earlier that originates from the GPS receiver, the use of a 24 MHz clock to measure time, and time jitter introduced by the digital electronics used to measure phase count. Even allowing for noise, the phase count data in Figure 13 appears to be increasing slightly during the period from lock at 0.35 h to about 5 h; beyond 5 h, the phase count seems to be on average relatively steady. Statistical (regression) analysis confirms this impression and indicated that the slope of phase-count versus time was (0.122 ± 0.009) counts per hour during the period 0.35 h < t < 5 h and was consistent with 0 for $t \geq 5$ h.

A change of phase count of 0.122 in one hour indicates that the Rb oscillator frequency was slightly in error. The maximum phase count change, corresponding to a change of phase of 2π radians, is 240. Thus, the fractional change in phase, during the one hour time period, was 0.122 / 240 = 5.08 × 10^{-4}. Equation 1 also expresses the change in phase, measured in radians, that would occur during a time period of length t resulting from an error, δf_R, in the frequency of the Rb oscillator: $\Delta\theta / 2\pi = -\delta f_R t$. Combining these two, $\delta f_R = -0.122 / (240 \times 3600 \text{ s}) = -0.14$ μHz, a very small error.

The control voltage, shown in Figure 13, exhibits a slight increase during the period 0.35 h < t < 5 h, reflecting the correction necessary to halt the slight increase in phase count discussed in the preceding paragraph. Beyond 5 h, the control voltage is relatively stable. The residual variation in the control voltage, after accounting for the long-term slopes, is about 1.2 mV. From Equation 12, we see that a change in control voltage of 1 V will produce an approximate change in the frequency of the Rb oscillator of 9 mHz. Thus, the residual random variation of the Rb oscillator frequency error is about 1.2 mV × 9 mHz / V = 11 μHz. Based on this and the earlier results, I think the long-term agreement of my Rb oscillator with the GPS standard, when using the GPS system to fine tune its frequency, is about ± 20 μHz, that is, 2 parts in 10^{12}. I do not have the equipment necessary to measure the short-term time jitter, or equivalently phase noise, of my Rb oscillator. Others have done these measurements, however, and report phase noise at 0.1, 1, 10, 100, and 1000 Hz and greater of –60, –76, –96, –135, and < –150 dBc/Hz, respectively.

My main motivations for this project were to determine that my Rb frequency standard was working properly and also as an educational undertaking. I learned a number of things, especially about the GPS system, serial interfaces, digital filters, and phase-locked-loops. Also, I now have a frequency standard that is extremely accurate. I use it to calibrate an HP frequency counter I purchased on eBay, and my transceiver. I cannot calibrate these units to accuracies any better than 0.1 Hz and 10 Hz, respectively, so the fact that my standard is accurate to ± 20 μHz instead of 3 mHz is really not important. Lately, I have been thinking about designing and building a receiver for use in the ARRL's periodic frequency measuring test that could make better use of this frequency standard.

Bill Kaune, W7IEQ, is a retired physicist (BS, 1966; PhD, 1973). He is married, has two grown daughters, four grandchildren, and a standard poodle. Bill spent most of his career collaborating with biologists and epidemiologists researching the biological effects of power-frequency electric and magnetic fields. Along with Amateur Radio, Bill spends his time hiking and backpacking. Bill was first licensed in 1956 as a Novice and then a General, became inactive while in college, and was licensed again in 1998. He upgraded to the Amateur Extra class in 2000. Bill is currently the president of the Jefferson County Amateur Radio Club, a member of the ARRL and the ARRL RF Safety Committee, and a fellow of the IEEE.

Jeremy Clark, VE3PKC

500 Duplex Ave, Apt 506, Toronto, ON M4R 1V6, Canada; **clarkj@rogers.com**

Build Amateur Radio Systems Using Scicoslab/Modnum

Simulation software gives us powerful tools to analyze the operation of a communications system before actually building any hardware.

I find that a good way to understand a circuit or system is to build a model of the circuit, and study the model's performance. *Scicoslab* and the *ModnumToolbox* are powerful freely available open source tools that allow you to quickly see how your system behaves.[1, 2] If you have a great idea about a new Amateur Radio project, why not build it in software just to make sure it behaves the way you want it to, before buying all the components? By laying out the various modules of your circuit in software, you will find new insights into your design that you were not even aware of.

[1]Notes appear on page 42.

Download and install *Scicoslab* first. It is available for PC, Mac and Linux. Next download and install *Modnum*. *Scicoslab* has a terminal like desktop. *Scicos* is the graphical user interface (GUI) that runs on top of *Scicoslab*. *Modnum* is one of the toolboxes available in *Scicos*. Start *Scicoslab* and open the editor. The editor runs script or *C* language like programs.

Open the *Modnum* **loader.sce** file in the editor and run it. (This file is part of the *Modnum* installation package.) Then under Applications, launch *Scicos*. You can also download a short tutorial on using *Scicoslab* and *Modnum* at the Scicos website.[3]

Figure 2 shows the layout of a hypothetical SSB modulator and demodulator circuit that we want to test. The file is available for download from the ARRL *QEX* files website.[4] Go to www.arrl.org/qexfiles and look for the file **11x13_Clark.zip**. Note the various blocks and their location in the Palette Tree shown in Figure 3.

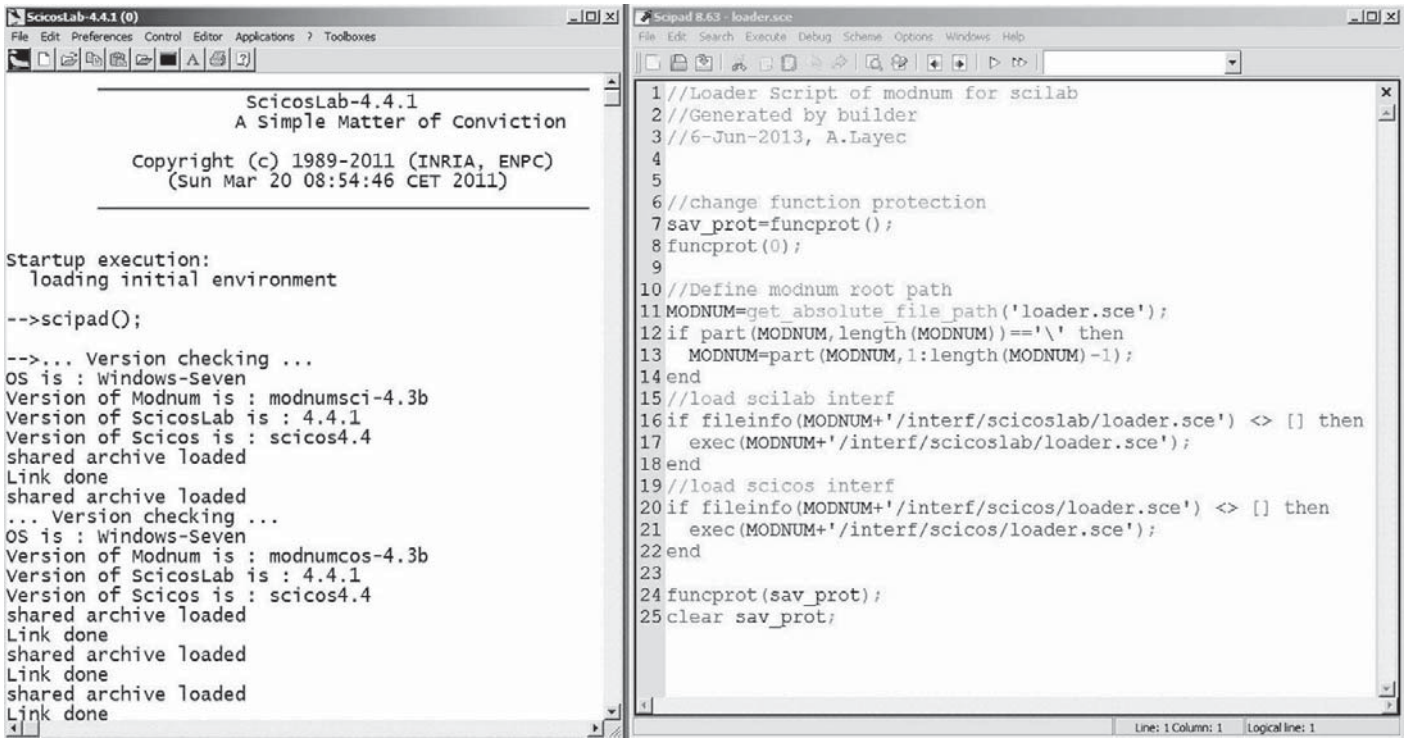

Figure 1 — This is a screenshot of the Modnum Loader File, with the file loader.sce open.

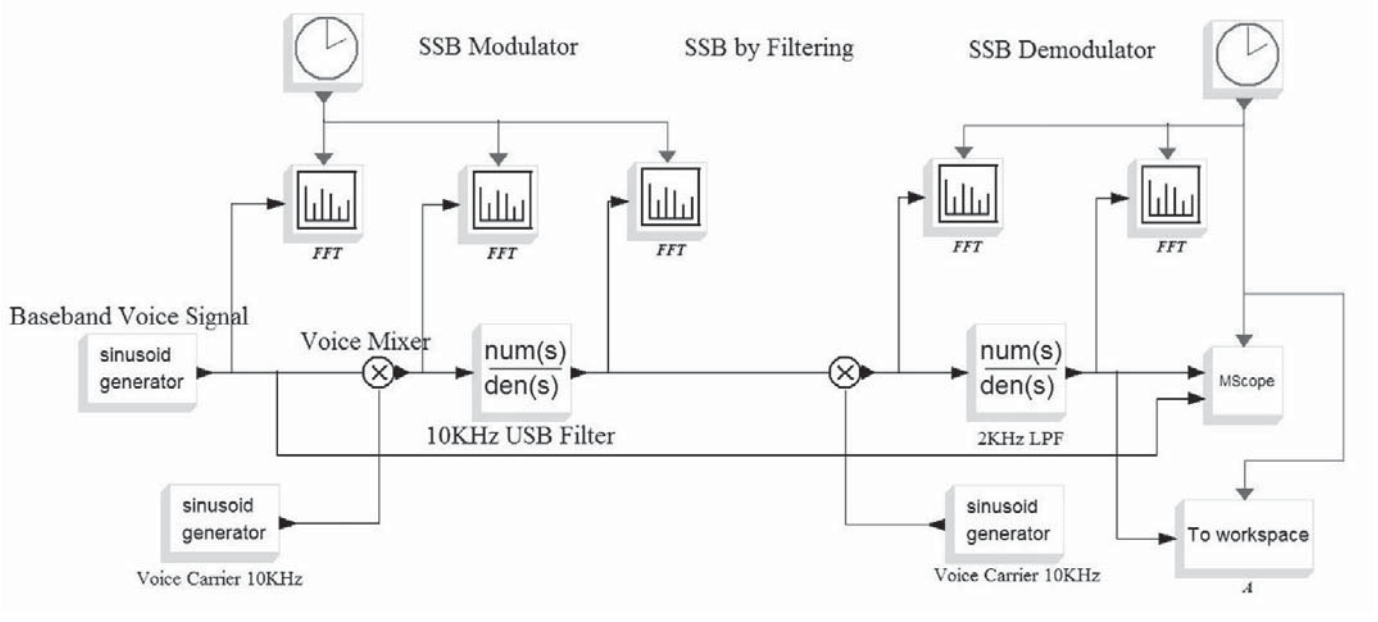

Figure 2 — SSB modulator and demodulator, from the file ssb_filtering_tone.cos.

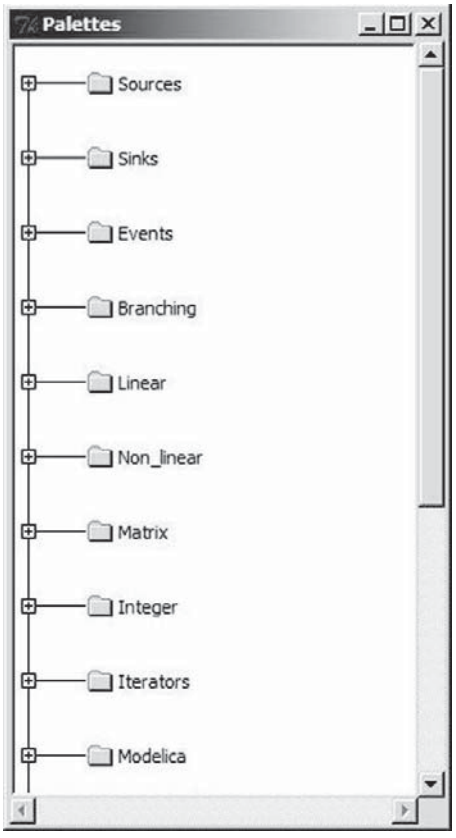

Figure 3 — Palettes Menu and Block Locations.

Scicos Block	*Palette Location*
Sinusoid Generator	Sources
Timer	Sources
FFT Spectrum Analyzer	Modnum/Sinks
Mixer	Non Linear
Transfer Function num(s)/den(s)	Linear
To Workspace A	Sinks
Text	Others

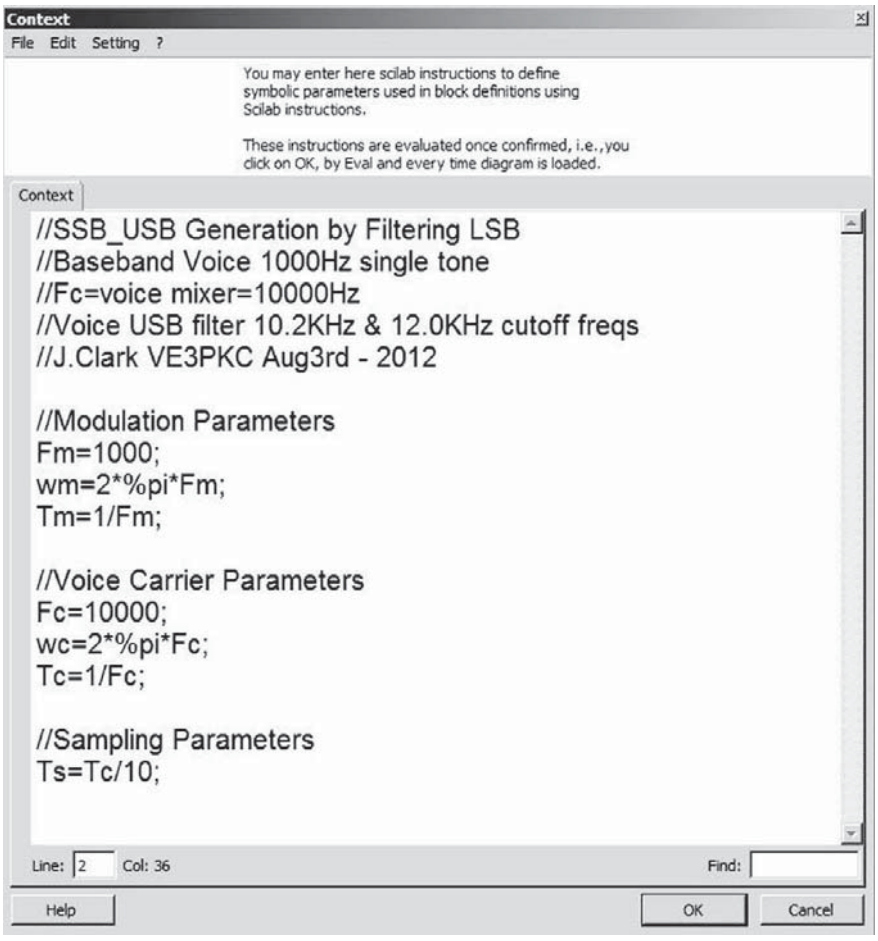

Figure 4 — Context Showing Definition of Run-Time Variables.

Locate the various blocks and drag them onto the open file. Save your file right away. Connect the modules by left clicking/holding on a source arrow, and dragging to an input. When you are over the input, release the mouse button. To form a branch, double click/hold on the wire and drag it to the required input. You may want an intermediate click to form a right angle turn. The next thing to do is define the run time variables. You do this in the "Context" menu. This is available under the "Diagram" menu item. See Figure 4. You can enter data into all the various blocks, but this becomes difficult to modify when you have many blocks. It is more convenient to assign a variable and give it a value in the Context, which can be changed any time.

In our example, we are defining the Voice band frequency of 1 kHz and the Voice carrier frequency of 10 kHz. Note that we also define the angular frequency $\omega = 2\pi f$, as this is required for the Sinusoidal generator. Note that in Scicoslab, π is denoted by "%pi." We also define a clock frequency. I usually choose 10× the highest frequency in the diagram, so that waveforms look smooth and not piecewise linear. Note that in order to use the FFT spectrum analyzer, you have to have a clock frequency at least twice 2× the highest frequency.

Once you have defined the run time variables, save them and enter them into the various blocks. Figure 5 shows examples of entering data into blocks.

In this case we enter the angular frequency, ωm, and sampling period, Ts. Of particular interest is the setup of the spectrum analyzer FFT and scope. This is shown in Figure 6.

For the FFT spectrum analyzer, the default settings are used except for the Sampling period, which is set to "Ts" and the Inherit, which is set to "0" for use with an external clock. For the scope, all default settings are used except for Ymin/max settings, which are adjusted to reflect the required voltage ranges, and the refresh period, which is set to equal the Setup run time. The "Accept herited events" is also set to "0." The scope can have more traces if required, just enter "1" into each Input Port size as required, and match with Ymin/max and Refresh periods.

The Setup time is found under the Simulation menu. Generally you need to have this set so that you have enough samples for the FFT. If the simulation results in no graph on the FFT, then increase the setup time.

Let's consider the filter designs using the linear transfer function num(s)/den(s). For a Butterworth normalized ($\omega c = 1$) low pass filter of order n, H(s) is as defined by Wikipedia.[5] Table 1 gives the transfer

Table 1
Butterworth Normalized Low Pass Filter Transfer Function D(s)

n = 1	$(1 + s)$
n = 2	$(1 + 1.4142\ s + s^2)$
n = 3	$(1 + 2s + 2\ s^2 + s^3)$
n = 4	$(1 + 2.6132\ s + 3.4143061\ s^2 + 2.6132\ s^3 + s^4$

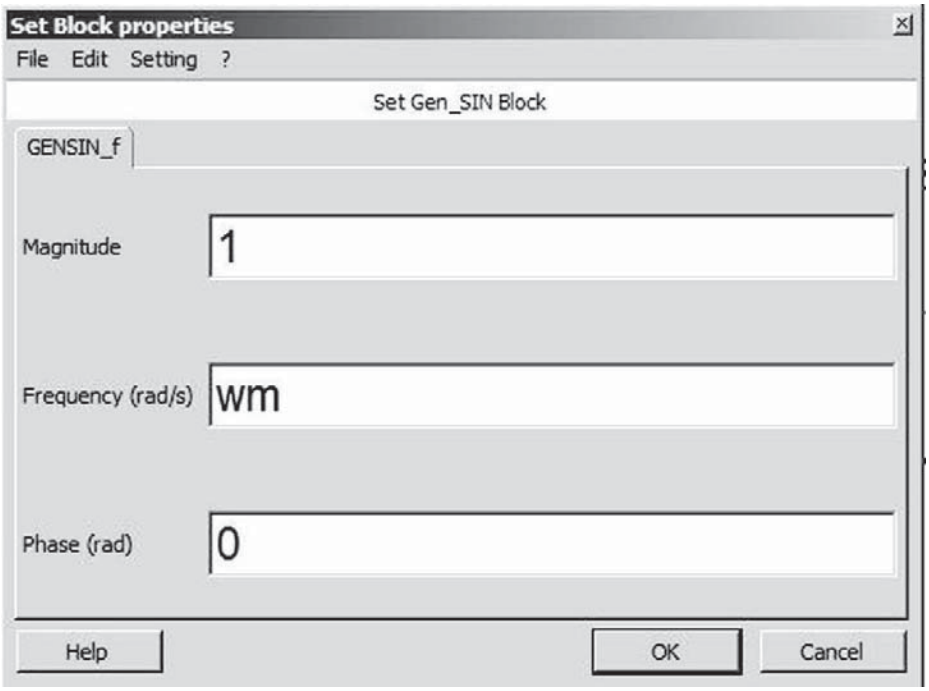

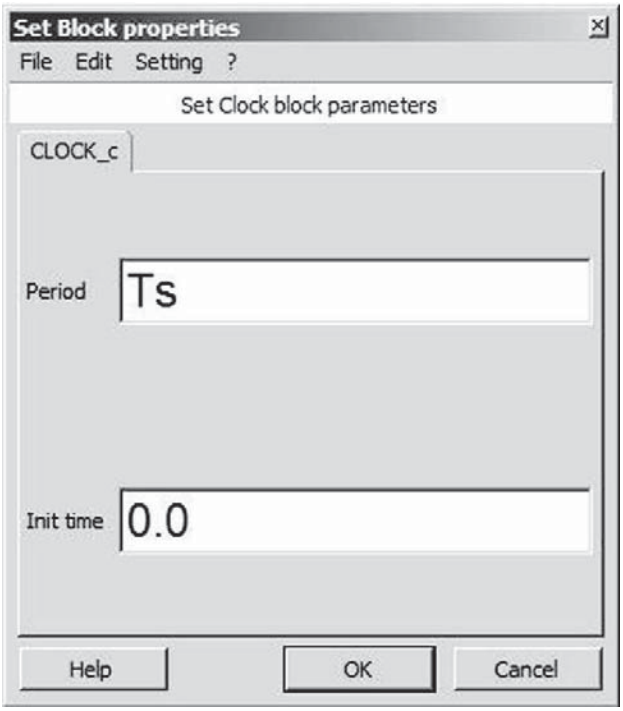

Figure 5 — Entering Variables into Blocks.

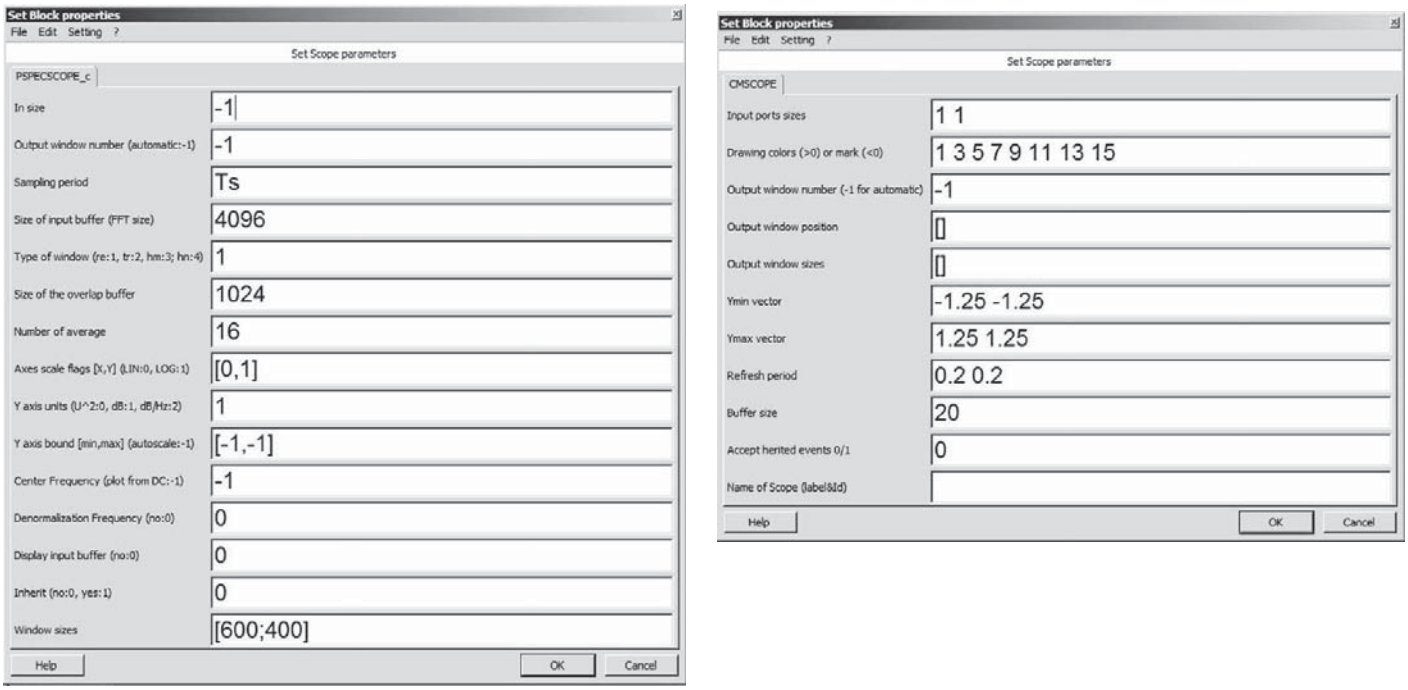

Figure 6 — Spectrum Analyzer and Scope Settings.

functions for n = 1, 2, 3 and 4. We can then write the normalized polynomials D(s), in Equation 1.

$$H(s) = Gain \times \frac{N(s)}{D(s)} = \frac{Gain}{D(s)} \quad \text{[Eq 1]}$$

To convert a normalized low pass filter to a low pass filter, high pass filter or band pass filter, we use the transformations given in Table 2. (See *Digital Signal Processing* by Andreas Antoniou, page 516.[6])

Now we can design the 10 kHz USB filter according to the following rules.

- Lower 3 dB Frequency = 10.2 kHz, ωp1 = 2 × %pi × 10.2 kHz = 64.089 krad/s.
- Upper 3 dB Frequency = 12.0 kHz, ωp2 = 2 × %pi × 12.0 kHz = 75.398 krad/s.
- B = Filter Bandwidth = ωp2 – ωp1 = (12.0 – 10.2) × 2 × %pi = 11.310 krad/s.
- ω0 = sqrt (ωp1 × ωp2) = 69.514 krad/s.
- n = Filter order = 2 nd

The file **bpf_butt2_10k_usb.sce** is a script file that generates the polynomial H(s) that can be used to generate the 10 kHz USB filter. The response is shown in Figure 7. Once we have H(s), then we can enter the polynomials into the Scicos block num(s)/den(s). You can use notepad to cut and paste the coefficients, and then modify them in the block. Figure 8 shows the coefficients. A similar file, **lpf_butt2_2k.sce** is used to generate H(s) for the 2 kHz receiver low pass receiver. This is shown in Figure 9.

Now that we have all the blocks completed, we can run the Scicos simulation. We can use the various spectrum analyzers to study the filter action at the various points of the circuit.

Figure 10A shows the single baseband tone of 1000 Hz at –6 dB. Figure 10B shows the mixing process, which produces two tones at 10 kHz ± 1 kHz = 9 kHz and 11 kHz at 0 dB. (The carrier amplitude is adjusted so that the tones are at the 0 dB reference level). Figure 10C shows the band pass filtering action selecting the USB tone at 11 kHz and rejecting the LSB tone at 9 kHz. The rejection is approximately 20 dB. More rejection could be accomplished by using a 4th order band pass filter, such as the one defined in the file **bpf_butt4_usb.sce**.

Figure 10D shows the receiver mixing action with the baseband tone at 1 kHz and the double carrier term at 20 kHz. Figure 10E shows the action of the receiver low pass filter knocking down the double carrier term by approx 40 dB. More rejection could be accomplished as before with a 4th order filter, as defined in the file **lpf_butt4_2k.sce**. Finally, Figure 10G shows the recovered 1 kHz tone versus the original transmit tone of 1 kHz. Note the transmission filter delay of approx 80 μs.

Scicos can be used to build almost any type of circuit, both analog and digital. Figure 11, for example, shows a QAM Modulator. QAM is a basic building block in all modern digital telecommunications systems.

For a complete guide to using Scicoslab including how to design your own functions and Scicos blocks, see *Modeling and Simulation in Scilab/Scicos with ScicosLab 4.4*.[7]

Table 2

Normalized Low Pass Filter Transformations to LPF, HPF, BPF

Normalized LPF to LPF	ωc = new cut-off frequency, rad/s	s = s / ωc
Normalized LPF to HPF	ωc = new cut-off frequency, rad/s	s = ωc / s
Normalized LPF to BPF	ωp2 = upper cut-off frequency, rad/s ωp1 = lower cut-off frequency rad/s B = (ωp2 – ωp1) = Filter Bandwidth ω0 = sqrt (ωp1 x ωp2)	$s = \frac{s^2 + \omega_0^2}{B \times s}$

```
//Band Pass Filter Butterworth 2nd order
//Fp1=lower band pass cutoff frequency
//Fp2=upper band pass cutorf frequency
//F0=band pass center frequency
//J.Clark Aug3rd - 2012

Fp1=10200;
wp1=2*%pi*Fp1;
Fp2=12000;
wp2=2*%pi*Fp2;
w0=(wp1*wp2)^0.5;
B=wp2-wp1;

clf()
s=poly([0],'s')
ns=1
ds=1+1.4142*s+s^2
ds=horner(ds,((s^2+wp1*wp2)/(B*s)))
hs=ns/ds
fr=0.01:10:100000;
wr=2*%pi*fr;
hf=freq(hs(2),hs(3),%i*wr);
hm=abs(hf);
plot2d1(wr,20*log10(hm),logflag='ln')
```

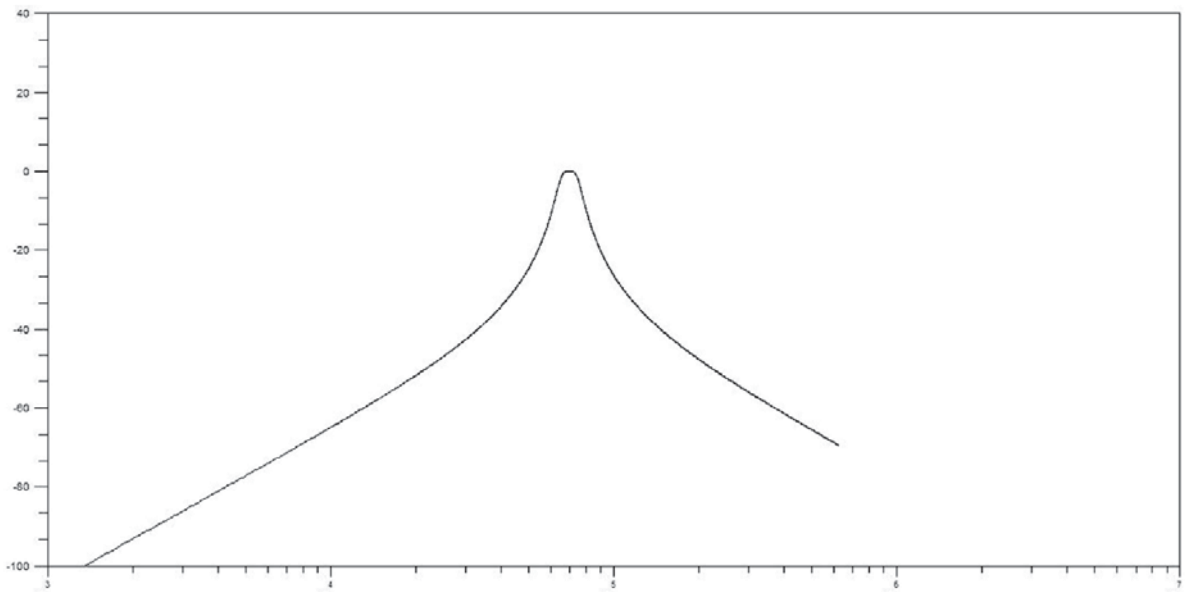


```
hs =

                        2
              1.279D+08s
-----------------------------------------
                                          2
2.335D+19 + 7.729D+13s + 9.792D+09s
                    3    4
    + 15994.225s  + s
```

Figure 7 — Part A shows the file bpf_butt2_10k_usb.sce and Part B shows the filter response.

Jeremy Clark, VE3PKC, is an ARRL Member who earned his Amateur Radio Operator's Certificate in 1966 (VE2BOT). He earned his Advanced Radio Operator's Certificate in 1973. He holds a Bachelor's Degree in electrical engineering from McGill University and a Masters Degree in electrical engineering from Concordia University in Montreal, Canada.

Jeremy worked in the Canadian Telecommunications industry for 21 years as a Transmission Systems Engineer, primarily working with UHF and Microwave relay systems. He then taught Telecommunications Engineering Technology in the Canadian College system for 16 years. He now works as a design engineer, specializing in remote area telecommunications and simulation systems. He holds several US patents on telecom design. He is also the author of Learning Telecommunications by Simulation.

Notes

[1]For more information and to download the Scicoslab software, go to: **www.scicoslab.org/**.

[2]The Modnum Toolbox is available for download at: **www.scicos.org/ScicosModNum/modnum_web/web/eng/eng.htm**.

[3]There is a short course on using Scicoslab and Modnum on the Scicos.org website: **www.scicos.org/Download/learn_tel_by_sim_short.zip**.

[4]The files described in this article are available for download from the ARRL *QEX* files website. Go to **www.arrl.org/qexfiles** and look for the file **11x13_Clark.zip**.

[5]To learn more about Butterworth filters and their design, see: **en.wikipedia.org/wiki/Butterworth_filter**.

[6]Andreas Antoniou, *Digital Signal Processing*, McGraw-Hill, ISBN 0-07-145424-1.

[7]Stephen L. Campbell, Jean-Philippe Chancelier, and Ramine Nikoukhah, *Modeling and Simulation in Scilab/Scicos with ScicosLab 4.4*, Springer ISBN 978-1-4419-5526-5.

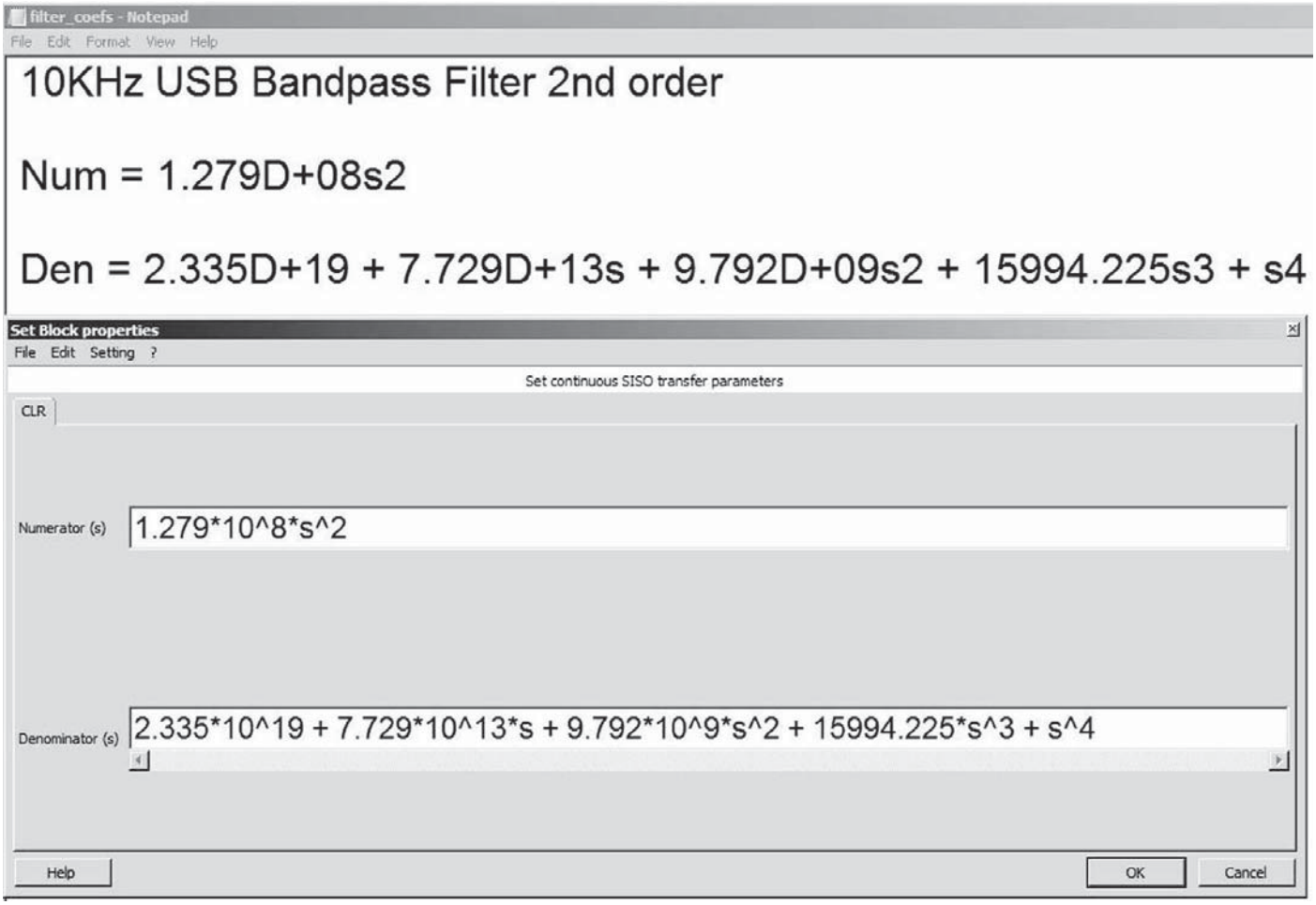

Figure 8 — Entering Coefficients into num(s)/den(s) for 10 kHz USB Filter.

Scipad 8.63 - lpf_butt2_2k.sce

File Edit Search Execute Debug Scheme Options Windows Help

```
1 //Low Pass Filter Butterworth 2nd order
2 //J.Clark Aug3rd - 2012
3 Fc=2000;
4 wc=2*%pi*Fc;
5
6 clf()
7 s=poly([0],'s')
8 ns=1
9 ds=1+1.4142*s+s^2
10 hs=ns/ds
11 hs=horner(hs,s/wc)
12 fr=0.01:1:10000;
13 wr=2*%pi*fr;
14 hf=freq(hs(2),hs(3),%i*wr);
15 hm=abs(hf);
16 plot2d1(wr,20*log10(hm),logflag='ln')
```

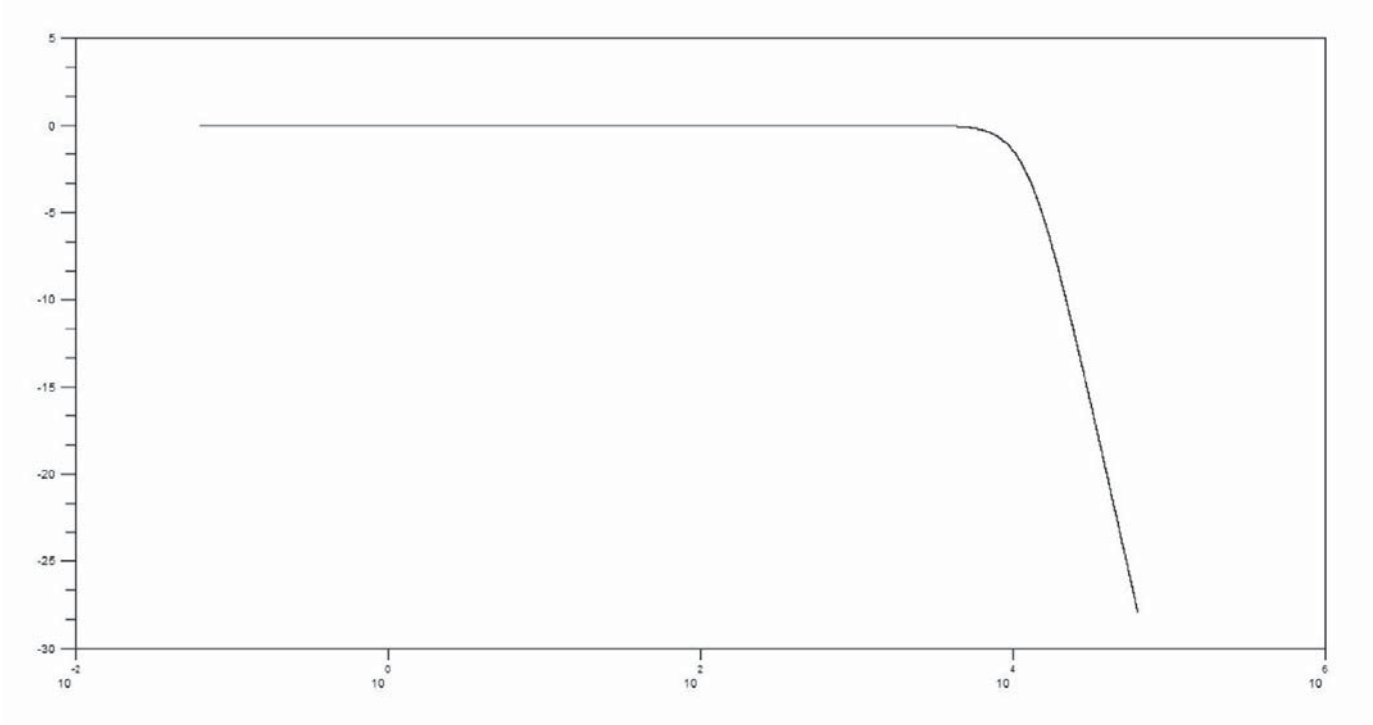

$$hs = \frac{1}{1 + 0.0001125s + 6.333D\text{-}09s^2}$$

Figure 9 — Part A shows the file lpf_butt2_2k.sce and Part B shows the filter response.

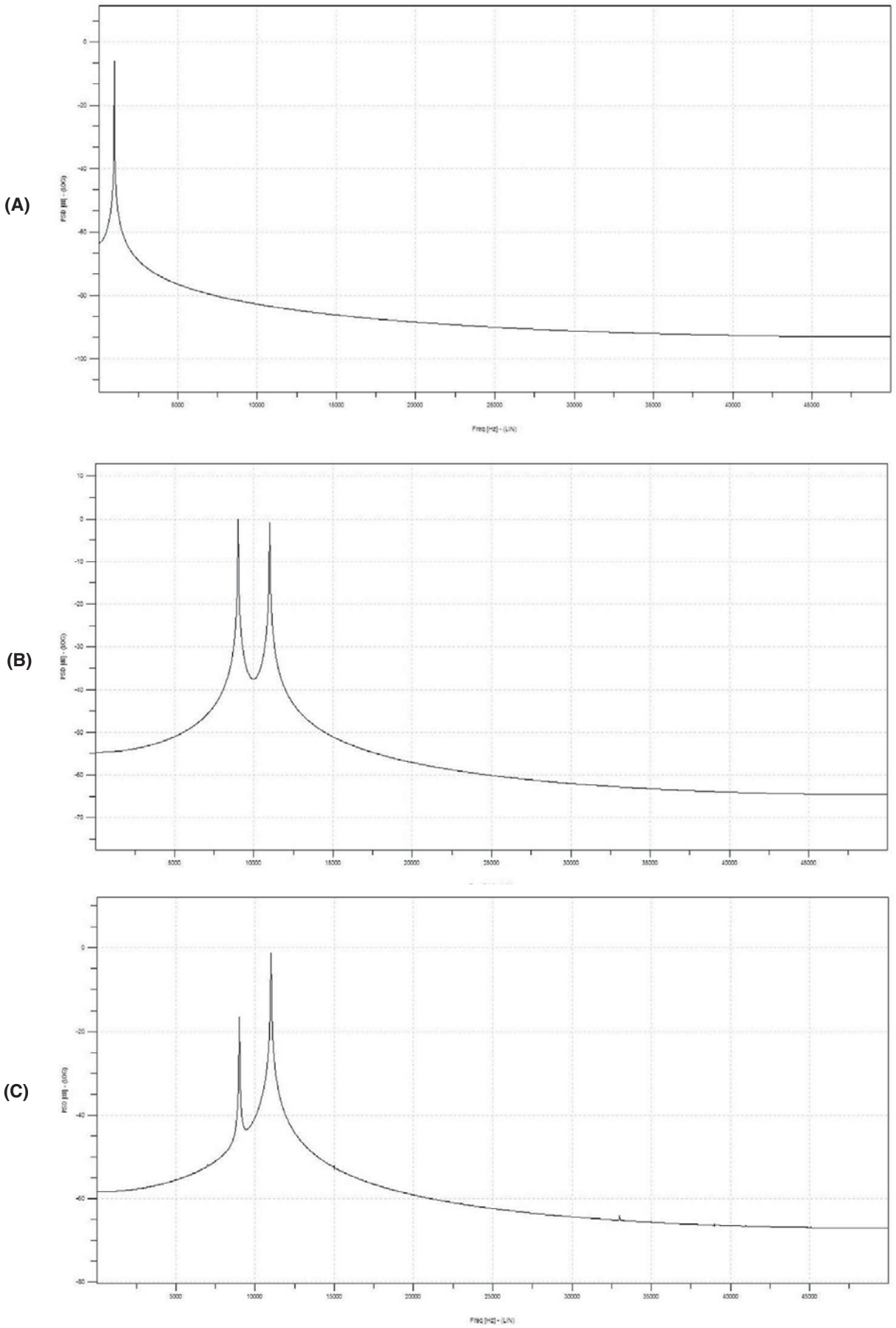

Figure 10 — Various spectrum analyzer responses to the simulation we have created. See the text for explanations of each plot.

(D)

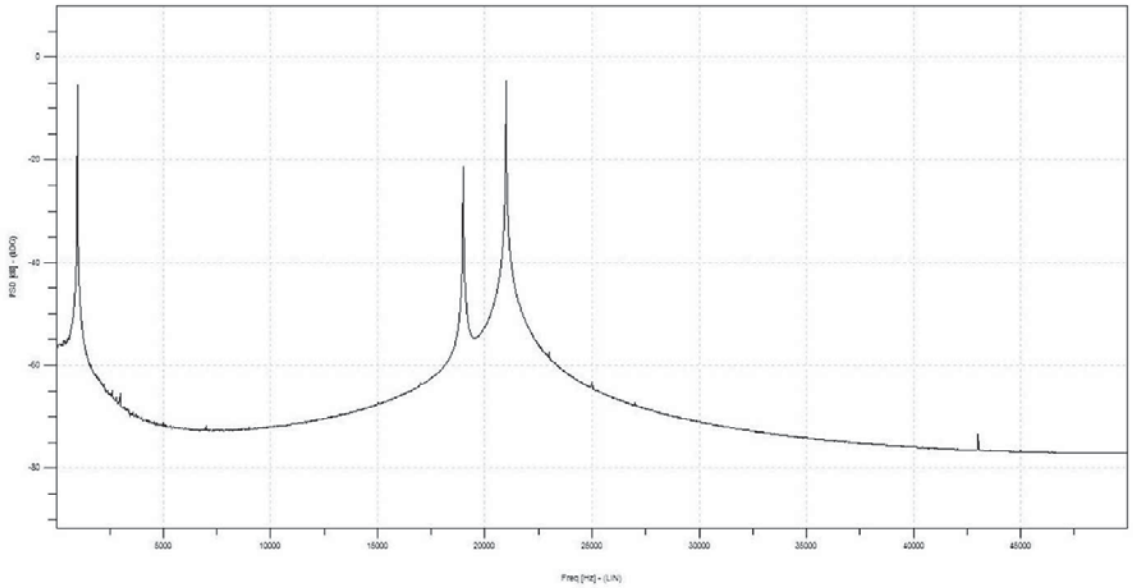
0
-20
-40
-60
-80
5000
10000
15000
20000
25000
30000
35000
40000
45000

(E)

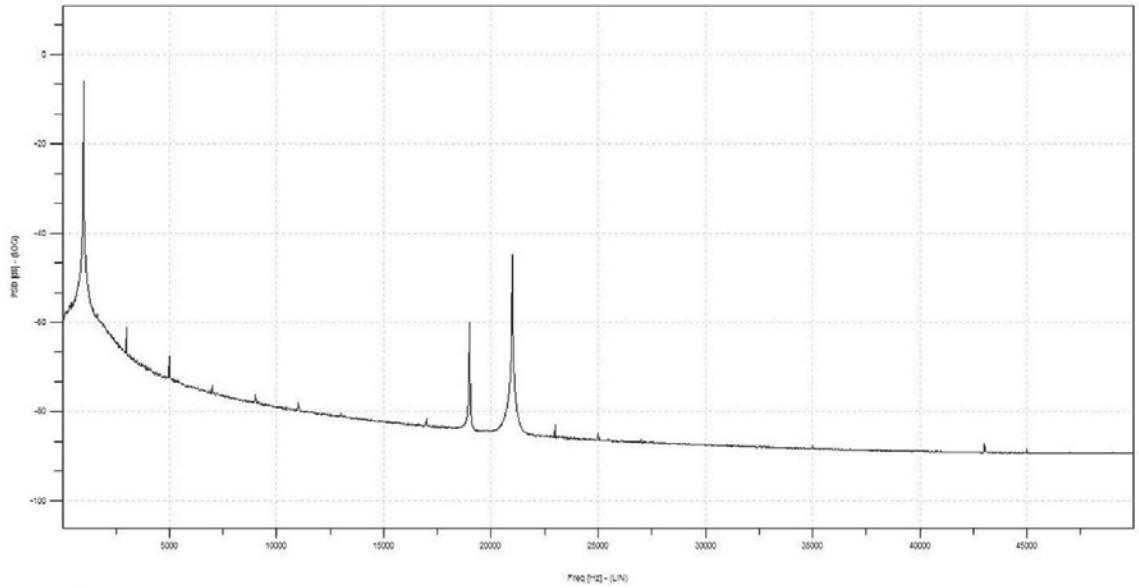
0
-20
-40
-60
-80
-100
5000
10000
15000
20000
25000
30000
35000
40000
45000

(F)

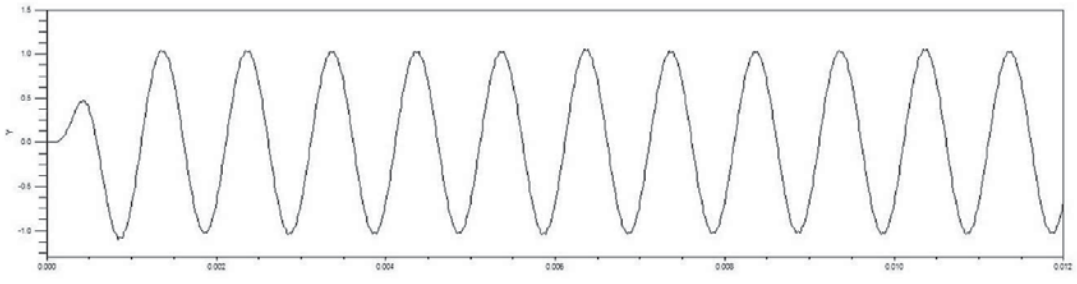
1.5
1.0
0.5
0.0
-0.5
-1.0
0.000
0.002
0.004
0.006
0.008
0.010
0.012

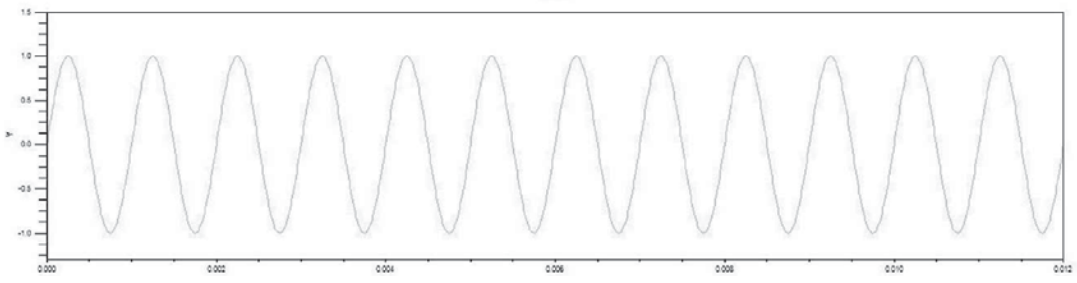
1.5
1.0
0.5
0.0
-0.5
-1.0
0.000
0.002
0.004
0.006
0.008
0.010
0.012

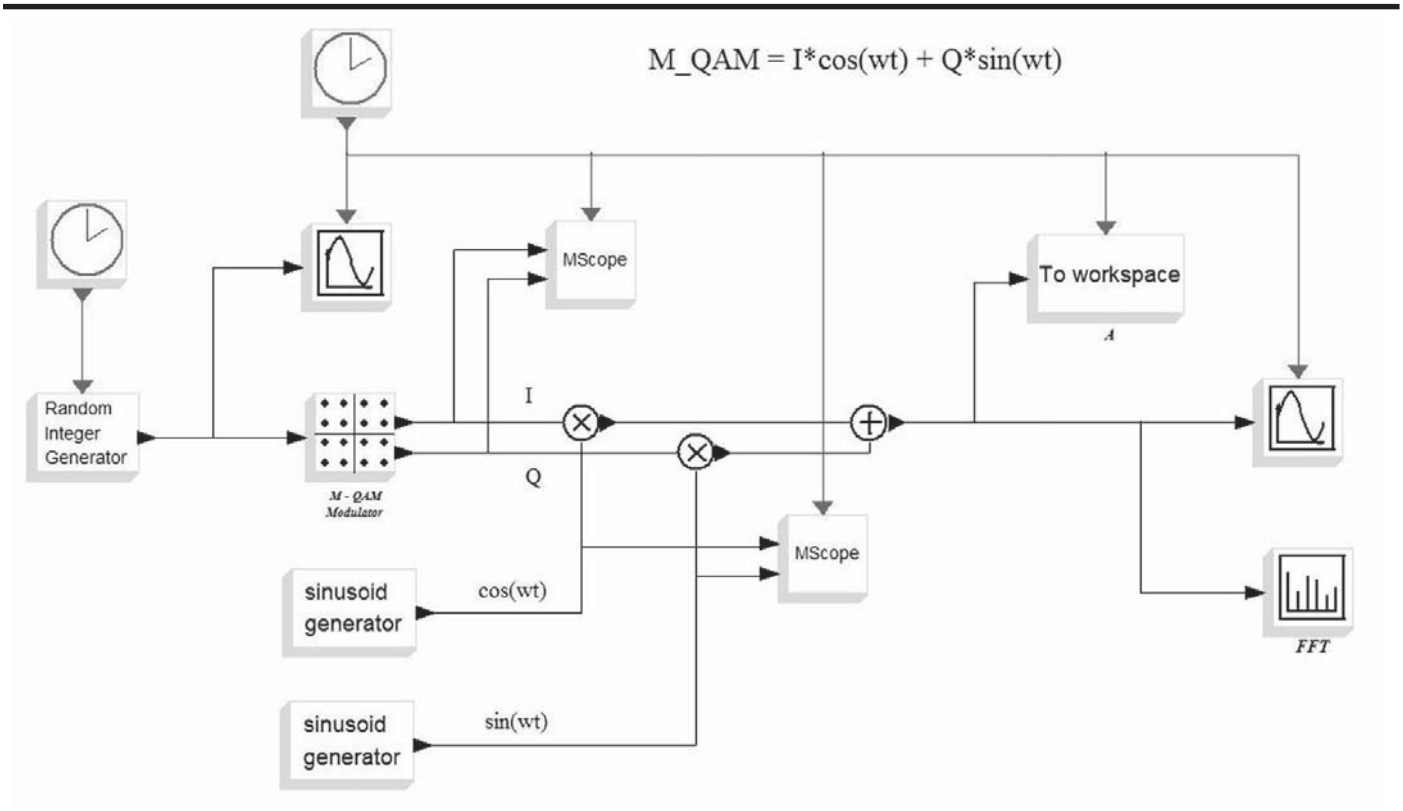

Figure 11 — QAM Modulator displayed from the file qam_rnd_data.cos

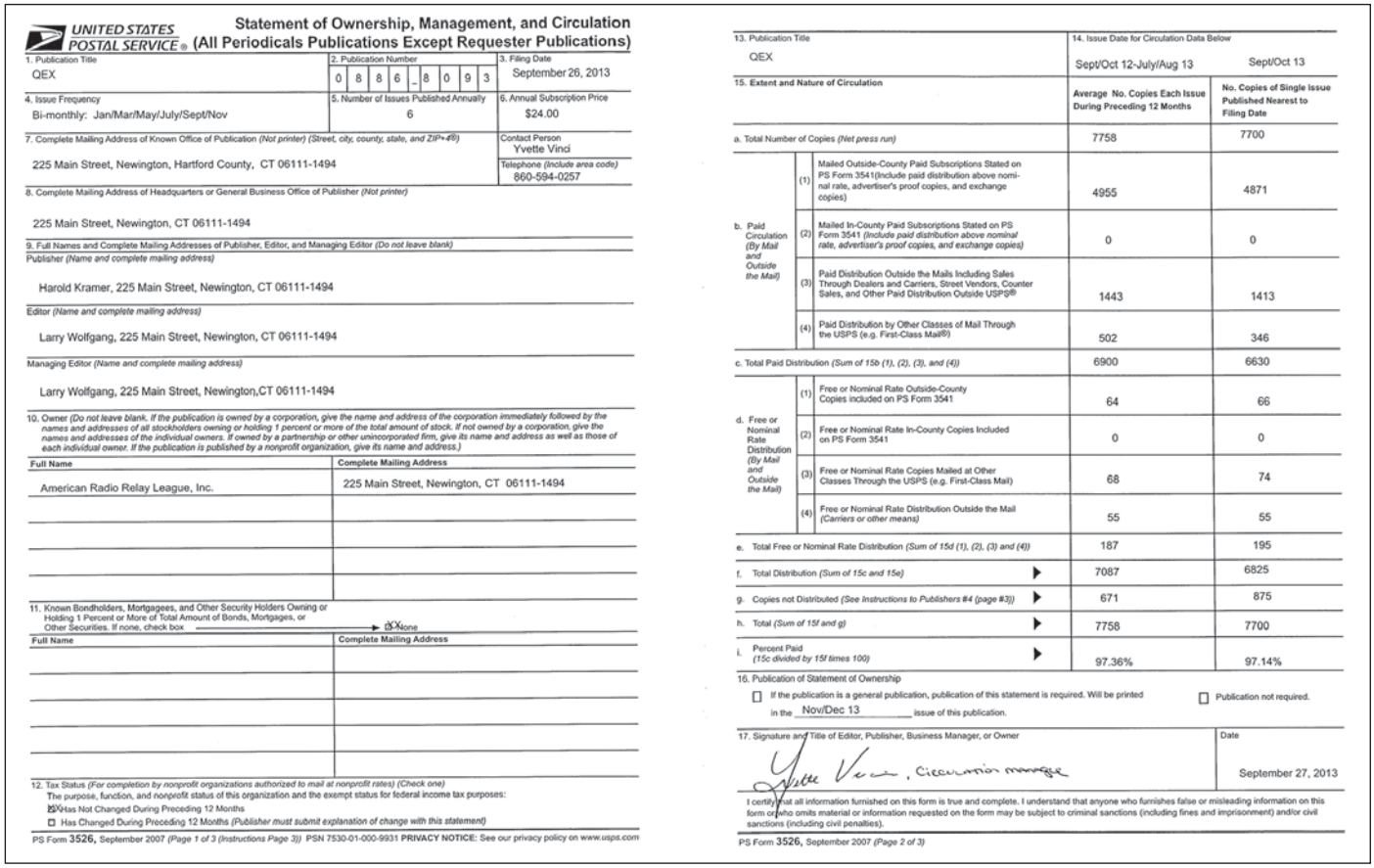

UNITED STATES POSTAL SERVICE®

Statement of Ownership, Management, and Circulation (All Periodicals Publications Except Requester Publications)

1. Publication Title	2. Publication Number	3. Filing Date
QEX	0 8 8 6 - 8 0 9 3	September 26, 2013
4. Issue Frequency	5. Number of Issues Published Annually	6. Annual Subscription Price
Bi-monthly: Jan/Mar/May/July/Sept/Nov	6	$24.00

7. Complete Mailing Address of Known Office of Publication (Not printer) (Street, city, county, state, and ZIP+4®)
225 Main Street, Newington, Hartford County, CT 06111-1494
Contact Person: Yvette Vinci
Telephone (Include area code): 860-594-0257

8. Complete Mailing Address of Headquarters or General Business Office of Publisher (Not printer)
225 Main Street, Newington, CT 06111-1494

9. Full Names and Complete Mailing Addresses of Publisher, Editor, and Managing Editor (Do not leave blank)
Publisher (Name and complete mailing address)
Harold Kramer, 225 Main Street, Newington, CT 06111-1494
Editor (Name and complete mailing address)
Larry Wolfgang, 225 Main Street, Newington, CT 06111-1494
Managing Editor (Name and complete mailing address)
Larry Wolfgang, 225 Main Street, Newington,CT 06111-1494

10. Owner (Do not leave blank. If the publication is owned by a corporation, give the name and address of the corporation immediately followed by the names and addresses of all stockholders owning or holding 1 percent or more of the total amount of stock. If not owned by a corporation, give the names and addresses of the individual owners. If owned by a partnership or other unincorporated firm, give its name and address as well as those of each individual owner. If the publication is published by a nonprofit organization, give its name and address.)

Full Name	Complete Mailing Address
American Radio Relay League, Inc.	225 Main Street, Newington, CT 06111-1494

11. Known Bondholders, Mortgagees, and Other Security Holders Owning or Holding 1 Percent or More of Total Amount of Bonds, Mortgages, or Other Securities. If none, check box → ☒ None

Full Name	Complete Mailing Address

12. Tax Status (For completion by nonprofit organizations authorized to mail at nonprofit rates) (Check one)
The purpose, function, and nonprofit status of this organization and the exempt status for federal income tax purposes:
☒ Has Not Changed During Preceding 12 Months
☐ Has Changed During Preceding 12 Months (Publisher must submit explanation of change with this statement)

PS Form 3526, September 2007 (Page 1 of 3 (Instructions Page 3)) PSN 7530-01-000-9931 PRIVACY NOTICE: See our privacy policy on www.usps.com

13. Publication Title	14. Issue Date for Circulation Data Below	
QEX	Sept/Oct 12-July/Aug 13	Sept/Oct 13
15. Extent and Nature of Circulation	Average No. Copies Each Issue During Preceding 12 Months	No. Copies of Single Issue Published Nearest to Filing Date
a. Total Number of Copies (Net press run)	7758	7700
b. Paid Circulation (By Mail and Outside the Mail) (1) Mailed Outside-County Paid Subscriptions Stated on PS Form 3541(Include paid distribution above nominal rate, advertiser's proof copies, and exchange copies)	4955	4871
b. Paid Circulation (By Mail and Outside the Mail) (2) Mailed In-County Paid Subscriptions Stated on PS Form 3541 (Include paid distribution above nominal rate, advertiser's proof copies, and exchange copies)	0	0
b. Paid Circulation (By Mail and Outside the Mail) (3) Paid Distribution Outside the Mails Including Sales Through Dealers and Carriers, Street Vendors, Counter Sales, and Other Paid Distribution Outside USPS®	1443	1413
b. Paid Circulation (By Mail and Outside the Mail) (4) Paid Distribution by Other Classes of Mail Through the USPS (e.g. First-Class Mail®)	502	346
c. Total Paid Distribution (Sum of 15b (1), (2), (3), and (4))	6900	6630
d. Free or Nominal Rate Distribution (By Mail and Outside the Mail) (1) Free or Nominal Rate Outside-County Copies included on PS Form 3541	64	66
d. Free or Nominal Rate Distribution (By Mail and Outside the Mail) (2) Free or Nominal Rate In-County Copies Included on PS Form 3541	0	0
d. Free or Nominal Rate Distribution (By Mail and Outside the Mail) (3) Free or Nominal Rate Copies Mailed at Other Classes Through the USPS (e.g. First-Class Mail)	68	74
d. Free or Nominal Rate Distribution (By Mail and Outside the Mail) (4) Free or Nominal Rate Distribution Outside the Mail (Carriers or other means)	55	55
e. Total Free or Nominal Rate Distribution (Sum of 15d (1), (2), (3) and (4))	187	195
f. Total Distribution (Sum of 15c and 15e)	7087	6825
g. Copies not Distributed (See Instructions to Publishers #4 (page #3))	671	875
h. Total (Sum of 15f and g)	7758	7700
i. Percent Paid (15c divided by 15f times 100)	97.36%	97.14%

16. Publication of Statement of Ownership
☐ If the publication is a general publication, publication of this statement is required. Will be printed in the Nov/Dec 13 issue of this publication. ☐ Publication not required.

17. Signature and Title of Editor, Publisher, Business Manager, or Owner — Date
Yvette Vinci, Circulation Manager — September 27, 2013

I certify that all information furnished on this form is true and complete. I understand that anyone who furnishes false or misleading information on this form or who omits material or information requested on the form may be subject to criminal sanctions (including fines and imprisonment) and/or civil sanctions (including civil penalties).

PS Form 3526, September 2007 (Page 2 of 3)

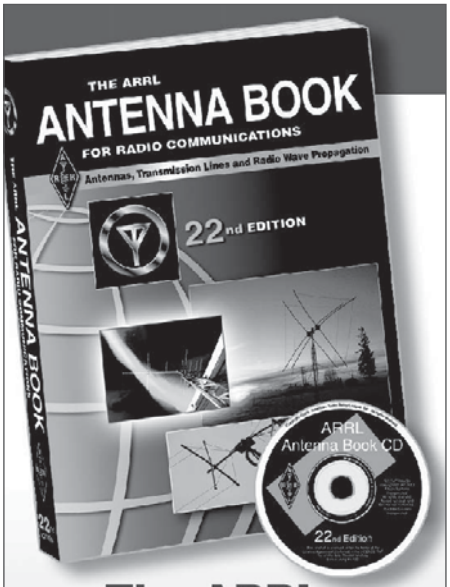

The ARRL Antenna Book

Build One Antenna, and You'll Quickly Find Yourself Planning the Next!

22nd Edition

The *ARRL Antenna Book* includes everything for complete antenna systems—from planning, to design and construction. You'll find antennas for nearly any frequency range and operating application: from the HF low bands through VHF, UHF and microwave; fixed station, portable, mobile, satellite and more.

Includes:

- Antenna Fundamentals
- Dipoles and Monopoles
- The Effects of Ground
- Loop Antennas
- Multielement Arrays
- Log-Periodic Dipole Arrays
- Antenna Modeling
- Single-Band MF and HF Antennas
- Multiband HF Antennas
- HF Yagi and Quad Antennas
- Long-Wire and Traveling-Wave Antennas
- HF Antenna System Design
- VHF and UHF Antenna Systems
- VHF and UHF Mobile Antennas
- Antennas for Space Communications
- Special Applications & Portable Antennas
- Stealth and Limited Space Antennas
- Mobile and Maritime HF Antennas
- Receiving and Direction-Finding Antennas
- Transmission Lines
- Antenna Materials and Construction
- Building Antenna Systems and Towers
- Antenna System Troubleshooting

Softcover Book with CD-ROM
ARRL Order No. 6948
Only $49.95*

*plus shipping and handling

ARRL *The national association for AMATEUR RADIO®*
SHOP DIRECT or call for a dealer near you.
ONLINE WWW.ARRL.ORG/SHOP
ORDER TOLL-FREE 888/277-5289 (US)

QST 5/2013

NEW!

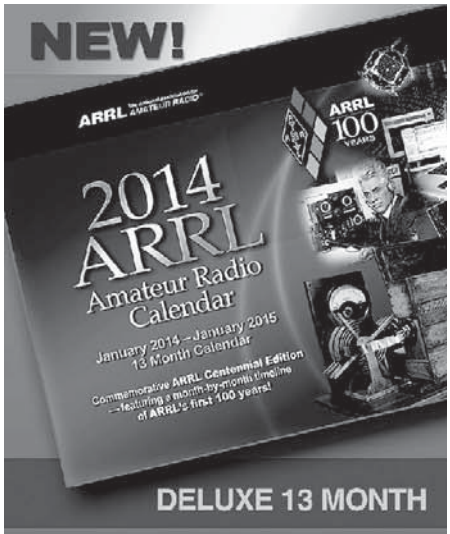

DELUXE 13 MONTH

Amateur Radio Calendar 2014

Commemorative ARRL Centennial Edition—
Featuring a month-by-month timeline of ARRL's first 100 years!

Includes:

- ARRL contests and other major ham radio contests
- National event dates: ARRL Field Day, Kids Day, Jamboree On The Air, and more!
- Phases of the moon
- Meteor showers
- Holidays and other important dates
- 2014 Monthly Planner
- Guide to ARRL Membership Services

2014 ARRL Calendar
ARRL Order No. 0062
Only $12.95*

***Plus shipping and handling.**

ARRL *The national association for AMATEUR RADIO®*
SHOP DIRECT *or call for a dealer near you.*
ONLINE WWW.ARRL.ORG/SHOP
ORDER TOLL-FREE 888/277-5289 (US)

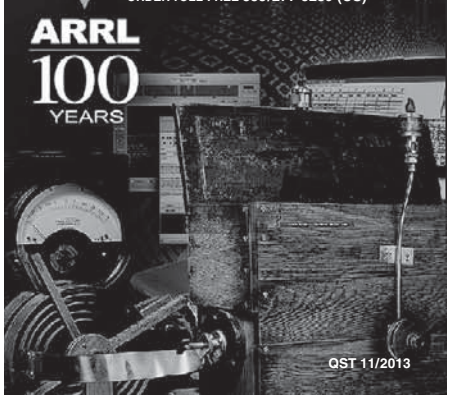

QST 11/2013

NATIONAL RF, INC.

VECTOR-FINDER
Handheld VHF direction finder. Uses any FM xcvr. Audible & LED display
VF-142Q, 130-300 MHz
$239.95
VF-142QM, 130-500 MHz
$289.95

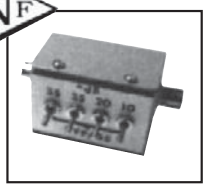

ATTENUATOR
Switchable, T-Pad Attenuator, 100 dB max - 10 dB min BNC connectors
AT-100,
$89.95

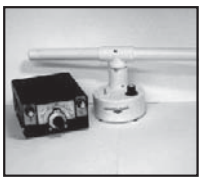

TYPE NLF-2 LOW FREQUENCY ACTIVE ANTENNA AND AMPLIFIER
A Hot, Active, Noise Reducing Antenna System that will sit on your desk and copy 2200, 1700, and 600 through 160 Meter Experimental and Amateur Radio Signals!
Type NLF-2 System:
$369.95

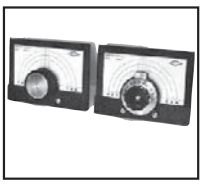

DIAL SCALES
The perfect finishing touch for your homebrew projects. $^1/_4$-inch shaft couplings.
NPD-1, $3^3/_4$ x 2 3/4, 7:1 drive
$34.95
NPD-2, $5^1/_8$ x 3 $^5/_8$, 8:1 drive
$44.95
NPD-3, $5^1/_8$ x 3 $^5/_8$; 6:1 drive
$49.95

NATIONAL RF, INC
7969 ENGINEER ROAD, #102
SAN DIEGO, CA 92111

858.565.1319 FAX 858.571.5909
www.NationalRF.com

We Design And Manufacture To Meet Your Requirements

***Protoype or Production Quantities**

800-522-2253

This Number May Not Save Your Life...

But it could make it a lot easier! Especially when it comes to ordering non-standard connectors.

RF/MICROWAVE CONNECTORS, CABLES AND ASSEMBLIES

- Specials our specialty. Virtually any SMA, N, TNC, HN, LC, RP, BNC, SMB, or SMC delivered in 2-4 weeks.
- Cross reference library to all major manufacturers.
- Experts in supplying "hard to get" RF connectors.
- Our adapters can satisfy virtually any combination of requirements between series.
- Extensive inventory of passive RF/Microwave components including attenuators, terminations and dividers.
- No minimum order.

NEMAL
Cable & Connectors for the Electronics Industry

NEMAL ELECTRONICS INTERNATIONAL, INC.
12240 N.E. 14TH AVENUE
NORTH MIAMI, FL 33161
TEL: 305-899-0900 • FAX: 305-895-8178
E-MAIL: INFO@NEMAL.COM
BRASIL: (011) 5535-2368

URL: WWW.NEMAL.COM

HPSDR is an open source hardware and software project intended to be a "next generation" Software Defined Radio (SDR). It is being designed and developed by a group of enthusiasts with representation from interested experimenters worldwide. The group hosts a web page, e-mail reflector, and a comprehensive Wiki. Visit www.openhpsdr.org for more information.

TAPR is a non-profit amateur radio organization that develops new communications technology, provides useful/affordable hardware, and promotes the advancement of the amateur art through publications, meetings, and standards. Membership includes an e-subscription to the *TAPR Packet Status Register* quarterly newsletter, which provides up-to-date news and user/technical information. Annual membership costs $25 worldwide. Visit www.tapr.org for more information.

NEW!

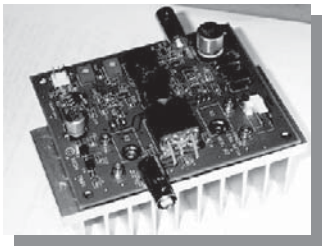

PENNYWHISTLE
20W HF/6M POWER AMPLIFIER KIT

TAPR is proud to support the HPSDR project. TAPR offers five HPSDR kits and three fully assembled HPSDR boards. The assembled boards use SMT and are manufactured in quantity by machine. They are individually tested by TAPR volunteers to keep costs as low as possible. A completely assembled and tested board from TAPR costs about the same as what a kit of parts and a bare board would cost in single unit quantities.

HPSDR Kits and Boards

- **ATLAS** Backplane kit
- **LPU** Power supply kit
- **MAGISTER** USB 2.0 interface
- **JANUS** A/D - D/A converter
- **MERCURY** Direct sampling receiver
- **PENNYWHISTLE** 20W HF/6M PA kit
- **EXCALIBUR** Frequency reference kit
- **PANDORA** HPSDR enclosure

TAPR
PO BOX 852754 • Richardson, Texas • 75085-2754
Office: (972) 671-8277 • e-mail: taproffice@tapr.org
Internet: www.tapr.org • Non-Profit Research and Development Corporation

Array Solutions Your Source for Outstanding Radio Products

Top-ranked Measurement Equipment from Array Solutions

Announcing the: PowerAIM 120
Vector Impedance Analyzer for Broadcast Engineers

- Patented, unique technology offers the broadcast engineer the full capabilities of a single port network analyzer
- Small, lightweight, software-driven instrument
- Easy to carry on airlines and in the field.
- Very simple to set up and use.
- Safe measurements in RF-dense broadcast environments.
- Time Domain Reflectometer (TDR) Functions.

Vector Network Analyzer Model VNA 2180

Measures impedance magnitude, phase and transmission parameters for antennas, filters, and discrete components - using one or two ports.

- Frequency range is 5KHz to 180MHz.
- Data plots include: impedance, SWR, return loss, S11 and S21.
- Plots can be saved for before and after comparisons.
- Dual Smith charts with zoom and rotation.
- Time Domain Reflectometer (TDR) Functions.
- New – 6 port VNA multiplexer for measuring directive arrays including Phase/Magnitude vector scope software.

Bird Wattmeter Digital Display Conversion Kits

Upgrade for your Bird analog watt meter that will transform your Model 43 into a state of the art digital meter!

AS-43A Average Power Reading Bird Wattmeter Kit Digital meter kit
AS-43AP Peak Power Reading Bird Wattmeter Kit Digital meter kit

AIM *uhf* Analyzer

- Frequency range from 5 kHz to 1 GHz.
- Data plots include SWR, RL, R + X, series and parallel, magnitude, phase, and more.
- Dual Smith charts with rotation and 20 markers.
- Plots and calibration files can be saved and used anytime in cvs and dynamic formats.
- AIM 4170C is still in production covering 5kHz to 180 MHz.
- Time Domain Reflectometer (TDR) Functions.

PowerMaster II

- New Larger, Sharp & Fast LCD Display
- Reduced Energy consumption
- USB and RS-232 interface built-in
- New - Both 3kW and 10kW couplers on one display - switched
- Hi / Lo Power Level Monitoring
- Supports 2 like couplers simultaneously (3kW & 3kW, 3kW & V/UHF, 10kW & 10kW)
- SWR Threshold Protection (with amp PTT bypass)

Single and Dual Rack Mount available
New "Power Master Basic" Software FREE!

ARRAY SOLUTIONS

www.arraysolutions.com

Sunnyvale, Texas USA
Phone 214-954-7140
sales@arraysolutions.com
Fax 214-954-7142

See our web site for other products and additional details.

Centennial Events & Programs

ARRL 100 YEARS

- **ARRL National Centennial Convention—July 2014**

- **Regional Centennial Events**
- **Donate Now to the Second Century Campaign for the ARRL Endowment**
  www.arrl.org/scc
- **Yearlong On-Air Operating Event and Awards**
- **Plus commemorative publications, regional events, special *QST* features, and more! Additional details coming soon…**

ARRL National Centennial Convention at the Connecticut Convention Center in Hartford, July 17-19, 2014

Thursday, July 17, 2014
All Day Training Tracks: public service, technology, radiosport, and more!

Friday & Saturday, July 18-19, 2014
- Exhibit Hall featuring ARRL exhibits, Amateur Radio manufacturers, equipment sellers, and an indoor flea market
- Dozens of forums & presentations
- License Exams
- Friday Night Banquet

July 17-20, 2014 (Thurs-Sun)
Tours of ARRL headquarters and W1AW

Hotel and Travel details available NOW

ARRL2014.org
Registration begins in January

Advancing the Art and Science of Radio—Since 1914
ARRL2014.org

Quicksilver Radio

See us at Hamfests
From Maine to Florida
Visit our Huge Display at Dayton

Discrete Component Analyzer

Identifies and measures transistors, MOSFETs, J-FETs, diodes, LEDs and more.
Pocket sized and battery powered.
Visit our Web Site for more details.

LCR Analyzer

Identifies and measures inductors, capacitors, and resistors. Optional tweezers for SMD components
More info and downloadable manuals on our Web Site.

Quicksilver Radio Products

Sign up on our Web Site for your free newsletter.
Ham Radio news, articles, & special discounts.

www.qsradio.com